A Finite Element Approach to Study Skeletal Muscle Tissue

Aron Teklemariam

A thesis submitted in partial fulfilment of the requirements of the Manchester Metropolitan University for the degree of Doctor of Philosophy.

2016

Abstract

This dissertation investigates force generation in muscle using a finite element (FE) approach to model electrical activity and mechanical force production within skeletal muscle. The work proposes new FE models design/formulations to answer specific research questions related to skeletal muscle properties. The focus is on two specific determinants of skeletal muscle force: the activation and the connective tissue. A FE model was created and designed to study the impact of the dielectric and geometric (pennation) properties of the muscle tissues on the electric activation signal detected on the skin surface by bipolar electrodes (surface electromyography, sEMG). The model shows that when considering parallel muscle fibres the tissue, attenuated mainly frequencies in the physiological range (92-542 Hz). This study revealed a strong impact of the muscle fibres pennation angle, on the detected signal (low pass filtering effect); suggesting that the low pass filtering behaviour observed in experimental data is due to the geometry (curvature or pennation) rather than the dielectric properties. The model informed recommendations for sEMG experimental protocol to increase the inter-electrodes distance when measuring sEMG of pennated muscles. A micromechanical model of the muscle tissue was created to explore the influence of the connective tissue properties (endomysium) on the total muscle force production. The constitutive model was used to study the mechanical consequence of clustering of fibres due to the remodelling of the motor units, which occurs with ageing. An FE model with a bundle of 19 fibres was designed and simulated activating 21% and 37% of the fibres in a distributed and clustered pattern. Results showed for both activation levels that the pattern of the strain distribution changed with an increased deformation toward the centre of the bundle. This could lead to excessive unbalanced stresses if higher deformations are involved. The micromechanical model can be used to study muscle force determinants at a fascicle level. It showed the importance of the fibre distribution during the muscle activation and the consequences of age related alterations on force production.

Declaration

No portion of the work referred in this thesis has been submitted in support of an application for another degree or qualification at this, or any other university, or institute of learning.

Date:

Signed:

Acknowledgement

" Glory to God, because of Your faithful love, because of Your truth."

I'd like to thank first of all, my supervisors team Dr. Glen Cooper, Dr. Emma Hodson-Tole, Prof. Neil Reeves, Dr. Nicholas Costen and recently Dr. Kirstie Andrew for giving me the opportunity to start a research/teaching career with this PhD. I thank my DoS of studies Dr. Glen Cooper for his support and encouragement, and for pushing me to develop a critical mind. A warm thank you to Dr. Emma Hodson-Tole for her pastoral support and her will to make us part of a disciplinary research team. I have tried my best to consider all your advices to become a mature researcher. Many thanks to my supervisors Neil Reeves, Nicholas Costen and Kirstie Andrew for always being available, and for giving me advices whenever it was needed. I am thankful to my office mates/friends/colleagues Canras, the sisters Elisa and Elisabetta, Andres, Ramzan, Simon, Dean, James, Mike, Gary, Prabhav, Khattab, Hassan, Fayad and Daniel. They made this journey enjoyable and full of meaning. Specifically I am very grateful to Canras, Elisa and Elisabetta for their support and caring. I wish them the best for their career and future families.

This PhD was not just research, but also teaching which I have loved a lot. I am therefore very grateful to Dr. Hong Li and Dr. Sravanthi Shashikumar for giving me the opportunity to teach. I could not have had better mentors and examples.

I think our department was blessed by the presence of staff that care about the research students. I was surprised and glad to see the dedication of our Head of Department Ms.

Margaret Fowler and the Head of School Dr. Georgina Harris to provide support to us, research students.

Finally yet importantly, I'd like to mention my family. My parents Teklemariam, Mehret and my sister Ruth. They taught me not to follow and believe the world but to have faith in God and the gift He gave us.

If my PhD is meaningful, it is because of the relationships I have built and the people I have worked with. I hope to work with them again, and I wish them all to find their ways.

Table of Contents

List of Figures

List of Tables

List of Abbreviations

ACh	Acetylcholine
ADP	Adenosine Diphosphate
ATP	Adenosine Triphosphate
CE	Contractile Element
CSA	Cross Sectional Area
ECM	Extracellular Matrix
EEG	Electroencephalogram
EMG	Electromyography
FE	Finite Element
FEA	Finite Element Analysis
FEM	Finite Element Model
F-L	Force-Length relationship
F-V	Force-Velocity relationship
IED	Inter-Electrode Distance
iEMG	Intramuscular Electromyography
MRI	Magnetic Resonance Imaging

MUAP	Motor Unit Action Potential
MUs	Motor Units
Na	Sodium
PCSA	Physiological Cross Sectional Area
sEMG	Surface Electromyography
SNR	Signal-to-Noise Ratio

Publications based on this work

A. Teklemariam, G. Cooper, E. F. Hodson-Tole, N. D. Reeves and N. P. Costen, "A Finite Element Model simulation of surface EMG signals based on muscle tissue dielectric properties and electrodes configuration," *Communication Systems, Networks & Digital Signal Processing (CSNDSP), 2014 9th International Symposium on*, Manchester, 2014, pp. 193-197. doi: 10.1109/CSNDSP.2014.6923823

Teklemariam, A., Hodson-Tole, E. F., Reeves, N. D., Costen, N. P. and Cooper, G. (2016) 'A Finite Element Model Approach to Determine the Influence of Electrode Design and Muscle Architecture on Myoelectric Signal Properties.' *PLoS One*, 11(2) p. e0148275.

Introduction

Appropriate skeletal muscle function is essential for survival as it is required for many fundamental aspects of life, such as breathing and swallowing, and also underpins the ability to maintain independence and a good quality of life by enabling us to move and interact with our environment (e.g. reaching and grasping, locomotion). This thesis aims to improve fundamental understanding of muscle force production through a modelling approach with implications for ageing and other conditions. With ageing people lose the ability to be independent and perform activities of daily living. Limb muscle strength can be reduced to 30% [1] in old age in comparison to younger people and changes in skeletal muscle are responsible for this deterioration.

The main characteristics that make skeletal muscle different from other biological materials and tissues are the activation dependent force generated by an electric signal and the force transmission mediated by the connective tissue. Experimental investigations of these components in human subjects can only go some way to explain function, as they require invasive methods, approximations or specialist tools. Modelling is a way to overcome this issue, offering the advantages of controlling the parameters and ability to study different scenarios for the same conditions. Recent finite element models, FEM, of the muscle have contributed to moving towards this goal but there is still more improvement needed. Other non-invasive experimental methods such as surface electromyography or ultrasound can be effective but anatomical differences and experimental protocol and measurement noise can be problematic.

Therefore, this thesis uses the FE method, to explore and simulate skeletal muscle tissue behaviour and the determinants of its force producing capability using experimental inputs. The focus will be the electrical input (activation) and the force transmission through the connective tissue. In order to understand how to implement FEM, it is necessary to be familiar with aspects of skeletal muscle physiology and function, electrical activation and muscle modelling fundamentals, described in detail in chapter 1: *Muscle Anatomy & Modelling Fundamentals*.

Many other researchers have used FE modelling approaches to understand skeletal muscle function. These are described in a literature review of past and recent muscle models, chapter 2, concentrating on models related to the detection of the activation signal and the contribution of connective tissue to force production. Promising approaches using micromechanical models from Blemker [2-4] and electrical limb models from Lowery [5, 6] were discussed and lead to the specific aims and objectives of this thesis at the end of the chapter. The thesis then addresses problems to improve understanding of muscle force production, specifically problems with electromyography, EMG, measurements using FEM to perform a design study of surface electromyography, sEMG, electrodes based on an electrical model of the muscle that produce recommendations on experimental protocol (chapter 3). It then describes skeletal muscle tissue mechanical properties, detailing current understanding of connective tissue. From this a new micromechanical FE model formulation is developed and implemented, providing a means of simulating a bundle of muscle fibres, which was used to test the hypothesis of lateral force transmission using an adapted analytical formulation (chapter 4).

Chapter 5 uses the model described in chapter 4 to simulate a bundle of fibres (fascicle). The effects of different fibre packing configurations, which may result from age, related motor unit re-innervation, and different activation patterns on force production was investigated.

The outcomes of the presented studies, outlines of the main contributions, implications of the work and potential future research directions are then discussed, chapter 6.

1 Muscle Anatomy & Modelling Fundamentals.

In this chapter, an insight on muscle mechanics, activation signal, and age related degeneration is given. Moreover, the fundamentals of muscle modelling are discussed. This will lead to the thesis main aim.

1.1 Skeletal Muscle Anatomy and Modelling Fundamentals

Skeletal muscles are striated muscle tissues connected to bones via elastic tendons. One function of skeletal muscle is to move the body, and specifically the body joints. Each joint has a specific range of movement, position that determine the muscle properties. Different intrinsic factors influence the muscle's ability to produce force and influence the muscle's strength-force generating capabilities. The length of the fibres composing the muscle and the length of the muscle's moment arm (the arm of the torque generated by the muscle force about the joint) influence the motion. The primary intrinsic factors that influence the muscle's force are: muscle size, strain of the muscle, contraction velocity, level of muscle fibre recruitment and muscle fibre types composing the muscle [7]. The overall performance of the muscle is then characterized by the muscle-tendon and joint architecture. Each of these characteristics needs to be studied separately and as interacting components, to enable the functional significance of each to be fully understood. The following section therefore provides a description of skeletal muscle anatomy, starting from the muscle-tendon unit to the single fibre and the interaction with the connective tissue.

1.1.1 The Musculo-tendon Unit

Skeletal muscles transfer force to the joints through the tendon, and together these two structures form the musculo-tendon unit. The direction of the muscle fibres (hence of the force) is not always aligned with the tendon but can have different architectural configurations (fibre orientation and curvature) creating a gearing effect (i.e. see Figure 1.1). Different architectural configurations are strictly related to the muscle function (force/power needed, range of motion, shortening velocity and anatomy) and when not considering the moment arm (muscle force × distance from the joint point of rotation), it is possible to make a functional consideration of how the architecture could influence the force-length relationship of the muscle. The force-length relationship of the muscle fibres refers to the maximum capacity of the fibres to exert an isometric force at a specific fibre length. The architecture can influence the range of length changes the muscle can undergo and consequently the maximum force it can exert. The most commonly studied muscle configurations are: parallel muscles and pennate muscles. Parallel muscles have fibres disposed along the force direction while pennate muscles have fibres oriented with a certain angle with respect to the force direction (see Figure 1.1).

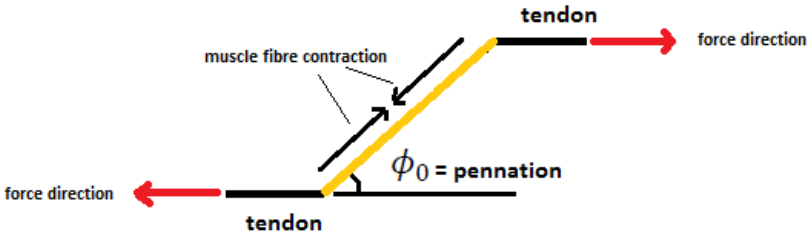

Figure 1.1 Scheme of a pennated muscle. The pennation angle defines the gearing between the force exert by the muscle and the pulling force at the tendon

Skeletal muscles are composed of contractile elements arranged in a connective tissue in a clearly defined hierarchical structure: from sarcomeres, to myofibrils, to fibres, to fascicles to the muscle (Figure 1.2).

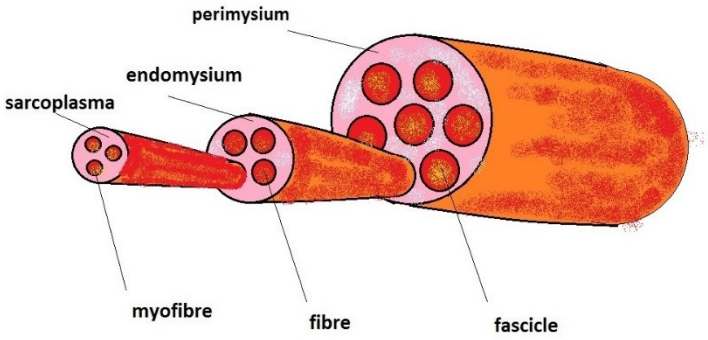

Figure 1.2 Muscle fibres hierarchal structure. Muscle fibres follow a hierarchal structure, from the myofibres to the fascicle, similar to a tendon structure.

Figure 1.3 (left) shows a scheme of the muscle interfaces: the intracellular space within myofibers, the basal lamina or membrane and the endomysium. The extracellular matrix consists of fibrous proteins (predominantly collagen) embedded in a hydrated

polysaccharide gel. The basal lamina is made of a laminar pattern of collagen that envelops individual myofibers and different proteins such as costameres and adhesive glycoproteins [8]. Costameres (Figure 1.3 right) are sub-membranous, Z-line associated structures found in striated muscle [9]. It is believed that lateral force is transmitted through costameric proteins such as vinculin, talin, and integrin, situated in the basal lamina and connecting the sarcomere cytoskeleton to the external collagen network (intramuscular connective tissue) [8-10].

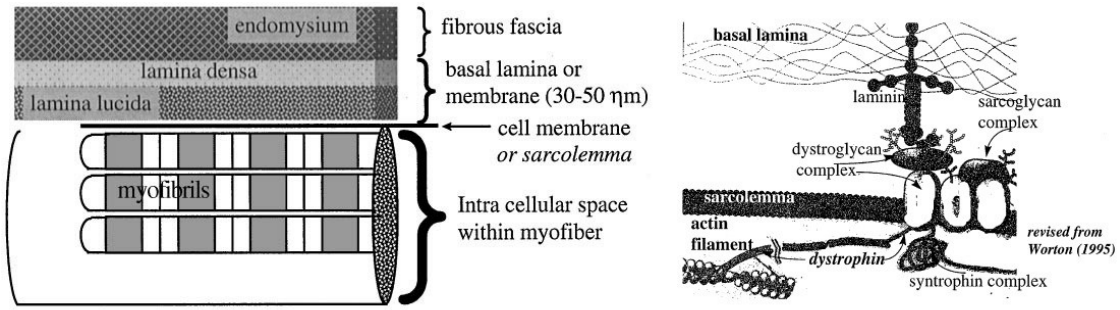

Figure 1.3 The fibre – matrix interface. (Left) muscle-endomysium substrates. (Right) dystroglycan costameric complex. (Adapted from[8])

The intramuscular connective tissue can be divided into: endomysium (within fibers), perimysium (within fascicle) and epimysium (envelops the entire muscle). New perspectives were presented by Purslow [11] on the role of the different levels of connective tissue. If the endomysium functional role is to distribute the stress transversally to the fibres direction, the perimysium function is believed to satisfy the need of accommodating the fascicles to shape changes. This theory was supported by

Purslow [12] study on the bovine semitendinosus (see Figure 1.4 b). The fascicles were marked with ink across their direction and the deformation of the muscle induced a misalignment between fascicles but not within fascicles as the endomysium presence links the fibres through frictional forces. On the other hand, the epimysium compartmentalization, creates a pressure that could increase the muscle contraction efficiency [11].

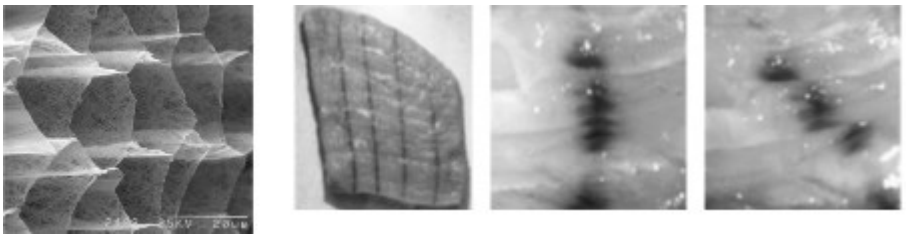

a b

Figure 1.4 Scanning electron micrograph of fibres. a) Purslow and Trotter [13] scanning electron micrograph of fibres within the fascicles of the bovine sternomandibularis muscle after sodium hydroxide treatment to remove myofibres. This early image revealed the collagen pattern surrounding the muscle fibres, creating a sort of tunnels where fibres operate. b) A study on the bovine semitendinosus. The fascicles where marked with ink across their direction. When the muscle is deformed, large shear displacement occur between the fascicles, but not within fascicles (adapted from[12]).

1.1.2 Motor Units and Activation

The smallest controllable unit in the muscle is the motor unit. A motor unit is an α-motor neuron, its axon and all the fibres it innervates [14] as represented in Figure 1.5. A motor unit action potential is triggered from the motor neuron. This input signal travels along the nerve axon to the axon pre-synaptic terminal and, following chemical chain reactions, ends up in the release of acetylcholine (Ach). The acetylcholine diffuses across the synaptic cleft and increases the permeability of the postsynaptic terminal to Na^+. The Na^+ flux depolarizes the membrane until the motor unit action potential (MUAP) is generated. This action potential changes the permeability of the surrounding ion channels which will in turn change permeability of adjacent channels, creating a chain reaction of depolarization and repolarization along the fibre that propagates at a certain conduction velocity and creates trains of travelling action potentials (MUAP) [15]. These action potentials will trigger and regulate the release of calcium that will activate the mechanical contraction of the fibres, as explained in Appendix A.

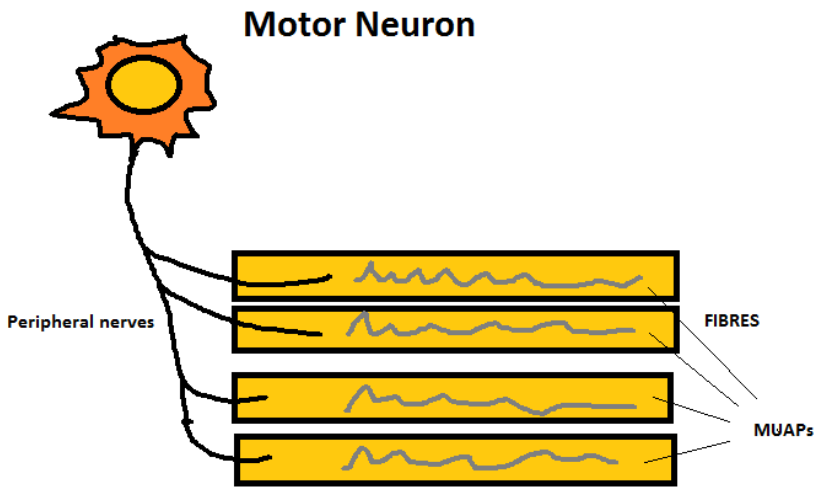

Figure 1.5 Scheme of a motor unit.

From a mechanical perspective, motor units can be classified (but their properties could be mixed) into three different types: slower, faster fatigable and faster fatigue-resistant [16]. Slower motor units have smaller fibre diameters and transduce energy at a relatively slow rate, implying a contraction at slower velocities. Faster fatigable units generate more force; have fibres with greater cross-sectional area and higher contraction velocities but can fatigue rapidly. The faster fatigue resistant units still have a fast contraction velocity, however are able to maintain the force production over longer time periods due to their high oxidative capacity.

Understanding motor unit recruitment patterns is fundamental to understanding function of the neuromuscular system in health and disease. The classic recruitment theory is the size principle, which states that motor units are activated in order of size, from the smallest to the largest [17]. Considerations were made by Clamann [18]on the benefit of having recruitment from the weakest to the strongest motor units. There are analogies with Weber's law on sensory perception; such as the fact that the gradual force increases can be a percentage of the current cumulative force and the smallest increment added by new motor unit recruitment becomes greater as the force of contraction increases [18]. Whilst such patterns of recruitment have been widely found, it is also possible that tasks demanding greater mechanical power production could rely on different, task dependent recruitment patterns [19, 20].

Another field of interest regarding motor units is their distribution in the muscle. Experimental studies [21, 22] indicate that fibres belonging to a motor unit can be spatially localised within a small region of the muscle, while the fibre distribution within that region showed a random distribution in most of the results. The size of the territory

occupied by a motor unit depends on the muscle and motor unit type [21], which is variable in human muscles. Monitoring the muscle electrical activity (MUAPs) can open the door to derive the recruitment pattern and the motor unit distribution. This is a factor which is considered in more detail in the literature review (see chapter 2).

1.2 Age-Related Changes in Muscle Tissue

Demographic ageing is a consequence of the higher quality of life and improved healthcare services in many countries. Such demographic change requires an increased effort in studying age-related pathologies, which will, according to the European Commission [23], affect healthcare system sustainability and people's quality of life in coming years.

One consequence of ageing is loss of muscle mass termed sarcopenia. Sarcopenia is the result of cellular processes (denervation, mitochondrial dysfunction, inflammatory and hormonal changes), the consequences of which are decreases in muscle strength, decreased mobility and function, increased fatigue, increased risk of metabolic disorders and increased risk of falls and skeletal fractures[24]. The decline in the total lean body mass (LBM) is reported to be 18% in men and 27% in women, from the second to the eighth decade of life, with a greater decrease in the lower limbs (15%) than in the upper limbs (10%). The resulting qualitative (strength) decrease is greater than the quantitative mass decrease [25-28].

The loss of motor units is believed to be at the heart of sarcopenic decline [27]. The loss of motor neurons causes a decrease in the number of muscle fibres (hypoplasia) [29].

This atrophy generally affects all types of fibres with some exceptions. For instance in the vastus lateralis (a knee extensor in the quadriceps), the number of type II fibres decreases from 600, 000 to 323, 000 (50%) between 50 and 80 years of age [30]. This creates a change in the distribution of the motor units, the possible consequences of which are explored in Chapter 6 of this thesis, through a mechanical model of the muscle.

Several invasive (e.g. biopsy) and non-invasive (imaging) studies revealed that, rather than reduced muscle volume or CSA, the infiltration of fat and connective tissue are the biggest contributors to loss of contractile properties [28]. Quadriceps muscle biopsies to assess the fibre composition, suggested a loss of fibres and reduction in their size, with the loss of fibres contributing most to decreased muscle volume in older adults as summarized by Lexell in 1995 [28]. These losses have functional implications, which are a consequence of changes in muscle architecture (e.g. fascicle length and pennation angle) [29]. Ultrasound imaging *in vivo* has revealed changed properties of the musculo-tendon complex in elderly people (e.g see Figure 1.6).

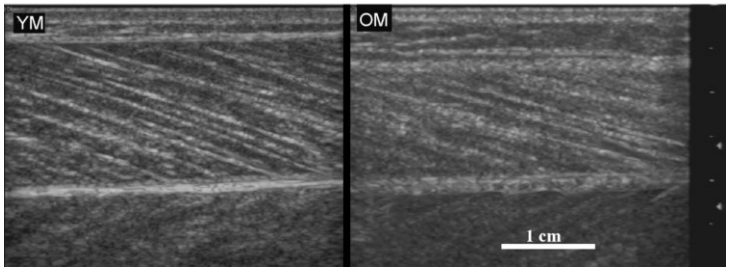

Figure 1.6 Sonography of the medial gastrocnemius. Sonography in the sagittal plane of the medial gastrocnemius in the same subject when younger (left) and older (right). The older subject shows lower pennation angles and fibres length. (adapted from [31])

The length of the muscle fascicles and their angle of insertion (pennation angle) were reported to be decreased in aged subjects [32]. Decreased fascicle length suggests a loss of sarcomeres in series, which will lead to a reduction in the maximal shortening velocity. Decreases in pennation angle suggest a loss of sarcomeres in parallel and hence reduced force producing capacity due to a reduced CSA [33]. Together these changes mean less force and power can be produced, which will affect a person's ability to properly accomplish a given motor task. For example, the vastus muscles stabilize the knee joint during the heel strike of the gait cycle (a phase of the walking cycle). Less power means less capacity to absorb the knee eccentric destabilization, leading to a possible risk of injury.

Ultrasound imaging techniques were used to find the stress-strain relationship of the tendon *in vivo* and obtain its Young's Modulus in young and old subjects [34]. These studies showed a lower tendon Young's modulus in older adults that did not depend on a change in the size, but on changes in intrinsic properties (e.g. Stiffness). These changes result in a left shift of the length-tension relation, hence a decline of the force for a given fibre length. Measurement of the rate of force/torque production revealed the association between tendon stiffness and contractile speed, with older tendons tending to damp the transmission of fast forces, resulting in functional limitations particularly related to faster movements [29].

Muscle is a living tissue, which means that each change in its architecture, composition, or neural drive, could somehow induce a spontaneous reorganization of its components (reinnervation, fibres pennation, specific force) to regain its original functionality. Nonetheless, this does not imply a complete restoration of functionality. For instance, the side effect of the loss of faster MUs is denervation of associated muscle fibres. Consequently, these fibres are incorporated in the remaining, generally slower, MUs, resulting in an increase in the level of innervation [25]. The newly innervated fibres will change their properties according to the new MU they have joined, increasing their size and fibre density.

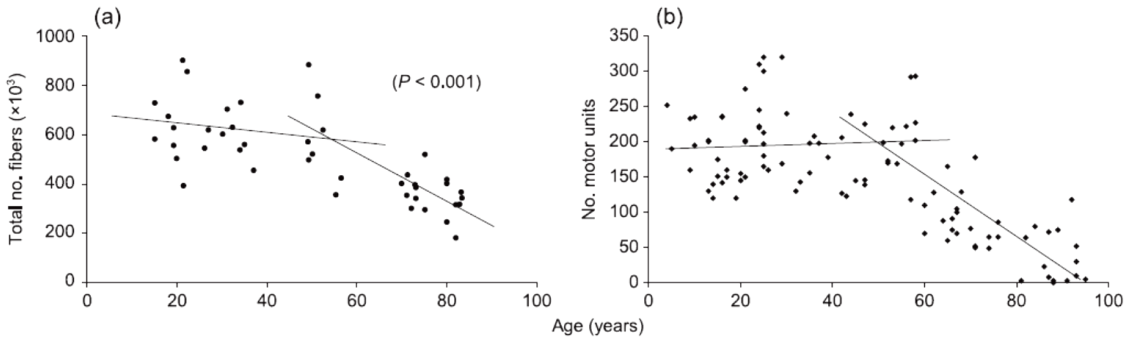

Figure 1.7 Relationship between age and number of muscle fibres and motor units.. (left,[35]) Decrease in the number of fibres (vastus lateralis muscle) and (right,[25]) motor unit (extensor digitorum muscle) during aging. The regression starts from 50 years old.

Due to muscle plasticity, it is possible to actively reduce the effects of sarcopenia and slow its progress, for example through the use of endurance exercise [27, 36]. This has been confirmed by different aged population studies that relate physical activity with functional independence [37] and physical health [38]. However, there is still a need to deepen knowledge of muscle function to identify further methods of preventing or slowing the progress and consequences of sarcopenia and assess the most influential determinant of reduced muscle force producing capability.

1.3 Skeletal Muscle Modelling

Early research in muscle modelling has led to understanding of properties such as the isovolumetric contraction [39] and the muscular-tendinous structure being defined [40]. According to Huxley [41] in the last century, three revolutions changed the way the muscle was conceived. The first revolution [42, 43] was the acknowledging of the ATP-ADP hydrolysis reaction as being the source of the filament folding. The second revolution [44] was the relationship between the energy liberated during contraction and the muscle's mechanical state, which led to the widely used Hill's based lumped parameters model. The third revolution (1953) was the discovery of the sliding proteins that generate the muscle contraction (through links called cross-bridges). The last two revolutions lay the foundations for mathematical muscle models that can be classified in two ways: i) structure and ii) rheological (or phenomenological) [15]. Structure models describe the mechanisms that characterize the behaviour of a system while rheological models consider the system as a black box, and describe the relationship between the input and the output through a transfer function. Structure models can be used to study the link between chemical properties such as rate of cross-bridges attachment and the force exerted by the muscle [45] while rheological models are widely used to study the overall musculo-skeletal biomechanics, linking the joint motion with the muscle force production [46]. Therefore, if structure models helped to find out how the muscle works, rheological models aim to study the consequences of muscle property changes on the force exerting capacity and the joint movements and coordination. This thesis will focus on rheological models as the research focusses on understanding the microstructural effects on force production.

1.3.1 Hill-based Rheological Models

Hill's type muscle models describe the muscle as a contractile active element (CE), whose dynamic behaviour is described in equation 1.2, acting in parallel with a passive non-linear element (PE) that represents the passive behaviour of the fibres (Figure 1.8).

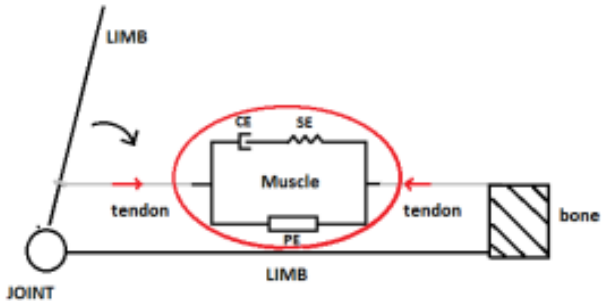

Figure 1.8 A scheme of the Hill's based muscle model. The contractile element (fibres) works in parallel with the passive element (passive tissue). The in series element (inertia of fibres) is usually neglected[47].

Hill based models characterize the fibre force-length (F-L) and force-velocity (F-V) relationships [47]. These functions are usually expressed with normalized values in order to have dimensionless curves (Figure 1.9). The F-L relationship of the muscle is a bell shape function that reaches the maximum value at a fibre length defined as the optimal length. This function, at a muscle macroscopic level, is a smoothed version of the discontinuous (see Appendix A) force-length relationship at a sarcomere level. The force-velocity relationship (from equation 1.1) is an inverted sigmoid; the maximal velocity is reached when the muscle is unloaded (force = 0, v_0 = max) while when the muscle is lengthening the force increases and it reaches a maximal value which usually

is 1.5 times the isometric force. When the force F is equal to the isometric maximal force $F_0$the velocity v is equal to zero according to Hill's results in equation 1.1, where:

$$v = \frac{b}{(F+a)}(F_0 - F) \quad (1.1)$$

b = costant with unit velocity

a = constant with unit force

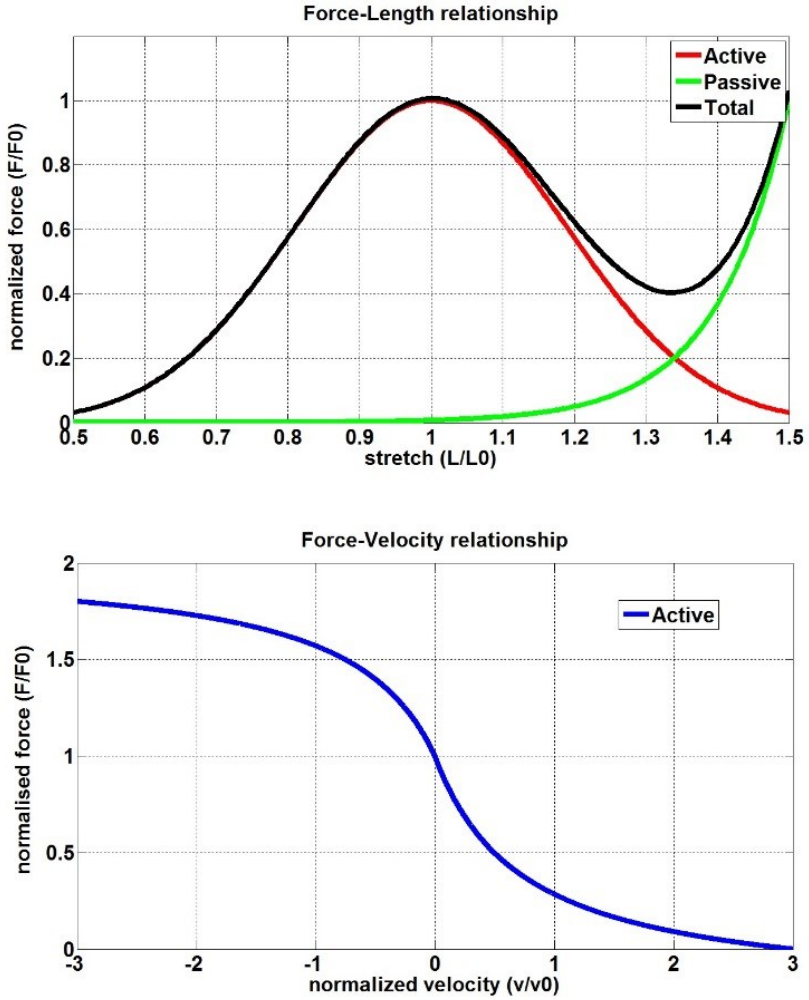

Figure 1.9 Hill's F-L, F-V graphs

(Top) The F-L relationship of the muscle. The force and the fibre length ranges are both normalized within respect the maximal isometric force at optimal length and the fibre optimal length respectively. The red line correspond to the passive tissue contribution the blue line is (Bottom) The F-V relationship of the muscle. It is a sigmoid function where the middle point distinguish between eccentric (while muscle is lengthening) muscle contractions and concentric muscle contractions. The max velocity is reached when the muscle is unloaded.

1.3.2 Rheological Hill-based Models

Buchanan *et al*. [48] proposed a model (Figure 1.10) to assess a biomechanical forward dynamic of the muscle that includes neural input. The main equations were based on the Hill type model incorporated by Zajac [47] into a musculo-tendon complex.

In this new model, the final force exerted by the musculo-tendon system is a function:

$$F^{MT} = f(a, l^{MT}, v^{MT}, F_0^M, l_0^M, l_s^t, \phi_0) \quad (1.2)$$

Where:

a : activation function from EMG measurements

l^{MT}: length of the musculotendoncomplex

v^{MT}: velocity of contraction

F_0^M: maximal isometric force

l_0^M: optimal fibre length

l_s^t: tendon slack length (assumed to be known)

ϕ_0: pennation angle at optimal length (pennation is a function of fiber length)

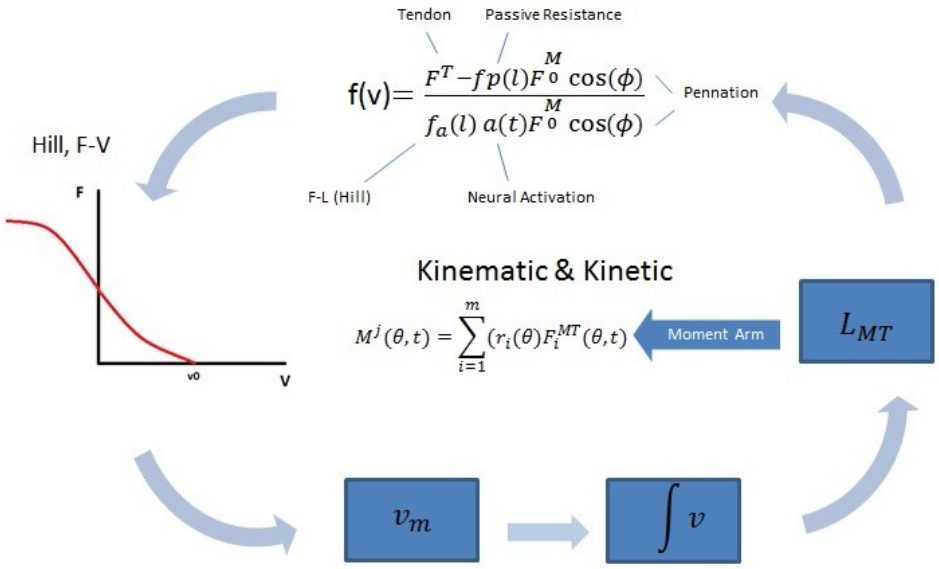

Figure 1.10 Buchanan *et al.* [48] forward biomechanical muscle model scheme. The model rearranges the system forces equations to isolate the force dependent from the velocity (from F-V relationship), from which the velocity of contraction can be derived and, through integration, the fibre length can be determined to calculate the moment arm. Knowing the anatomy means the torque at the joint can be obtained.

Once the resultant moment arm and the anatomical geometry of the joint are known, it is possible to calculate the joint torque. For an estimation of the muscle force, the parameters to consider in Hill-type models are: the pennation angle, optimal subject specific Hill's parameter estimation (optimal fibre length, maximal isometric force, maximal velocity of contraction, a, b) and the PCSA [49]. Hill's model parameters of human skeletal muscles can be found in literature [50-52] and many more data can be found for animals. Ward *et al.*,[52] provided the mean values taken from 21 human cadaveric specimen with the main objective of updating previous data from literature

with new high fidelity set of data along with muscle functional considerations. The fibre length was normalized by sarcomere length so that it was possible to compare muscles between different subjects, since the fibre length could have been affected by the sarcomere tensional condition during the measurements. Despite it being a less complex model, Hill based musculo-tendon modelling of the total human body might require a subject specific estimation of 54 muscle parameters, which will result in more than 270 parameters being estimated [53]. Consequently, clinical research toward biomechanical disorders (e.g. gait pattern disorders) had mainly applied inverse dynamic to estimates joint torque. Inverse dynamics is a mathematical tool to extract muscles and joints, forces and torques, from kinematic measurements. This approach does not guarantee a realistic estimation of the single muscle contribution to the force exerted, which might be of relevant importance for such studies. Indeed the typical equation (see equation 1.3) that describes the relationship between the movement and the muscle forces is generally redundant with a number of unknown muscles exceeding the number of equations.

$$M(q)\ddot{q} + C(q,\dot{q}) + G(q) + R(q)F_{MT} + E = 0 \qquad (1.3)$$

Where:

M = system mass matrix C = centrifugal Coriolis loading G = gravitational loading

q = kinematic variable $\mathrm{R(q)F_{MT}}$ = muscle torques E = external forces

On the other hand, forward analysis (estimating kinematics from generated forces) requires higher computational costs and is not always feasible. These problems can be solved by reducing the number of muscles combining them or by using optimization principles that might add further muscle constraints [54]. However, optimization functions are based on assumptions that may not reflect the real muscle behaviour. An attempt to overcome these limits was made by Sartori *et al*., [55], who considered more degrees of freedom of the musculo-tendon unit. When considering more degrees of freedom during a joint movement (which means the kinematics on different planes), the redundancy of the muscle forces is reduced (less possible solutions), allowing a more reliable result without sacrificing accuracy.

1.3.3 Neural Drive

The neural drive is the neural input to the motor neuron that determines the level of activation (how many cross-bridges formed) and the recruitment of the fibres. The activation level is usually described in muscle models as a function that modulates the amplitude of the maximal muscle force through EMG (electromyography) measurements. The EMG is the measurement of the sum of the motor units action potentials (MUAPs) detected at the surface of the muscle (sEMG) or in the muscle (iEMG), depending on whether signals are recorded using surface electrodes or intramuscular electrodes. The activation function can be a simple input scaling factor or could represent the dynamic patterns of motor unit recruitment [47]. In the latter case, an EMG-to-activation dynamic is used. EMG acquisition to assess muscle activation and force, requires previous knowledge of the nature of the EMG-muscle force relationship,

the difference in temporal characteristics between EMG and force signals, normalization of EMG amplitude and the effects of muscle contraction dynamics [56]. Equations 1.4, 1.5 shows the EMG-to-activation function proposed by Buchanan *et al*. [48].

$$u(t) = \alpha\, e(t-d) - \beta_1 u(t-1) - \beta_2 u(t-2) \tag{1.4}$$

$$a(t) = \frac{e^{AU(t)}-1}{e^{A}-1} \tag{1.5}$$

The function $u(t)$ is a second order discretized differential equation representing the muscle fibre's twitch response when activated. α, β_1, β_2 are the coefficients of the second order dynamic and *d* is the electromechanical delay. *a*(*t*) which is a function of $u(t)$, is the non-linear activation function that modulates muscle force. These models assume homogenous activation across muscle fibres, however, this is not the case in the muscle itself as different types of muscle fibres are recruited at different times[17]. The classical recruitment theory is the size principle that indicates MUs are activated in and orderly fashion from the smallest (usually slower) to the largest (usually faster) [17]. More recent studies [19] suggest that this recruitment pattern is not always respected, and task dependent recruitment patterns may occur. Wakeling *et al*. [20] compared classical models of muscle force-velocity relationship with a new differential recruitment model that considers independent activation of fast and slow twitch fibres with different curvature of the muscle force-velocity relationship, showing that independent activation led to better force predictions of the force compared to traditional Hill's type models. The activation function was determined with a time-frequency analysis of the EMG signal. Through wavelet analysis it is possible to separate the signal into different

bands of frequencies. In this study faster fibres contribute to the higher band (240-423 Hz), and slower fibres in the lower band (82-247 Hz).

1.3.4 Limitations of Classic Models and Introduction to Finite Element Models

The research community is focusing on developing new muscle models that can include complex features such as the interaction between the connective tissue and the fibres (lateral force transmission), the architecture and the motor unit distribution/activation. The main goal motivating this effort is the need to realistically estimate the muscle force (forward dynamic) when certain subject specific muscle parameters (Hill's model parameters, architectural parameters, connective tissue parameters) and the level of activation are known. Furthermore, there is a need to study synergies of different muscles acting on the same joint and further improve the understanding of functional significance of musculo-skeletal anatomy and physiology. The different levels of modelling are represented in Figure 1.11. The core is the muscle model, which has the neural drive as input.

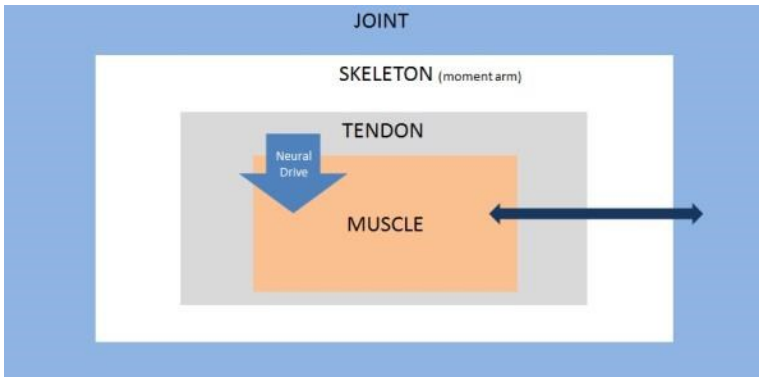

Figure 1.11 Musculoskeletal modelling levels

Hill-based models consider the muscle's overall behaviour without taking into consideration the interactions between adjacent fibres or compartments or between the muscle fibres with the surrounding connective tissue. Recent research has focused on incorporating the connective tissue contribution into the models [3, 60]. The main mathematical tool that allowed this progress in modelling is the Finite element analysis (FEA). FEA is a mathematical method used mainly in engineering, to simulate physical models in the continuum space. Muscle models that use the FEA approach, were able to investigate the influence of the neural drive, the tissue properties and the three dimensional configuration of the fibres on the outcome force [3, 57-60]. A further exposition of this method and its applications will be made in the literature review of chapter 2.

2 Literature Review: Mathematical Models of Skeletal Muscle

This chapter will review past and recent muscle models. The review is divided into two main sections: i) The modelling of the dielectric properties of the muscle, detailing the activation electric signal (MUAPs) and how it is detected on the muscle surface; ii) Review of mechanical models of the muscle. Specifically how the connective tissue can be modelled and which age related changes of the muscle could be explored through modelling. The review outlines what is missing in literature and identifies improvement, which can be added, leading to the specific objectives of the thesis, which are detailed at the end of each topic review.

2.1 sEMG Models

2.1.1 sEMG

The electric activity of the muscle can be measured through electrodes placed on the surface (sEMG) or intramuscularly (iEMG). EMG measurements are considered the gold standard way to monitor the muscle activity. Surface electrodes have the advantage of being non-invasive, but the resulting measurement will be the superimposed electric activity that belongs to more than one motor unit as the fibres are randomly distributed across the muscle. The fibre electric potential is affected by nuisance signals due to environmental electric activity (*e.g.* 50 Hz electric interference) which can be of the same order of amplitude as the EMG signal. These nuisance signals are at different random frequencies (white noise) and can be partially eliminated with a bipolar differential acquisition that eliminates the common signal (since two electrodes, separated by a small distance will have the same noise). Furthermore, the waveform of the detected action potential depends on the orientation of the bipolar electrodes with respect to the fibre orientation. If the electrodes are aligned along the fibres' direction, the action potential observed will have a biphasic shape. The generated action potential runs along the fibre in opposite directions from the nerve end plate (see Figure 2.1), hence if the electrodes are situated on the left side or right side of the nerve end plate, the potential will be observed at different phases [61]. Early analytical models of the generation and detection (EMG) of action potentials were able to investigate the influence of electrodes size, distance and orientation. These studies introduced the concept of spatial filtering. Lynn et al. [62] two and three dimensional analytical models, confirmed the low impact of the electrode size on the amplitude and shape of the

detected waveform. In addition, distant fibres were found to have less amplitude and high frequency content (smoother). Fuglevand et al. [63] model of the motor unti action potential (based on Rosenfalck model [64] confirmed these results. Most of the detected signal energy was coming from motor units within 10-12 mm from the electrode. The size of the electrode did not give any advantage in term of depth resolution and differences were found only in term of integration of the signal over a wider area. A greater IED increased the detection distance (higher risk of cross talk), while smaller IED increased the selectivity of the EMG. These models showed how EMG measurements are affected by the configuration of the electrodes, and which signals are representing.

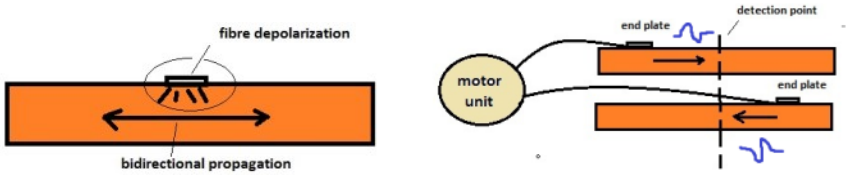

Figure 2.1 Schematic representation of action potential propagation. (Left) Propagation of a single action potential from the motor unit end-plate. (Right) Propagation with respect to the detection point.

It is possible to determine the motor recruitment pattern through sEMG [65], but the volume conduction effects of the biological tissue that affect the spatio-temporal characteristic of sEMG should be considered along with the fibres' architecture. Specifically the muscle tissue is composed of the muscle fibres, the adipose tissue (fat)

and the skin on the surface. These features are not considered in analytical models. Besides the fibres can assume a pennated architecture, which changes the direction of the propagation of the action potential with respect to the skin surface (see Figure 2.2).

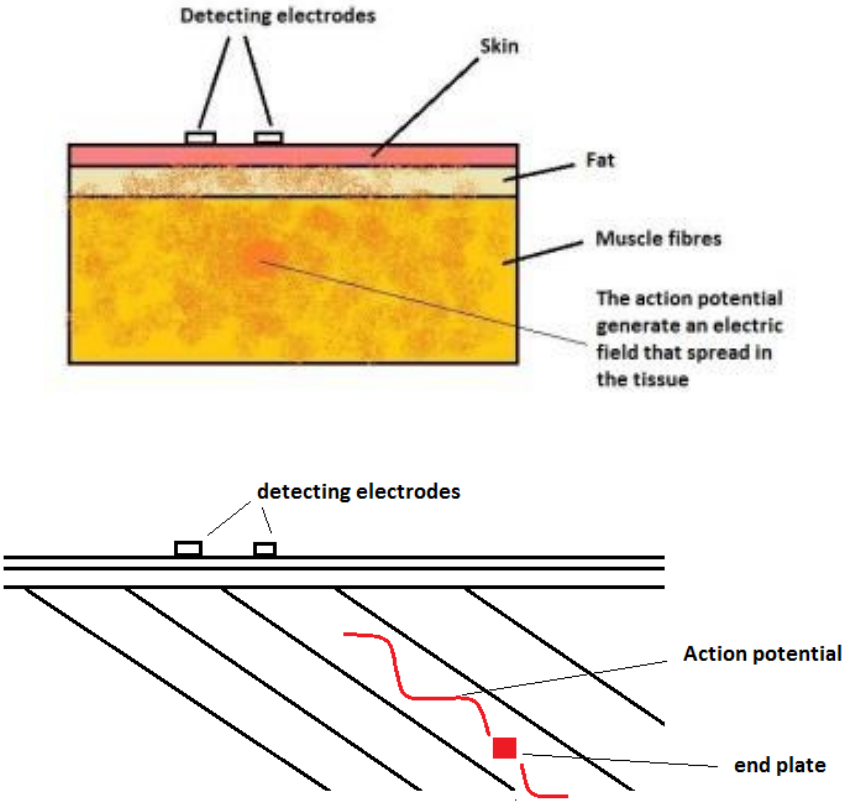

Figure 2.2 Schematic representation of the muscle tissue. (Top) The action potential is filtered by: the muscle, the fat tissue and the skin before reaching the detecting electrodes. (Bottom) Representation of a pennated muscle. Pennation changes the direction of propagation of the action potentials, hence changes the way the electrodes detect the signal.

Knowing how the electric field generated by the action potentials travelling along the fibres, sum up and spread up to the surface, can give an insight view of the EMG

measurements. This can lead to a better interpretation of the EMG signal and prediction of the influence of certain characteristics such as the curvature of the muscle the thickness of the skin, the fat tissue and the dielectric properties of the muscle. This topic motivated the implementation of analytical [66-69] and later on more accurate finite element (FE) models of the dielectric properties of the muscle tissue. FE models characterized the muscle tissue geometric and dielectric properties to study the motor unit action potentials detected on the surface [5, 6, 70-72], with a focus on predicting the sEMG from simulated action potentials generated in the muscle tissue.

2.1.2 EMG Modelling

Three main factors can affect EMG measurements: the design of the electrodes and their configurations, the characteristics of the tissue including the fascicle geometry (fascicle curvature, pennation) and the direction of propagation of the electric signal (Figure 2.3). In order to design or choose electrodes and their configuration (monopolar, bipolar, etc...) that maximize the significance of the measurements (e.g. provide the most appropriate signal to address specific questions within a given study), it is necessary to understand how independent factors affect the relationship between the physiological and the measured signal. One approach to better understand the feature of the detected signals is computer based, mathematical modelling.

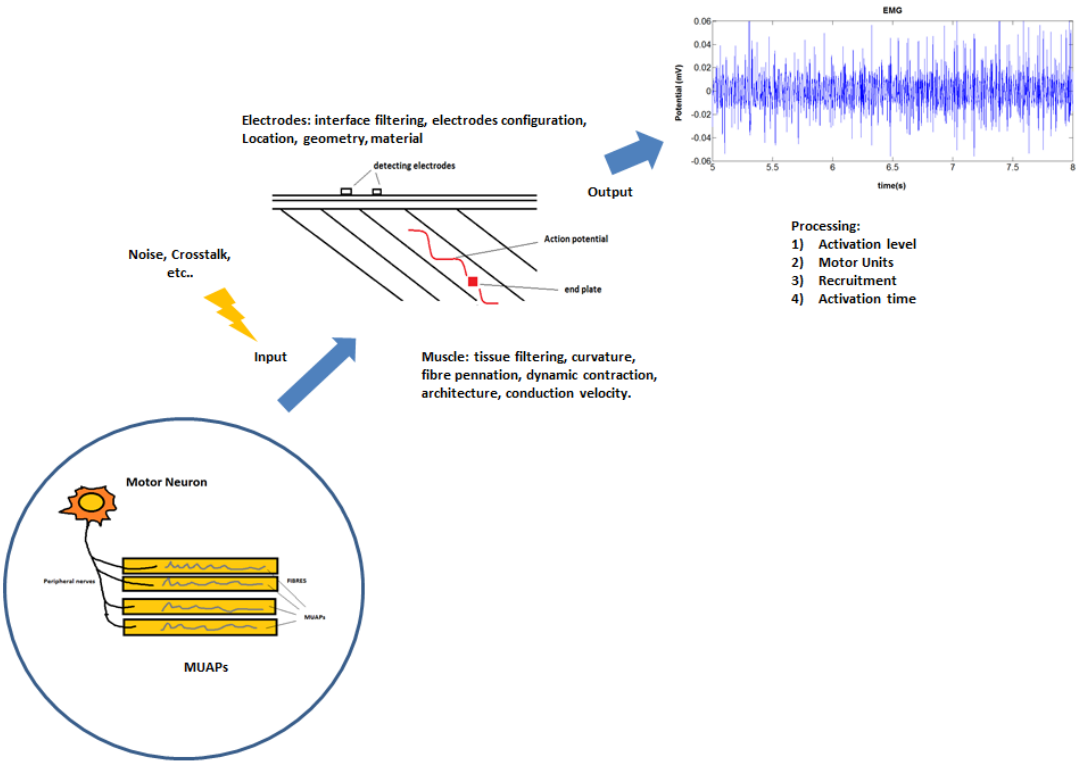

Figure 2.3 Features of sEMG, including desired and undesired components. The desired components are the MUAPs coming from the muscle or motor units that are being studied. The undesired components come from other inputs such as adjacent muscles or heart activity and other non-physiological noise such as movement artefacts or 50 Hz line noise. In addition, the signal is filtered in the frequency domain by the tissue and in the spatial domain by the electrodes and their configurations. Further features such as the muscle architecture (curvature, pennation) and MUAP conduction velocity, will determine the signal detected by the surface electrodes.

When simulating EMG, the first step is to model the source, i.e. the action potential. The action potential is due to the depolarization of the cell membrane. The work of Andreassen and Rosenfalck [68] was the base of several analytical models which will be discussed in subsequent sections [68]. They expressed the extracellular action potential as the numerical integration of the intracellular potential V_i [73]. The muscle tissue was considered anisotropic, where the longitudinal conductivity σ_z is considerably greater than the radial conductivity σ_r . Consequently, the extracellular potential was formulated as:

$$\phi_{an}(r,z) = \frac{a^2\sigma_i}{4\sigma_e} \cdot K(z) \cdot \int_{-\infty}^{\infty} \frac{\frac{d^2V_i}{ds^2}}{\sqrt{r^2\left(\frac{\sigma_z}{\sigma_r}\right)+(s-z)^2}} \cdot ds \qquad (2.1)$$

Where:

z, r are the distances along and perpendicular to the fibre axis

σ_i, σ_e are the conductivities of the intracellular and the extracellular medium

a is the radius of the muscle fibre

and : $K(z) = \frac{\delta\phi_e(a,z)}{\delta r} \frac{\delta\phi_e(a\cdot\sqrt{\frac{\sigma_z}{\sigma_r}},z)}{\delta r}$, $\phi_e = \sqrt{\sigma_z \cdot \sigma_r}$ (2.2)

Merletti *et al*. [66] modified the potential model to include a scaling factor λ and introduced a membrane current distribution:

$$V_m(z) = \text{m. action potential} = A(\lambda z)^3 e^{-\lambda z} - B \qquad (2.3)$$

$$I_m = \text{m. current dstribution} = C\frac{d^2V_m(z)}{dz^2} = CA\lambda^2(\lambda z)[6 - 6\lambda z + (\lambda z)^2]e^{-\lambda z} \qquad (2.4)$$

Where A is the amplitude of the action potential, B is the resting membrane potential and z is the distance along the fibre starting (=0) from the polarization front.

Following the depolarization membrane current has a triphasic shape (tripole, see Figure 2.4). This is represented by only three independent parameters: the amplitude of the poles, the distance between the first and the third pole and the asymmetry$\left(\frac{a}{b}\right)$.

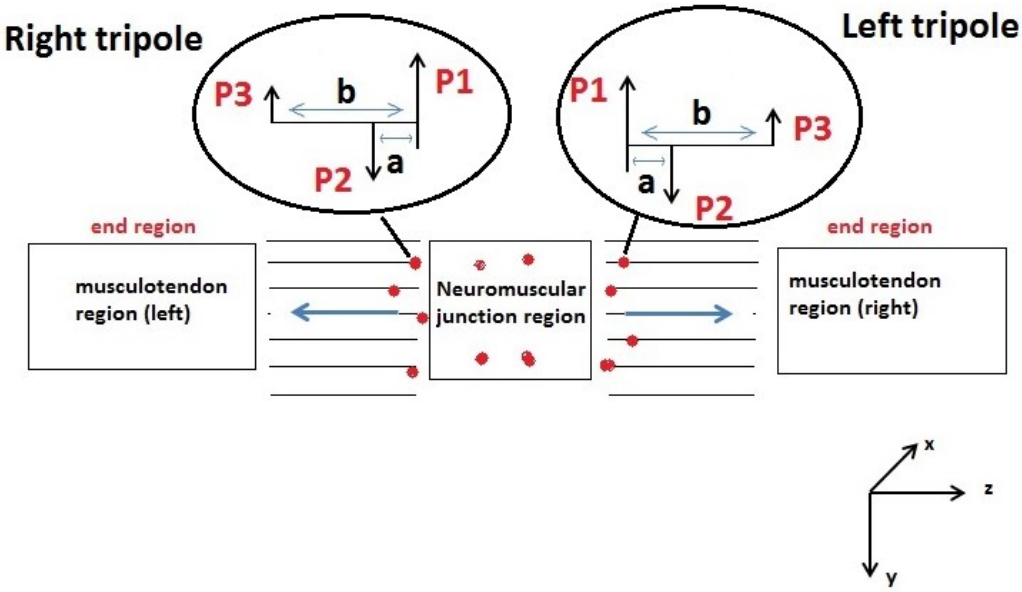

Figure 2.4 Schematic representation of Merletti and Lo Conte's [66] sEMG model. The action potentials are generated at the neuromuscular junction region and travel along the fibre to extinguish at the musculotendon region. A tripole (P1, P2, P3) was used to represent the current, where the parameter b is the distance between the first and the third pole and a is the distance between the first and the second. The tripole approximates the three phasic behaviour of the current model into three point of source or sink P_i. The surface potential was then derived from equation 2.5.

Assuming an infinite region of homogeneous tissue limited on top by the skin layer, the potential on the surface was expressed as:

$$\phi_j = \frac{1}{2\pi\sigma_r}\sum_{i=1}^{6}\frac{P_i}{\sqrt{((x-x_i)^2+y_i^2)k_a+(z-z_i)^2}} \quad (2.5)$$

$$\sigma_x = \sigma_y = \sigma_r, K_a = \frac{\sigma_z}{\sigma_r}$$

Merletti *et al*. [66] used four point-like electrodes to estimate the surface EMG with different configurations (single differential, double differential). This model was able to outline the importance of the electrode location. For instance, the distance from the termination and/or innervation zones, should be adequately greater than the inter-electrode distance in order to have meaningful EMG outcomes. In addition, larger inter-electrodes distance means an increased pick-up volume, which may enhance the contribution of the non-propagating signal (standing waves) at the termination regions. Farina and Merletti [74] extended the capabilities of analytical models by using a new approach which modelled the volume conductor properties and the fibre inclination with a transfer function in the frequency domain, whereas a 2-D spatial filtering was applied to represent the electrode's shape and configuration. The model also included tissue stratification (skin, fat, and muscle) and described end plate, end-tendon effects. Farina and Merletti's model [74] incorporated the anisotropic behaviour and the three tissues layers (skin, fat, muscle), but approximated the muscle geometry with three planar domains, infinite along two directions (along the planes) in a Cartesian coordinate system (Figure 2.5).

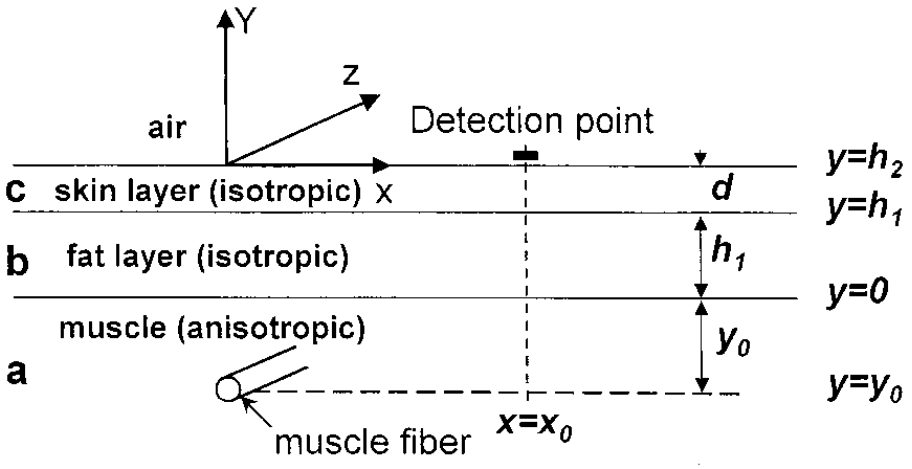

Figure 2.5 Schematic representation of the geometry of the model from Farina and Merletti [66]. Three planar layers were modelled in a Cartesian system. From the top the layers represent: the skin, the fat tissue and the muscle. The muscle fibre generate a signal from a certain distance from the detection region (adapted from [74]).

Gootzen *et al*. [75] provided a better volume conductor geometrical representation, modelling a cylindrical conductor with two layers (fat, muscle). Blok [76] extended the implementation to include the skin layer which contributes to the spread of the potential as suggested in models of the EEG [77] (Figure 2.6).

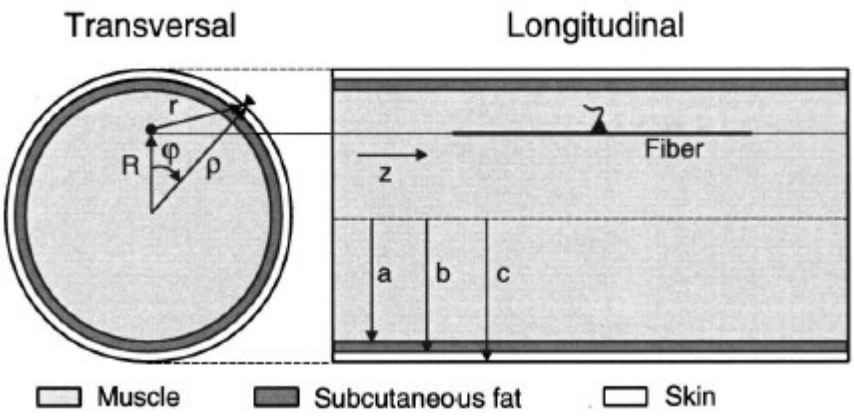

Figure 2.6 Schematic representation of the geometry of the model proposed by Blok [68]. A cylindrical three layers (skin, fat, muscle) concentric model was implemented by Blok (adapted from [76]).

Skeletal muscle tissues have a concentric structure and can be approximated with concentric layers of cylindrical geometry. This cylindrical symmetry gives the possibility to implement an analytical model. Consequently Blok's analytical model [76] solved the Poisson equation for the potential (considering a quasi-static volume conduction) in cylindrical coordinates for each layer (Figure 2.6). The computation results in three equations, which include Bessel functions given as the solution to Laplace differential equations of the electric potential. For each layer j, the potential Φ_j is given as a function of the radial distance of the electrode from the cylinder axis(ρ), the angle between the radial directions from the axis of the source and the electrode (ϕ)and the spatial frequency in the axial direction(k):

Muscle layer:

$$\Phi_1(\rho,\phi,k) = \frac{d}{2\sigma_{1_r}} K_0\left(r\sqrt{\frac{\sigma_{1_z}}{\sigma_{1_r}}}|k|\right) G(k) + \sum_{n=-\infty}^{\infty} e^{-in\phi}\left[A_n(k) I_n\left(\sqrt{\frac{\sigma_{1_z}}{\sigma_{1_r}}}k\right)\right], \quad (2.6)$$

Fat layer:

$$\Phi_2(\rho,\phi,k) = \frac{d}{2\sigma_{2_r}} K_0\left(r\sqrt{\frac{\sigma_{2_z}}{\sigma_{2_r}}}|k|\right) G(k) + \sum_{n=-\infty}^{\infty} e^{-in\phi}\left[C_n(k) I_n\left(\sqrt{\frac{\sigma_{2_z}}{\sigma_{2_r}}}k\right) + D_n(k) K_n\left(\sqrt{\frac{\sigma_{2_z}}{\sigma_{2_r}}}|k|\right)\right], \quad (2.7)$$

Skin layer:

$$\Phi_3(\rho,\phi,k) = \frac{d}{2\sigma_{3_r}} K_0\left(r\sqrt{\frac{\sigma_{3_z}}{\sigma_{3_r}}}|k|\right) G(k) + \sum_{n=-\infty}^{\infty} e^{-in\phi}\left[E_n(k) I_n\left(\sqrt{\frac{\sigma_{3_z}}{\sigma_{3_r}}}k\right) + F_n(k) K_n\left(\sqrt{\frac{\sigma_{3_z}}{\sigma_{3_r}}}|k|\right)\right]. \quad (2.8)$$

$G(k)$ is the Fourier function of the transmembrane current source density $g(z)$, The quantities I_n, k_n are the modified Bessel functions , while $A_n(k), C_n(k), D_n(k), E_n(k), F_n(k)$ are unknown solved from the boundary conditions. The boundary conditions between layers i,j should satisfy the continuity condition:

$$\Phi_i|_{\rho=a} = \Phi_j\big|_{\rho=a} \quad , \quad (2.9)$$

$$\sigma_{ir} \frac{\partial \Phi_i}{\partial \rho}\Big|_{\rho=a} = \sigma_{jr} \frac{\partial \Phi_j}{\partial \rho}\Big|_{\rho=a} \quad . \tag{2.10}$$

The model was used to simulate a current source at different depths. The effect of the fat layer and skin layer on the sEMG amplitude was studied. The fat component reduced the signal width and amplified the amplitude; on the other hand, the skin reduced the amplitude and spread the signal. The sEMG amplitude decline, observed in experimental studies, was found to not be reproducible with one-layer and two-layer models, meaning that a three-layer model is necessary to have results consistent with the actual experimental results.

Analytical models were able to simulate sEMG, investigating how the EMG signal originates and how features of the muscle, and the detecting electrodes, influence its pattern. Models were improved to add more components in their formulation, such as including the fat and skin tissue, which contribute to further filtering of the physiological signal. But analytical models can be applied only to specific symmetric geometries and the formulation can be unstable, leading to simplifications in the composition of the muscle tissue. For these reasons, finite element models started to be widely applied to simulate the electrical behaviour of the muscle. For example, Lowery *et al*. [6] used an FE cylindrical model that included the bone (

Figure **2.7**), whose presence gives unstable results in analytical models [76].

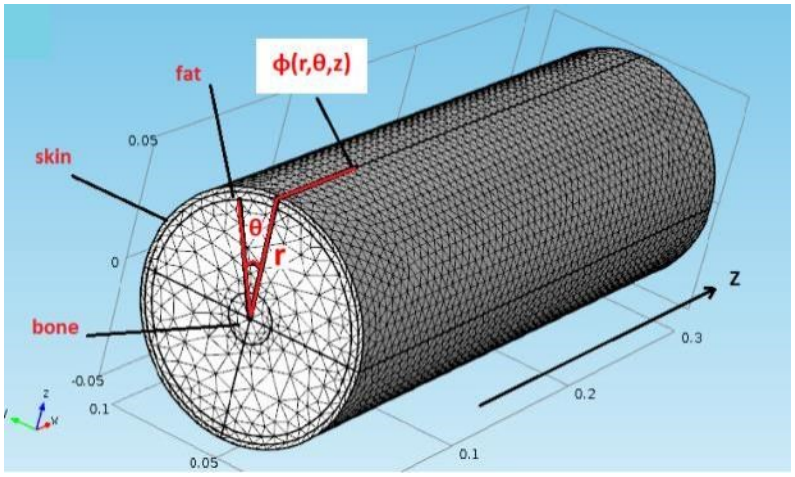

Figure 2.7 Representation of the model geometry proposed by Lowery *et al.*, [60]. This was a three layer cylindrical model, as was Blok's analytical model; however, the FE numerical approximation made it possible to include the bone.

The physics general problem consists of finding the solution (potential V) given a charge distribution to the Laplace's equation since a quasi-static approximation was applied:

$$\nabla^2 V = 0 \quad . \qquad (2.11)$$

This in cylindrical coordinates becomes:

$$\Delta\phi(r,\vartheta,z) = \frac{\partial^2\phi(r,\vartheta,z)}{\partial r^2} + \frac{1}{r}\frac{\partial\phi(r,\vartheta,z)}{\partial r} + \frac{1}{r^2}\frac{\partial^2\phi(r,\vartheta,z)}{\partial\vartheta^2} + \frac{\partial^2\phi(r,\vartheta,z)}{\partial z^2} = 0 \quad , \qquad (2.12)$$

where r is the radial distance from the cylinder axis, ϑ is the angular displacement and z is the axial coordinate.

When modelling the conductive properties of the muscle volume using a finite geometry, it is important to be able to properly model the boundary condition, since in the real body the current is free to flow and spread from the limb to the whole body (volume conductor effect). This was implemented in analytical models with infinite planes and extremities [74], or mirror symmetries [76]. In the model from Lowery *et al*. [6] the Bayliss-Turkel absorbing boundary condition was applied. The source formulation was based on [78] which related the intramuscular action potential current with the second derivative of the transmembrane voltage and the dielectric properties of each tissues were taken from Gabriel's extensive study, which reported the dielectric properties of human tissues at different frequencies [79-81]. The dielectric properties of the model proposed by Lowery *et al*. [6] were taken at 100 Hz, which is the typical surface EMG median frequency [81, 82]. The FE model investigated the EMG outcome when generating an intramuscular potential, which is detected on the surface of the skin using a bipolar electrode configuration. This model set up was also used to explore the selectivity of the sEMG signal and the effect of features such as the fat layer or the electrode configuration [72]. An anatomical based model was implemented (
Figure **2.8**) later, building the geometry from MR images [5]. In this case, the geometry was not infinite, but extended (grounded at the extremities) until the electric field drop was negligible. Another model also studied the capacitive effects and the dispersion in the time and frequency domain revealing the importance of establishing when the muscle can be considered a pure resistive volume conductor [70]. Low conductivity and high permittivity values should be chosen toward the middle of the available range from experimental reported data. Otherwise neglecting capacitive dispersive effects can lead to an estimation error of 75% in the high frequency band of the EMG.

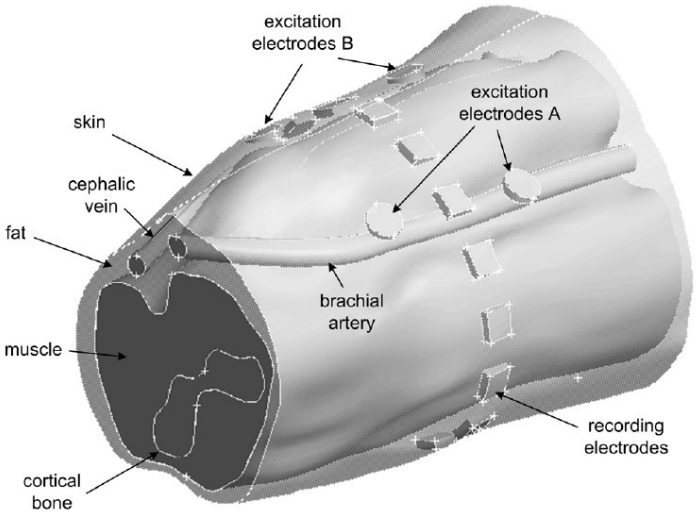

Figure 2.8 Representation of the FE model proposed by Lowery *et al.* [64]. The model geometry was constructed from MR images of the human upper arm (adapted from [5]).

The finite element model proposed by Mesin *et al*. [71] considered muscle volume conduction during shortening (concentric) contraction (Figure 2.9). To achieve this, a curve was defined to describe the path of the fibres and instead of having just a radial and axial conductivity; a conductivity tensor was defined. The tensor relates the axial and radial conductivity to the position in the curve, i.e. the shortening fibres.

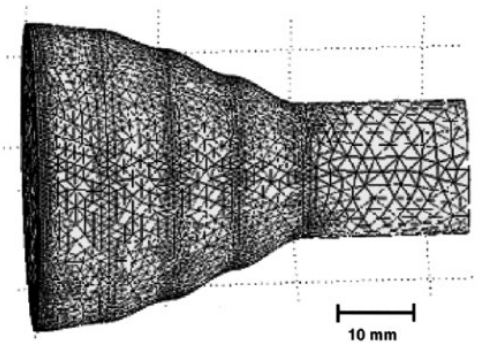

$$\underline{\underline{\sigma}} = \frac{1}{w^4 + z^2(x^2+y^2)} \begin{bmatrix} x^2z^2\sigma_l + (w^4+y^2z^2)\sigma_t & xyz^2(\sigma_l-\sigma_t) & -w^2xz(\sigma_l-\sigma_t) \\ xyz^2(\sigma_l-\sigma_t) & y^2z^2\sigma_l + (w^4+x^2z^2)\sigma_t & -yzw^2(\sigma_l-\sigma_t) \\ -w^2xz(\sigma_l-\sigma_t) & -yzw^2(\sigma_l-\sigma_t) & w^4\sigma_l + z^2(x^2+y^2)\sigma_t \end{bmatrix}$$

Figure 2.9 Schema of the FE model proposed by Mesin *et al.* [62] that included a tensor formulation of the conductivity, which depends on the geometry and hence changes while the muscle contracts. This allowed a study of the dielectric properties of the muscle while shortening (adapted from [71])

The FE model from Mesin *et al*. [71], showed how the amplitude and frequency content of the sEMG could change during dynamic contractions due to a change in the shape of the action potential. When the muscle is shortening the fibres move far from the detecting electrodes, while the end regions (tendon junction) get closer. This reverses the weight of the non-propagating source (the standing waves at the tendon junction) with respect to the propagating source (the traveling potential). The sensitivity of this effect differs depending on the configuration of the detecting electrodes and their distance from the fibre (superficial fibres are less affected). Lowery *et al.* [5] and Mesin *et al.*[71] models were able to represent for the first time, detailed anatomical features. Despite that, results cannot be compared (only the behaviour) with experimental data

because the experimental source signal is uncertain. Consequently, in their simulations a random source signal and MUs population were generated, disconnected from actual real EMG data.

Further discussions of FE mathematical formulations and a comparison with analytical models can be found in Mesin [83] literature review.

2.1.3 Identified Research Question and Related Thesis Objectives

Muscle motor unit activation information can be inferred from sEMG signals through decomposition algorithms [84, 85]. A common method to test the accuracy of these algorithms is the subject of discussion within the research community [86, 87]. Ideally, a concurrent measurement of intramuscular and surface EMG would lead to a better estimation of the decomposition algorithm; alternatively, a better detection system, which increase the selectivity of the motor units, would be preferable. Examples are multiple channel sEMG [88], linear electrode arrays [89] or high-density electrode arrays [90, 91]. Despite the increasing spatial resolution of electrode arrays, a bipolar electrode configuration offers the advantage of giving enough information to assess single muscle activity while requiring less signal input and fewer electrodes than the electrodes arrays or multiple channels. For applications where several muscles are involved and regional information is not needed, a bipolar configuration is still the preferable tool to record the muscle activity (reduced cross-talk, i.e. recording activity from muscles other than the target muscle) for certain applications. Despite that other configurations (monopolar, double differential) can still offer some advantages. In addition, electrode arrays can improve the spatial resolution of the EMG. By a weighted summation of the

electrode leads signals, it is possible to create spatial filters (normal double differentiating filter NDD, inverse rectangle filter IR, inverse binomial filter IB^2) that can increase the spatial selectivity of the EMG. The filters that provides an isotropic transfer function can further improve the signal to noise ratio but this is limited to motor units close to the electrode.

Other important aspects of the measurements are the electrode location, the inter-electrode distance, the electrode orientation respect to the fibre direction and the underlying muscle architecture (pennation). Furthermore, from EMG measurements, it is possible to estimate the motor unit population, the activation level, the recruitment, the muscle coordination, the muscle fatigue and even the muscle architecture (pennation). Despite these potential applications, a lot of uncertainty such as noise, tissue filtering and fibre architecture affects the EMG outcome, challenging current guidelines in term of EMG surface electrodes placement [92].

Past FE models have allowed researchers to study more aspects of muscle activity, from the anatomy and tissue composition, to the dielectric properties and the consequences of dynamic contractions, to the best electrode configuration that can improve selectivity and accuracy of recorded surface myoelectric signals. It is hard to align electrodes with the fibre direction and when the fibre curve toward the deep aponeurosis, as shown in Figure 2.2, the signal travels far from or toward the electrodes. For this reason, muscle with parallel fibres should have guidelines on electrode positioning which differ from muscle with highly pennate fibres. Thus, a model that can evaluate the loss of information when the muscle is highly pennate is needed, but has to be provided. This

thesis therefore considers the influence of the fibre orientation with respect to the electrodes and the geometry of the electrodes.

The first study in the thesis simulates an electrical model of the muscle, which aims to:

- Clarify the determinants of recorded surface EMG signal properties (dielectric properties, muscle architecture), with a focus on the influence of the effects of the orientation of the muscle fibres.

- Identify the best electrode design/configuration for the signal detection by conducting a sensitivity study on important parameters.

2.2 Muscle Biomechanical Models

Biomechanical muscle models can use a lumped parameter approach to describe the muscle or consider a continuum space that takes into account the material properties distributed in space. Lumped parameter models such as Hill based models, were used also to implement geometrical muscle models in order to resemble the muscle architecture. The simplest models were mechanically unstable, presenting a non-equilibrated torque as the tendons in a pennated muscle were not aligned [47] or when aligned, presented other geometrical simplifications which do not reflect the real muscle architectural conformation [93] as pointed out by Van Leeuwen and Spoor [94]. The geometrical planar model of a bipennated muscle reported by Van Leeuwen and Spoor [94], included a tendinous sheet and curved fibres to allow mechanical stability. A

dynamic model was also implemented to simulate the contraction of a squid's tentacle [95]. The model used Hill's force-velocity relationship and the results were consistent with the kinematic behaviour observed. Despite offering a good approximation, these models cannot faithfully predict all muscle properties, leading to, for example, underestimation of the fibres volume fraction [94]. The lower computational cost of such models enables real time analysis of muscle force estimation. Whereas a constitutive model in the continuum space involves continuum mechanics theory and exploits mathematical advanced theories such as finite element methods that require a higher computational cost.

2.2.1 Constitutive Mechanical Models

Hyperelastic models are higher-order forms of linear elastic models in which stresses are some function of the total strain or stretches [96]. These models are being used to describe the behaviour of the connective tissue of the muscle and other biological tissues. A hyperelastic material is defined through a strain energy function (see Appendix B and C for theory background) where it is possible to uncouple the deviatoric and the dilational (volumetric) component of the deformation/stress. The muscle connective tissue behaviour is similar to rubber (elastic nonlinear large deformations) and can be described with a Mooney-Rivlin strain energy as applied in the formulation from Johansson *et al*. [97, 98]:

$$W = \sum_{i+j=1}^{n} a_{ij} \left(I_{1,M} - 3\right)^{i} \left(I_{2,M} - 3\right)^{j} + \frac{k}{2} \left(I_{3,M} - 3\right)^{2} \quad , \qquad (2.13)$$

where $I_{i,M}$ = invariants of the deformation tensor and k = bulk modulus.

Based on the formulation of Johansson *et al*., activation of the fibres generates a stress in the direction of the fibres. These stresses are in terms of Cauchy Stresses (current stresses) and need to be transformed into the second Piola-Kirchhoff stresses S_{ij} to be conjugated with the Green-Lagrangian finite strain tensor:

$$S_{ij} = \frac{\partial W}{\partial E_{ij}} = 2\frac{\partial W}{\partial C_{ij}} \quad . \tag{2.14}$$

Furthermore [98] used a displacement pressure formulation [99] that is more stable and convergent than the pure displacement formulation in FE models.

The relation between the global stiffness matrix (K_{ij}^t) , the displacement/ pressure and the external forces (F_i^t) , (R^t) is:

$$\begin{bmatrix} K_{UU}^t & K_{UP}^t \\ K_{PU}^t & K_{PP}^t \end{bmatrix} \begin{bmatrix} \hat{u} \\ \hat{p} \end{bmatrix} = \begin{bmatrix} R^{t+\Delta t} \\ 0 \end{bmatrix} - \begin{bmatrix} F_U^t \\ F_P^t \end{bmatrix} \quad , \tag{2.15}$$

where the vector $\begin{bmatrix} \hat{u} \\ \hat{p} \end{bmatrix}$ contains the increment of the displacement and the pressure degree of freedom. The problem set is then based on the equilibrium of the virtual works:

$$\int_{V0}^{V} S_{ij} S_0 E_{ij} dV = R \text{ equilibrium of virtual works} \quad , \tag{2.16}$$

where R represents external pressures, discrete forces or constraints [98].

A constitutive behaviour of fibres based biological tissues (muscles, ligaments, tendons) was formulated by Weiss *et al*. using a form of strain energy for an isotropic fibre composed material:

$$W = F_1(I_1, I_2) + F_2(I_4) + F_3(I_1, I_2, I_4) \quad , \qquad (2.17)$$

where:

F_1 = material response of the isotropic ground substance matrix (deviatoric, distorsional);

F_2= contribution from collagen fiber family;

F_3= contribution from interaction between the fibers and matrix (dilational).

This method introduced directional dependence on the deformation explicitly into the strain energy through a vector representing the material preferred direction. Fibre stretch can be determined in term of the deformation gradient and the fibre direction, a^0, in the undeformed configuration as follow:

$$\lambda a = Fa^0 \quad , \qquad (2.18)$$

$$\lambda^2 \mathrm{a}\ \mathrm{a} = \lambda^2 = \mathrm{a}^0 \mathrm{F}^{\mathrm{T}} \mathrm{F} \mathrm{a}^0 = \mathrm{a}^0 \mathrm{C} \mathrm{a}^0 \quad . \tag{2.18}$$

Therefore, the invariants I_4 can be substituted by a dependence on the stretch:

$$\mathrm{I}_4 = \mathrm{a}^0 \mathrm{C}\ \mathrm{a}^0 \quad . \tag{2.19}$$

A novel FEM was described by Blemker *et al*., (2005) that implemented a 3D FE muscle model of the biceps brachii to explain the non-uniform strain of the fascicles that were observed in experimental data [100]. The muscle was considered as a composite nearly incompressible material where a decoupled constitutive behaviour was used to describe the dilational behaviour (matrix) and the deviatoric behaviour (fibres) [57]. The novelty of the model from Blemker *et al*. was their use of two of the new set of 5 invariants described by Criscione [101].

The typical (see equations 2.5-1, 2.5-2) representation of W $(\mathrm{I}_1, \mathrm{I}_2, \mathrm{I}_3, \mathrm{I}_4, \mathrm{I}_5)$ uses the invariants of the Cauchy-Green right deformation tensor $\mathrm{C} = \mathrm{F}^{\mathrm{T}} \cdot \mathrm{F}$, where:

$$\mathrm{I}_1 = \mathrm{tr}(\mathrm{C}) \quad , \tag{2.20}$$

$$\mathrm{I}_2 = \mathrm{tr}(\mathrm{C}^2)/2 \quad , \tag{2.21}$$

$$\mathrm{I}_3 = \det(\mathrm{C}) \quad , \tag{2.22}$$

$$\mathrm{I}_4 = \mathrm{M} \cdot \mathrm{CM} \quad , \tag{223}$$

$$\mathrm{I}_5 = \mathrm{M} \cdot \mathrm{C}^2 \mathrm{M} \quad , \tag{2.24}$$

and C is the Cauchy-Green right deformation tensor and M is the unit vector to specify the preferred material direction (reference direction), related with the current direction through the following transformation:

$$\mathrm{m} = \text{current direction} = (\mathrm{M} \cdot \mathrm{CM})^{-\frac{1}{2}}\mathrm{FM} \quad , \quad (2.25)$$

(m lies in the FM direction).

The new sets of invariants introduced by Criscione for the strain energy function $W(\beta_1, \beta_2, \beta_3, \beta_4, \beta_5)$, have the advantage of being ideally mutually orthogonal, hence their independence allows different parts of the strain energy function to be directly obtained. The relationships between the Green's deformation tensor deviatory invariants and the new set of invariants are:

$$\beta_1 = \frac{(\ln \bar{I}_3)}{2} \quad , \quad (2.26)$$

$$\beta_2 = \frac{(3 \ln \bar{I}_4 - \ln \bar{I}_3)}{4} \quad , \quad (2.27)$$

$$\beta_3 = \ln\left(\left(\frac{\bar{I}_1\bar{I}_4 - \bar{I}_5}{2\sqrt{\bar{I}_3\bar{I}_4}}\right) + \sqrt{\left(\frac{\bar{I}_1\bar{I}_4 - \bar{I}_5}{2\sqrt{\bar{I}_3\bar{I}_4}}\right) - 1}\right) \quad , \quad (2.28)$$

$$\beta_4 = \sqrt{\frac{\bar{I}_5}{\bar{I}_4{}^2} - 1} \quad , \quad (2.29)$$

$$\beta_5 = \frac{\bar{I}_1\bar{I}_4\bar{I}_5 + \bar{I}_1\bar{I}_4{}^3 + 2\bar{I}_3\bar{I}_4 - \bar{I}_5{}^2 - 2\bar{I}_2\bar{I}_4{}^2 - \bar{I}_5\bar{I}_4{}^2}{\left(\bar{I}_5 - \bar{I}_4{}^2\right)\sqrt{\bar{I}_1{}^2\bar{I}_4{}^2 + \bar{I}_5{}^2 - 2\bar{I}_1\bar{I}_4\bar{I}_5 - 4\bar{I}_3\bar{I}_4}} \quad . \quad (2.30)$$

These invariants respectively identify a specific aspect of the strain:

- Volume strain;
- Distortional fibre strain;
- Cross Fibre shear;
- Along fibre shear;
- Orientation of the along-fibre shear plane, relative to the cross-fibre shear diagonals.

The new strain energy implemented by Blemker *et al*. considered the muscle as a fibre-reinforced composite with transversely isotropic material symmetry and its equation is:

$$\psi(B_1, B_2, \lambda, \alpha, J) = W_1(B_1) + W_2(B_2) + W_3(\lambda(\bar{I_4}), \alpha) + \frac{k}{2}\ln(j)^2 \quad . \quad (2.31)$$

B_1, B_2 are the physically based strain invariants defined by Criscione (equations 2.5-14, 2.5-15) to describe the along-fiber and cross fibre shear strains, whose effects could not be considered independently in previous models. λ is the along fiber stretch, α the activation level and k is the bulk modulus. The last right side term of the equation describes the dilational (volume) changes.

The first right side terms express the shear strain behaviour:

$$W_1(B_1) = G_1 B^2{}_1 = G_1 \sqrt{\frac{\bar{I}_5}{\bar{I}_4{}^2} - 1} \quad , \tag{2.32}$$

$$W_2(B_2) = G_2 B^2{}_2 = G_2 \cosh^{-1}\left(\frac{\bar{I}_1 \bar{I}_4 - \bar{I}_5}{2\sqrt{\bar{I}_4}}\right) \quad , \tag{2.33}$$

where $\bar{I}_i$ are the deviatoric invariants and $\bar{I}_4, \bar{I}_5$ are the new invariants defined by Criscione. The stretch is defined as $\lambda = \sqrt{\bar{I}_4}$. The function $W_3(\lambda, \alpha)$ expresses the active part in terms of the Cauchy stresses.

When the muscle fibres exert a force, there are two components to take into consideration (equation 2.34), the active component (contractile element) and the passive non-linear element. The active element is a function of the activation, F-L relationship, F-V relationship and depends on the maximal isometric force (equation 2.35).

$$\sigma = \sigma_{active} + \sigma_{passive} \quad , \tag{2.34}$$

$$\sigma_{active=} \sigma_{isometric} f_t(t) f_v(t) f_l(t) \quad , \tag{2.35}$$

This stress can be expressed in term of the Cauchy stress:

$$\lambda \frac{\partial W_3}{\partial \lambda} = \sigma_{isometric} f_a(t) f_p(t) f_l(t) \quad . \tag{2.36}$$

The interaction between the connective tissue and contractile fibres are among the main characteristics still to be assessed when developing a realistic muscle model. Huijing [8] reviewed studies with evidence of a lateral force transmission between fibres through the connective tissue that allowed the muscle to be considered as a collagen fibre reinforced composite. In particular, a study of the interaction between a myofibre and the surrounding fibres revealed the existence of a lateral force when the myofibre strain was large enough to create passive shear stresses capable of deforming the surrounding fibres [102]. This force transmission is likely to be frictional rather than in plane [13, 103]. Recent research had been focusing on incorporating the architecture, the activation and the connective tissue contribution in muscle constitutive models. These models are based on finite element analysis. Chi *et al*., implemented a 2D approach to study the particular strain-stress behaviour of the aponeurosis. The fibres constitutive model was based on the work of Blemker *et al*. [57] and the matrix was described with a 5 coefficient Mooney-Rivlin strain energy function fitted to experimental data from a frog muscle. The model was able to explain the differences in strain due to different pennation angles. A similar approach was used by Rahemi *et al*. [60] to study the consequences of regional activation in the lateral gastrocnemius muscle on force production. In the constitutive model, the muscle and the tendon tissue were considered composite, thus with a fibre and a matrix material. The matrix or base material was modelled with a hyperelastic strain energy function, whose parameters were derived from an exponential fit of experimental data. Through this model, the same S-shaped fascicle trajectories observed in vivo from ultrasound image of the medial gastrocnemius [104] were predicted, revealing a feature that is important to maintain mechanical stability within the muscle [94]. In addition, regionalized muscle

activity resulted in changes in muscle force magnitude and direction, even if the muscle activity was the same. The constitutive model from Blemker *et al*., included a part directly linked with the muscle transverse to fibres and along fibres shear modulus. Sharafi and Blemker [2] used this model, to study the effect of fibres and fascicle geometry in a micromechanical constitution. Further implementations of the model from Blemker *et al*. [57] were applied at a microscopic level [3, 4] to study the fibres lateral force transmission through the endomysium and force at the myotendinous junction. Yucesoy *et al*. [105] used two domains to describe the fibres and the matrix (connective tissue). These two domains were linked through the mesh so that the fibre-matrix interface properties could be changed by changing the number of links between the two domains. Other models worth mentioning include structural features (multi-scale model) such as Huxley cross-bridge model based activation and the motor unit distribution [106] or tried to simplify the formulation to allow real time applications [107]. Blemker *et al.* [57] model was able to explore many architectural (fibres geometry) configurations [57, 58] and fibre/fascicle geometries [2-4]. In addition, its constitutive model parameters (Criscione's Invariants [101]) represent the longitudinal to fibres and transverse to fibres shear modulus. Others models like Mooney Rivlin hyperelastic model, do not have parameters that are directly linked to physical quantities. The limitation of Blemker's model is the numerical instability because Criscione's Invariants depends on transcendental functions. An alternative to avoid this issue would be to derive analytically the stress tensor components and include them in the FE solver code.

2.2.2 Identified Research Question and Related Thesis Objectives

In this thesis, the focus is on the altered mechanical properties of the muscle. Specifically the deterioration of the connective tissue and the muscle fibres is associated with an altered transmission of the force, which may lead to an increased risk of injury. This condition is typically present in age related pathologies such as sarcopenia, and is becoming more and more important as the older population increases. An effort is being made to deepen the knowledge [30, 32-34] of this pathology and find out new solutions or tools to slow down its progress and/or consequences. Knowing how specific muscle features (architecture, tissue composition, muscle activation) affect the functionality of the muscle [33, 34] could lead to a deeper insight into the link between this pathology and its debilitating consequences.

Capturing a range of different muscle properties in an experimental or laboratory-based environment is actually quite challenging and often unfeasible, so an alternative option is to develop models where hypotheses can be tested to help the understanding of mechanisms, which underpin loss of function/capabilities.

To accomplish this goal a muscle mechanical model was simulated to achieve a better understanding of the muscle tissue properties in term of force transmission capacity and age related alterations of the tissue such as active fibres clustering.

Specifically the objectives were to:

- Design a micromechanical model of the muscle to characterize the interaction between the myofibers and the connective tissue.

- Explore age related alterations in skeletal muscle fascicle properties and assess how these affect the force produced.

Specific literature with regard to model development and implementation has thus been reviewed and the key objectives for the thesis have been set. The next three chapters now detail the development and implementation of two models, designed to meet the sets of objectives defined.

3 A FE Design Study of the Dielectric and Geometric Properties of the Muscle

sEMG measurements, when processed can reveal a lot of information regarding the muscle activation. For instance the onset time (when the muscle is active), the fatigue of the muscle, the level of activation and the motor units involved. Despite this, the sEMG is not always accurate and it might contain undesired signals along with the desired EMG signal. For this reason the location of the electrodes and their configuration are crucial to guarantee a better accuracy and selectivity. This chapter present a new FE model and approach to study the effect of the muscle geometry (pennation) on the detecting sEMG bipolar electrodes. Sensitivity studies were performed on the configuration for each case.

(The work within this chapter has been published in PloS One in February 2016 [108])

3.1 Overview

Surface electromyography (sEMG) is the measurement of the electrical activity of the skeletal muscle tissue detected at the skin's surface. Typically, a bipolar electrode configuration is used. Most muscles have pennate and/or curved fibres, meaning it is not always feasible to align the bipolar electrodes along the fibres direction. Hence, there is a need to explore how different electrode designs can affect sEMG measurements.

A three layer finite element (skin, fat, muscle) muscle model was used to explore different electrode designs. The implemented model used as source signal an experimentally recorded intramuscular EMG taken from the biceps brachii muscle of one healthy male. A wavelet based intensity analysis of the simulated sEMG signal was performed to analyse the power of the signal in the time and frequency domain.

The model showed muscle tissue causing a bandwidth reduction (to 20-92- Hz). The inter-electrode distance (IED) and the electrode orientation relative to the fibres affected the total power but not the frequency filtering response. The effect of significant misalignment between the electrodes and the fibres (60 ˚- 90 ˚) could be reduced by increasing the IED (25-30 mm), which attenuates signal cancellation. When modelling pennated fibres, the source signal is low pass filtered due electrode detection. The effect of different IED seems to be enhanced in the pennated model, while the filtering response is changed considerably only when the electrodes are close to the signal termination within the model. For pennation angle greater than 20˚, more than 50% of the source signal was attenuated, which can be compensated by increasing the IED to 25 mm.

3.2 Introduction

A key component of the neuromuscular system is the motor unit, which is the link between neural activity and the production of muscle force. A motor unit is defined as an α-motor neuron, its axon and all the muscle fibres it innervates [14]. The motor unit action potential (MUAP) is the sum of the action potentials travelling along its fibres [15, 61]. It is possible to detect the interference pattern of these potentials using electromyography (EMG). Surface EMG (sEMG) is the measurement of the electric activity (i.e. MUAPs) detected at the skin's surface (passing through the muscle, fat and skin), and is a good non-invasive method to estimate the level of muscle activation of superficial muscles. In order to be reliable, the measurement should: i) be representative of the muscle activity; ii) select the desired signal with minimal contribution from other signal sources (e.g. other adjacent muscles); iii) have a high precision (i.e. low error variance) and iv) have a high signal to noise ratio (SNR). To increase the SNR a bipolar electrode configuration is usually used (see Figure 3.1), negating common node noise, but also resulting in an attenuated signal.

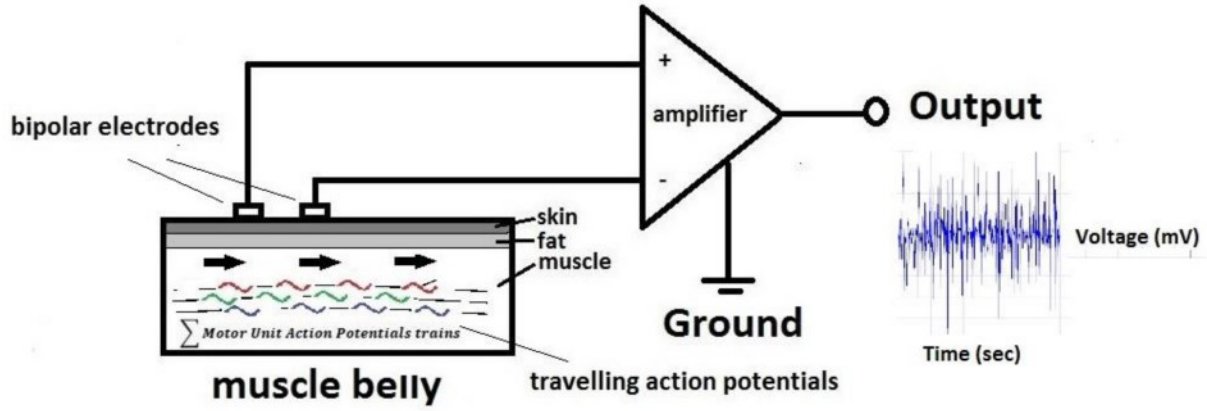

Figure 3.1 A typical Bipolar configuration scheme. Measurements are made as the difference between the signals of two sensing electrodes, separated by a known distance. The detected signal is the sum of the action potentials (MUAPs) travelling along the fibres.

An important feature of the bipolar configuration is the electrode orientation with respect to the muscle fibre direction; since both sensors are supposed to see the same action potentials as they propagate along the fibre (see Figure 3.1). Few skeletal muscles demonstrate such parallel fibre arrangements. In contrast, most muscles have pennate (obliquely orientated) and/or curved fibres [109, 110], meaning it is not always feasible to accurately align the electrodes along the long axis of the fibres. This means that the sensing electrodes may detect signals across different fibres and the potential detected at one electrode is not the same delayed signal detected at the other electrode. This will not allow derivation of the real frequency components of the action potentials travelling along the fibre or determination of the true activation level. Therefore, there is a need to explore how different electrode orientations and distances can affect the properties of recorded myoelectric signals.

One method of investigating the effects of electrode properties on recorded signals is to employ mathematical modelling approaches. An early implementation of an analytical model of skeletal muscle tissue was reported by Andreassen and Rosenfalck [68]. The model was used to investigate the intramuscular EMG electrodes' bipolar configuration, i.e., the orientation of the recording surfaces relative to the direction of the muscle fibres, the distance between the recording surfaces, and the area of the recording surfaces. The model parameters were the radius of the fibre; conduction velocity; anisotropy ratio of muscle tissue (difference in conductivity parallel to the fibre direction and perpendicular to it); and conductivity of the intracellular and extracellular medium. This model was able to give quantitative guidelines on the best feature set for the electrodes to provide the highest selectivity. Results suggested that a bipolar configuration with electrodes oriented perpendicular to the fibre direction gives the highest selectivity, thus recording the activity of a few fibres. This behaviour could still be considered similar if the electrode orientation angle was less than 45 ˚. An inter-electrode centre distance less than 50 µm still recorded activity in a few fibres, while inter-electrode centre distance greater than 200 µm gave measurements similar to that of two monopolar electrodes. This was shown by the fact that the potential amplitude decline was three times greater for the bipolar than the monopolar configuration when the fibre distance was at 200 µm, raising to five times at distances of 500 µm. This means the contribution from far fibres to the detected signal, is less in the bipolar configuration. Merletti et al., [66] modified the Andreassen and Rosenfalck [68] action potential model. They introduced a current distribution flow from the travelling transmembrane action potential to study the effect of the innervation and termination zones on the surface signal in a parallel fibred muscle. The model was applied and

compared against experimental results from sEMG signals detected from the biceps brachii muscle [67] and the model parameters set so that the model results would match the experimentally recorded signal pattern. This method gave important physiological information, for example the conduction velocity of the MUAPs and the location of the innervation zone, and provided important conclusions about the best location for electrodes, with reliable bipolar measurements possible between the innervation and termination zones, when they were sufficiently wider than the IED. However, the main limitation of this work was that the adipose tissue layer between the muscle and the electrode surface was not considered. Later Blok et al., [76] developed an analytical cylindrical volume conductor model which included the skin and fat layers to describe the muscle tissue, improving previous two layers models, which were sensitive to the depth of the potential source [75]. Wheeler et al., [69] extended these models by defining and modelling the motor units size, properties (e.g. conduction velocity), validating the simulated sEMG, and derived force by experimental observation. They reported a strong correlation between linear sEMG and force relationships found in both simulated and experimentally recorded signals. While these models have provided valuable guidelines, wider applications are limited by the fact that analytical models can only provide solutions for ideal geometries such as infinite cylinders or planar planes and symmetric geometries [5]. The potential to investigate properties of more realistic muscle geometric properties can however be done using a finite element model (FEM) approach.

FE modelling is a mathematical method that discretises a continual space into finite elements, turning differential equations into algebraic equations for which it is possible to find an approximate solution. FEMs therefore extend the possible range of studies,

specifically in terms of the complexity of the muscle fibre geometries that can be considered. For example, Lowery et al. [6] reported an FEM of a cylindrical three-layered muscle tissue which was further implemented into an anatomically based (real muscle geometry) model which included the bone and blood vessels, and showed how these additional components can change the amplitude of the EMG signal and the shape of the action potential. Pennated and curved fibres can change the action potential shape detected, and hence the frequency components of the EMG. This was shown by Mesin et al. [71] who studied conductivity property changes during shortening of a 3D fusiform shaped FE model of the muscle and, in agreement with previous analytical models [71], revealed changes in amplitude and frequency content of the action potential.

Previous FE models all make use of single MUAP trains, which makes it harder to validate against commonly recorded myoelectric signals, which represent the interference pattern of multiple MUAPs. In the present study, a different approach was used. The fibres of a motor unit cover a portion of the cross section of a muscle with a round irregular shape [111, 112] and the activity of a small number of fibres at a certain depth can be detected through intramuscular EMG (iEMG). Instead of modelling the current of a single fibre, the potential detected can be considered as the superimposed resultant potential at that depth, hence the source signal is the overall potential travelling at that depth, which can be detected through intramuscular measurements. Using this approach, it is possible to implement models that use a source signal acquired from experimental acquisition and is thus closer to the real signal than simulated data. This approach enables greater focus on the filtering properties of the muscle tissues and the surface electrodes configuration with respect to the fibres. The aim of this work was to simulate the muscle tissue volume conductive properties and test the effect of inter-

electrode distance, electrode orientation and muscle fibre pennation angle on the measured bipolar sEMG signal in terms of power loss and frequency filtering. This aim was pursued by implementing a three layer FEM of the muscle, fat and skin.

3.3 Method

3.3.1 FE Model

A three layer finite element muscle model (2 mm skin, 3 mm fat, 30 mm muscle, see Figure 3.2) was implemented in the time domain [113] using Comsol Multiphysics (version 4.4, Cambridge, UK) explicit finite element solver. A conjugate gradient iterative solver was used. A convergence h-refinement study was also performed for 6 levels of mesh density by refining the mesh globally from 3462 to 87353 elements. The parameter chosen to measure convergence was the root mean square of the signal, at the electrodes since it represents the signal total energy. The results converge to around $2.17 \times 10^{-6}\ \mathrm{mV}$ and $2.12 \times 10^{-6}\ \mathrm{mV}$ for the first and second electrodes. The mesh design of our FE model used 51053 solid tetrahedral elements.

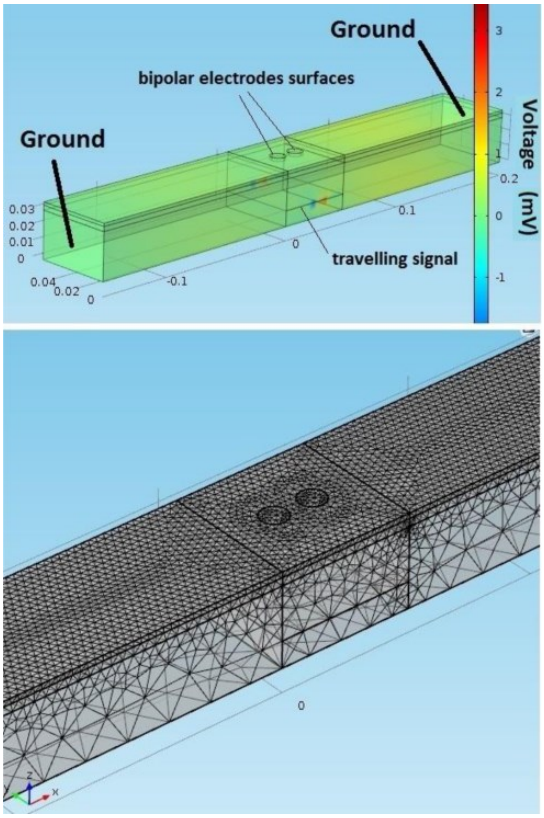

Figure 3.2 Three layers FE model of the muscle tissue. (Top) The simulated model consisted of an intramuscular travelling potential, which generated a potential on the surface of the model. The surface potential is then detected by two probe areas representing the electrodes. These probes record the average potential over the area, reflecting the behaviour of sEMG electrodes. The coloured bar represents the tissue electric potential. (Bottom) FE model four node tetrahedral mesh. A finer mesh was built in the electrodes areas.

The model set up was similar to that proposed by Lowery [5, 6, 72]. Specifically our model used a quasi-static assumption applied to the biological tissues [114], hence the muscle can be considered as a resistive tissue only (ignored effects from capacitance and inductance). The governing equation is a combined form of the continuity equation and Gauss's law in the differential form [115] (equation 3.1,3.2):

$$\nabla \cdot \mathrm{D} = \rho \qquad \text{(Gauss Law)} \tag{3.1}$$

$$\nabla \cdot \mathrm{J} = \frac{\partial \rho}{\partial \mathrm{t}} \qquad \text{(Charge continuity equation)} \tag{3.2}$$

$\rho = \text{charge density} \quad \mathrm{D} = \text{electric displacement} \quad \mathrm{J} = \text{current density}$

Ohm's law and the constitutive equation are used to relate the electric field with the electric displacement and the current density (equation 3.3, 3.4):

$$\mathrm{D} = \varepsilon_0 \varepsilon_\mathrm{r} \mathrm{E} \tag{3.3}$$

$$\mathrm{J} = \sigma \mathrm{E} \tag{3.4}$$

$\mathrm{E} = \text{electric field} \quad \varepsilon_0 = \text{vacuum permittivity} \quad \varepsilon_\mathrm{r} = \text{relative permittivity}$

$\sigma = \text{electrical conductivity}$

The skin and fat tissue were considered as isotropic while the muscle anisotropy ratio (longitudinal conductivity over transversal conductivity) was set to 5 [5, 116]. Table 3-1 reports the dielectric properties used in the model. The dielectric properties were taken at a frequency of 100 Hz which is the typical median frequency of an EMG spectrum [5].

Table 3-1 Dielectric Properties of the muscle tissues [117]

	Conductivity (S/m)	Permittivity
Muscle	0.26671 (transverse)	9329000
Skin	0.00046112	45298
Fat	0.02081	457060

Combining Gauss's law and the continuity equation, by eliminating the charge density a single equation is obtained (equation 3.5, 3.6):

$$\nabla \cdot (\sigma \mathrm{E} + \frac{\partial \varepsilon \mathrm{E}}{\partial \mathrm{t}}) = 0 \tag{3.5}$$

In a quasi-static approximation the electric potential (V) is given as equation 3.6:

$$\mathrm{E} = -\nabla \mathrm{V} \tag{3.6}$$

Substituting equation 3.6 into equation 3.5 results in equation 3.7 :

$$-\nabla \cdot (\sigma \nabla \mathrm{V} + \frac{\partial \varepsilon \nabla \mathrm{V}}{\partial \mathrm{t}}) = 0 \quad (3.7)$$

Equation 3.7 is the governing equation for time-dependent electric currents.

Boundary conditions are specified at material interfaces and physical boundaries. At the interface between two media (skin, fat, muscle), the Neumann boundary condition is given for the current density (equation 3.8):

$$\mathrm{n}_2 \cdot (\mathrm{J}_1 - \mathrm{J}_2) = -\frac{\partial \rho}{\partial \mathrm{t}} \quad (3.8)$$

Where n_2 is the outward normal from medium two. In a resistive media, the current density should be continuous (equation 3.9):

$$\mathrm{n}_2 \cdot (\mathrm{J}_1 - \mathrm{J}_2) = 0 \quad (3.9)$$

The portion of muscle simulated was considered electrically isolated at its boundaries since the conductivity of the surrounding space (air) can be assumed to be zero; therefore, there is no normal current flow (equation 3.10):

$$\mathrm{n} \cdot \mathrm{J} = 0 \quad (3.10)$$

The ground was applied at the extremities of the model, where the electric potential V is null (Dirichlet boundary condition).

3.3.2 Input Data

The model simulates the whole intramuscular MUAP interference pattern and evaluates the surface potentials at two areas representing sEMG electrodes. To simulate the MUAP signal, the implemented model used a recorded iEMG signal (sample frequency 5 kHz, amplifier gain 1000) from fine-wire electrodes (3 mm bared tips) inserted in the long head of the biceps brachii muscle (see data in S1 datafile). The measurements were taken from one healthy male, adult volunteer. The participant provided written informed consent and the study was approved by the local ethics committee at the Faculty of Science and Engineering, Manchester Metropolitan University, in accordance with principles of Declaration of Helsinki. The iEMG was recorded at a 20 mm depth during 10% maximum voluntary contraction isometric conditions.

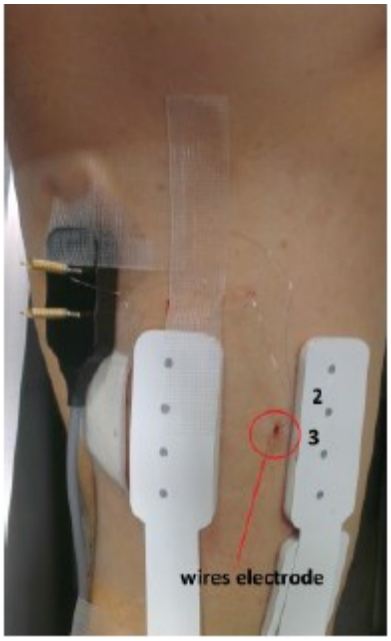

Figure 3.3 Experimental set up. Electrodes wires were inserted in the biceps brachii

A 50Hz notch filtered 1 sec portion of the iEMG was applied as the source signal in the simulation. This source signal was set as an electric potential $V(t)$ that travelled for one second along a surface within the muscle domain (equation 3.11):

$$V(t) = \text{signal}\left(t - \frac{x}{v}\right) \tag{3.11}$$

Where x is the coordinate along the fibre direction, and v is the speed of propagation (4 m s-1). The source signal travels along a distance of 0.05 m while the tissue extends to 0.15 m at both sides (see Fig. 2), a distance by which the potential is no longer affected by the boundaries of the model. To define this distance a correlation study was conducted to assess the minimum extension length for which the outcome distance is not affected by the drop of the electric field at the end of the signal route (see Table 3-2).

Table 3-2 Correlation between the RMS of the resultant bipolar potentials at different muscle lengths (extension). After a length of 100 mm, the results are strongly correlated.

Length (mm)	0	50	100	150	200	250	300
0	1	0.66751	0.567246	0.552953	0.542169	0.5422	0.546311
50	0.66751	1	0.837897	0.84586	0.850144	0.848236	0.853335
100	0.567246	0.837897	1	0.998694	0.997279	0.996393	0.997045
150	0.552953	0.84586	0.998694	1	0.999275	0.998708	0.999119
200	0.542169	0.850144	0.997279	0.999275	1	0.999665	0.999854
250	0.5422	0.848236	0.996393	0.998708	0.999665	1	0.999595
300	0.546311	0.853335	0.997045	0.999119	0.999854	0.999595	1

Two probe circular areas (radius, 50 mm) on the skin represent the electrodes (see Figure 3.4). The average potential on these areas were recorded and post processed.

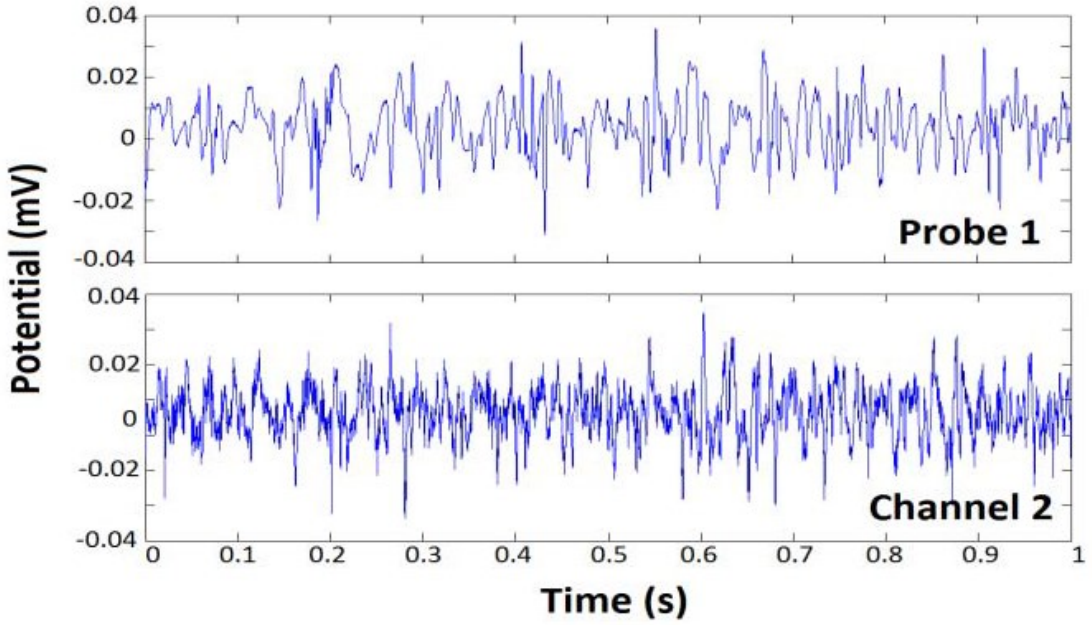

Figure 3.5 Simulated (top) VS. Experimental signal (bottom).

A bipolar electrode configuration was investigated by changing three different parameters: the inter-electrode distance, the orientation of the electrodes and the pennation angle of the fibre along which the signal travelled (see Figure 3.4 A, B, C). The inter-electrode distance was set at 15, 20, 25, 30 mm; the orientation of the electrodes was varied to 0°, 10°, 30°, 60°, 90° and the fibre pennation angle changed to 5°, 10°, 15°, 20°, 30°. In the parallel case the signal travels at 20 mm depth from the surface.

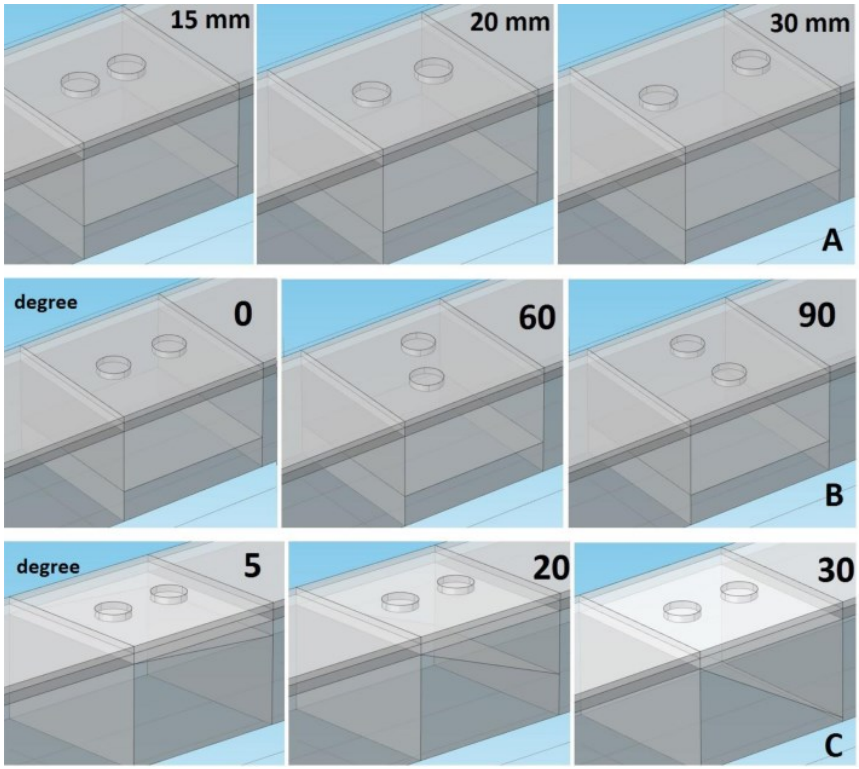

Figure 3.4 Representations of some of the bipolar configurations simulated. A) inter-electrode distances (mm); B) electrodes orientation (Degree); C) fibre pennation angle (Degree). The signal travels along the horizontal plane in the muscle tissue at a depth of 20 mm. For the pennated case, the plane is inclined at different angles.

3.3.3 Signal Processing

Matlab (version r2013a, Cambridge, UK) was used for post processing. A wavelet based intensity analysis of the simulated sEMG signal was performed [118]. This method uses a filter bank of non-linearly scaled wavelets developed specifically for EMG time frequency analysis, with applications to both experimental and simulated signals described in detail elsewhere [65, 119, 120] . Briefly, based on the source sample

frequency (5000 Hz), a set of 16 wavelets with centre frequencies spanning 6.9Hz to 804Hz (see equation 3.12) was defined in the frequency domain (see Figure 3.5).

$$F\Psi(f, cf, scale) \coloneqq \left(\frac{f}{cf}\right)^{cf \cdot scale} \cdot e^{\left(\frac{-f}{cf}+1\right) \cdot cf \cdot scale} \tag{3.12}$$

The EMG signal is then convolved with the wavelet set, essentially band-pass filtering the signal with the same frequency components as the wavelets [119]. Using this method, an intensity can be calculated which approximates the power of the signal [121]. This method enables investigation of the filtering effects (power attenuation) of electrode configuration and fibre geometries at the central frequencies of the wavelet analysis.

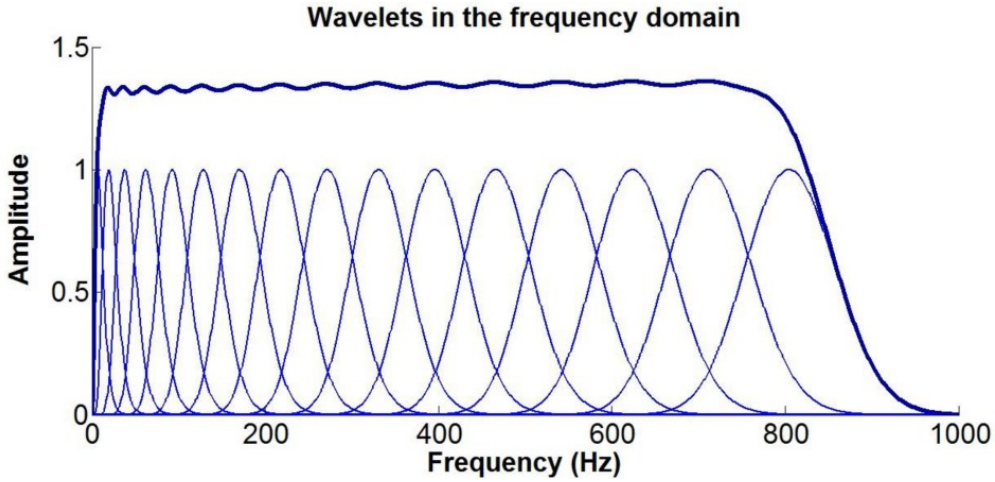

Figure 3.5 The 16 wavelets set in the frequency domain. The sum of the wavelet (thick line) gives the total band of the filter. Each peak is the central frequency of the single wavelet.

The mean power of the sEMG bipolar signal, expressed as a percentage of the mean power of the iEMG (source) signal was used to interpret the results.

3.4 Results

3.4.1 Properties of the iEMG Source Signal

The source signal contained bursts of activity at short time intervals, which indicate the activation of recorded motor units (see Figure 3.6 A). Typically, the bursts occur at higher frequencies (indicating appropriate ranges), and are evident in the total power plot (Figure 3.6 B) as amplitude peaks. From the time-central frequency power plot (Figure 3.6 C) it is also evident that lower frequencies (<62 Hz) contribute minimally to the recorded signal.

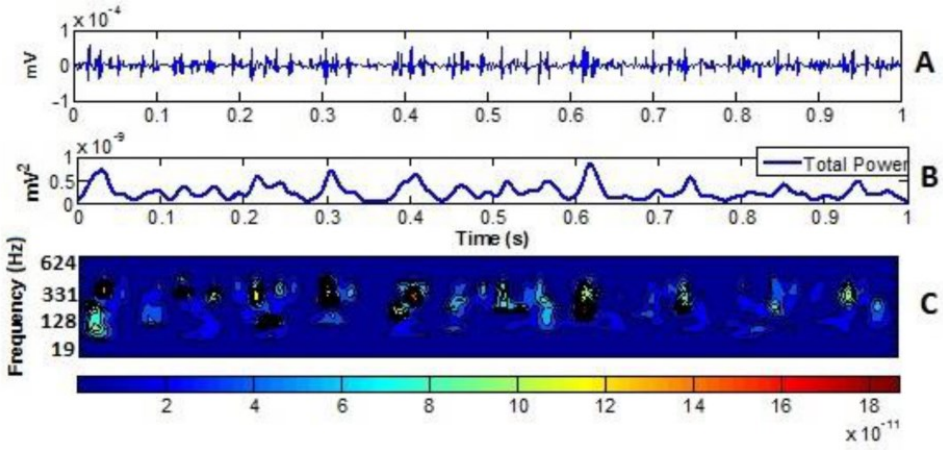

Figure 3.6 The source signal power in time and frequency domain. The 1 sec sample from intramuscular signal that was used as source signal is shown at the top (A) . The total power of this signal is shown in the time domain (B) and in the frequency-time domain (C). From this plot it is possible to distinguish bursts of activity that occur during the isometric contraction.

In Figure 3.7 the source signal mean power for each central frequency is reported. The mean power of the intramuscular source signal had peak values around the central frequency of 395 Hz.

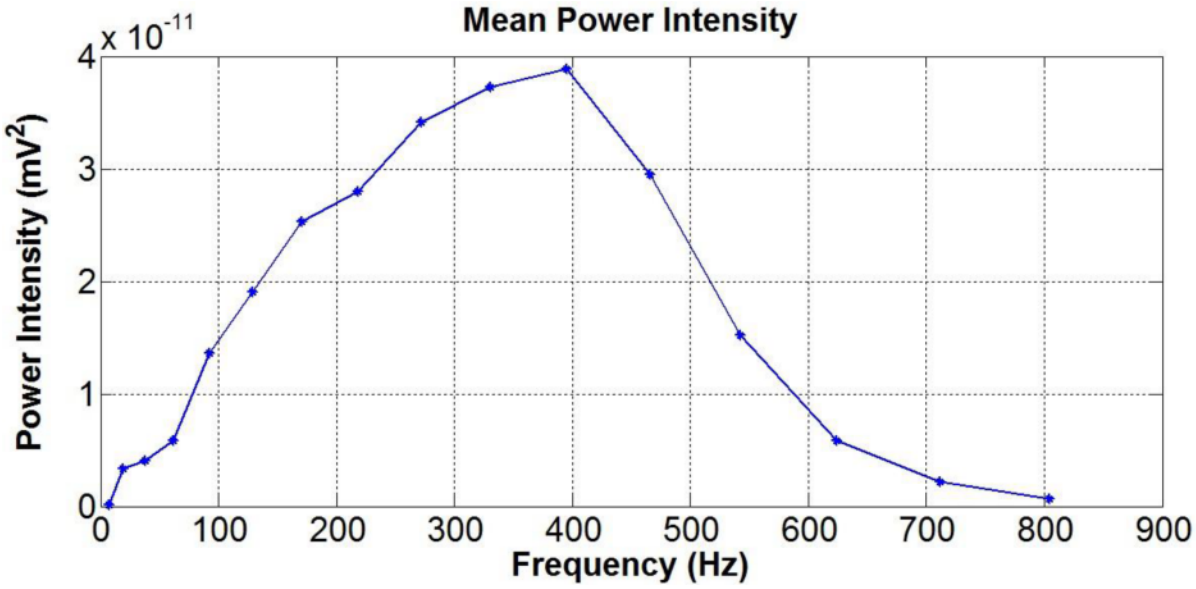

Figure 3.7 The source signal mean power. The source signal mean power over 1 sec calculated for each frequency component of the source signal.

3.4.2 Influence of inter-electrode distance & orientation

The overall energy of the signal was assessed by evaluating the total power measured at the simulated surface electrode. A positive linear relationship was found between the IED and the total power, while a negative decay was found as the electrode alignment deviated from the signal direction toward a perpendicular orientation (see Figure 3.8). The difference in the total power as a percentage of the source signal power between the lowest and the highest parameter was just 3% when varying the inter-electrode distance, IED, and around 2% when the electrode orientation was varied.

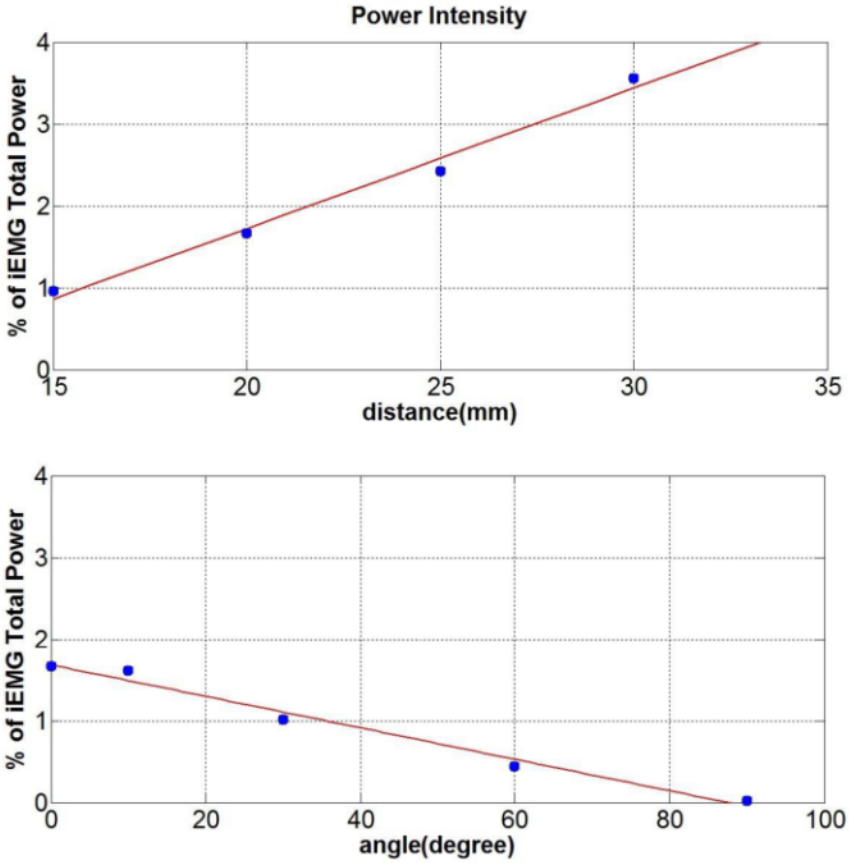

Figure 3.8 Total Power expressed as percentage of the source signal total power. (Top) Total power for different IED, showing a positive linear trend as the distance is increasing (Bottom) Total Power at different orientation, showing a decay as the electrodes alignment deviate from 0° to 90°.

The mean power of the bipolar surface signal for each central frequency was also obtained (see Fig. 3.8). The mean power increased as the IED was increased, but this occurred only for lower (<92 Hz) and higher (>542 Hz) frequencies, while in the range 92-542 Hz the signal was filtered out. The same frequency filtering occurred at different electrode orientations.

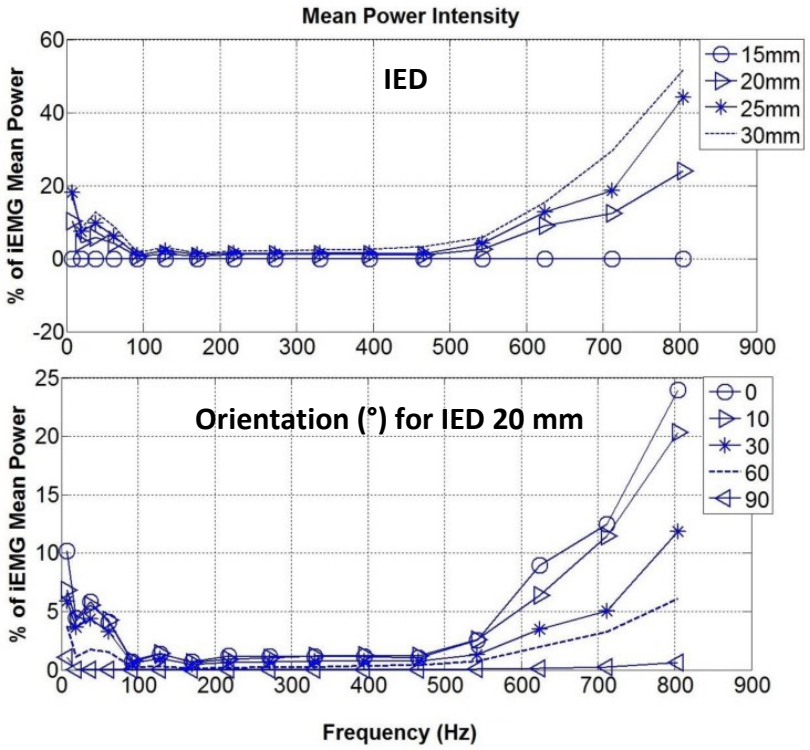

Figure 3.9 Mean Power of the bipolar signal in the frequency domain. The general trend reveal a band stop filtering in the range 92- 542 Hz (Top) Mean power at different IED. As the distance increases, the mean power increases as well. (Bottom) Mean power at different orientations. As the electrodes deviate from the direction of the signal, the mean power decreases, until reaching almost zero at 90°.

3.4.3 Influence of Fibre Pennation Angle

The amplitude of the sEMG from a signal travelling along a simulated pennated muscle fibre was also increased and of the same order of amplitude as the source signal. As the pennation angle increased the total power of the bipolar signal was considerably

attenuated (up to 13 %, Figure 3.10 top). Combining the effect of changing the inter-electrode distance with a 20° pennation angle showed an enhanced effect on the total power (see Figure 3.10 bottom). A 7 % difference in the total power between the lowest and the highest IED case was found, while it was just of 3 % without pennation.

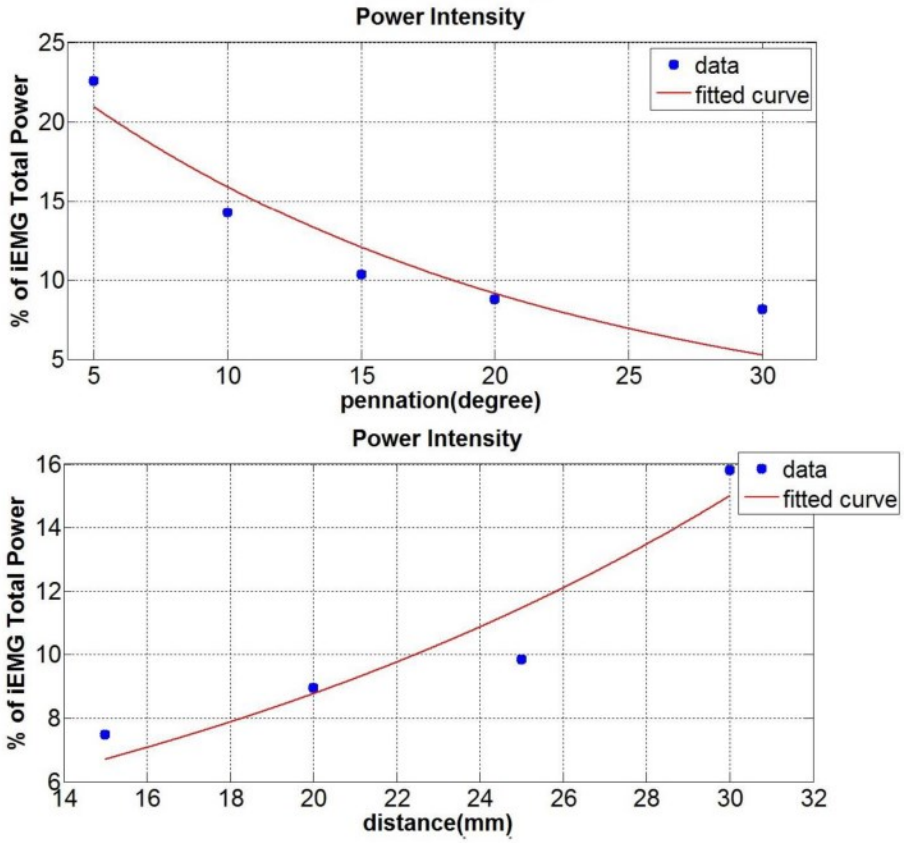

Figure 3.10 Total Power of the bipolar configuration. (Top) Total power at different fibre pennation angles. There is a linear decrease of the power as the pennation increase for a fixed IED of 20 mm. (Bottom) Total Power for a pennated model at 20° while changing the IED. The increase in the power as the distance increase is almost double as that found in the parallel fibres model.

The fibre pennation angle strongly affected the outcome signal, which was low pass filtered, retaining frequencies lower than the central frequency of 170 Hz (see Figure 3.11 top). The IED did not seem to affect the filtering response except when the electrode was relatively close to the termination side of the signal (see Figure 3.11 bottom). In that case (IED 30 mm) a narrower band and prominent peak at the central frequency of 62 Hz was found.

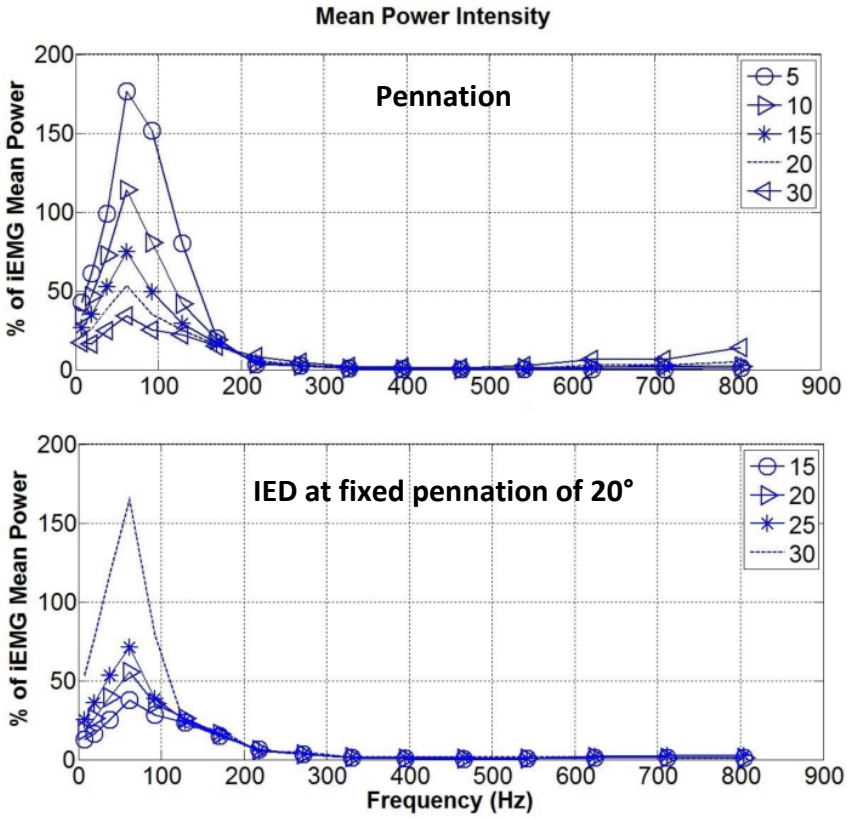

Figure 3.11 Mean Power of the bipolar signal in the pennated case. (Top) The mean power at different pennation is low pass filtered and the amplitude increase as the pennation decrease. (Bottom) Mean power for the pennated case at 20° while changing the IED. There is an enhanced peak for the IED of 30 mm for which the electrodes are close to the terminating point.

3.5 Discussion

A FEM of the muscle, skin & fat tissue was simulated to study the performance of different sEMG electrodes in bipolar configurations. During experimental data collection, the configuration of the electrodes is important to avoid cross-talk [122] and to assess the detection volume [63]. Bipolar measurements are more selective since they show a lower detection range [68], but are sensitive to their orientation with respect to the direction of the muscle fibres and the distance between the two electrodes [68].

3.5.1 Orientation and IED

From the work presented here, it is clear that the orientation of the electrode areas should give a differential signal similar to that of the IED, since the signal considered in the first two simulations is travelling horizontally across the tissue layer. As the electrodes become misaligned with respect to the signal direction, the signal detected will give a bipolar measurement equivalent to that from electrodes that have a smaller inter-electrode distance than that of the actual electrodes (considering an area across which MUAPs are homogeneous). The case in which the electrode areas are aligned at 90° with respect to the signal direction can be associated with the case of a null inter-electrode distance, hence the differential measurements cancel out. Andreassen and Rosenfalck [68] concluded that for an angle above 45 °(less than 45 ° according to their reference system), the iEMG electrodes will act as a perpendicular oriented electrode pair. In the simulations performed here the IED and the electrode orientation seems to play a minor role when the signal is travelling along a plane parallel to the electrode

plane. The influence of these features is to change the power amplitude while leaving the tissue filtering properties unchanged. Fig. 8 shows that the main attenuation of the signal intensity occurs between 92-542 Hz, which is a range that includes frequencies of physiological relevance. Slower motor units operate in the frequency range between 82-247 Hz, while faster in the range 240-423 Hz [20, 120]. Higher frequencies (>542 Hz) are less attenuated and the effect of different IED and electrode orientation is more remarkable, but these frequencies are generally discarded by researchers, as they are not in the physiologically relevant frequency range. When the misalignment (see Fig. 8 bottom) between the electrodes and the fibres is significant (60 ˚- 90 ˚) it is suitable to increase the IED distance (25-30 mm) to reduce the chance of the signal cancelling out in a bipolar configuration. By choosing the IED, other features considered in previous models should be also evaluated. The IED should not be too large in order to avoid the termination end effects [66]. Moreover, the thickness of the fat tissue increases substantially the pick-up volume, which is further extended by the IED [72]. This can lead to the occurrence of cross-talk [123] with other muscle activities.

3.5.2 Pennation angle

When dealing with pennated fibres, the signal travels along a diagonal plane.. The muscle tissue acted as a band stop filter (attenuating the wavelet frequency range between 92-542 Hz) when parallel fibres were modelled. In the case of pennation the bipolar configuration resulted in a low pass filtering of the signal. (Figure 3.11). This change in the frequency response can be explained as a consequence of the bipolar configuration, with the higher contribution to the sEMG signal coming from the

electrode which is closer to the source signal [124] and changes in the detected potential shape as occurring as predicted by the analytical pennated model proposed by Mesin and Farina [125]. The effect of a different IED seems to be enhanced in the pennated model in terms of total power, while the filtering response is changed considerably only for IED where the electrodes are close to the signal termination points (IED 30 mm). In addition, the amplitude of the sEMG is generally increased in the pennated simulation due to the small distance between the signal and the muscle surface as it starts to travel toward the deep aponeurosis. For the isometric condition studied here, Figure 3.11 suggests that for pennation angles greater than 20° (more than 50 % of the source signal is attenuated) it is suitable to increase the IED, i.e. IED of 20-25 mm. In our simulation, the signal is the sum of the MUAPs, hence a simplification was made in considering it travelling from the top to the bottom toward the deep aponeurosis. Muscle fibre's motor units end plate are usually located in the middle of the fibres [126]. This implies that in pennated fibres, the single action potentials travel in both directions toward the deep and the superficial aponeurosis. Nevertheless the direction of the potential detected, depends on the relative position between the bipolar electrodes, the fibres and the motor unit end plate [127]. Therefore, the source signal could have been represented in different ways, which might depend on the muscle that is being studied and its pennation. One major feature that this model predicted is the fact that the potential depends on the signal arriving at the superficial aponeurosis (closer to the electrodes), while the signal ending at the deep aponeurosis is strongly attenuated. This make it possible for signals to be recorded from different groups of muscle fibres and provide spatially localized information [128].The geometry of the fibres can also change as the muscle is contracting as addressed in Mesin et al. [71] analytical model. Despite

the limitation of not including the skin and connective tissue, they showed the importance of considering dynamic changes, specifically for recording the activity of deeper fibres, which are more affected as the distance from the detecting electrode is changed [111]. They also showed that the shortening of the muscle influenced the weight of the non-propagating components (standing waves) in the signal. Therefore, the model presented in this paper refers only to the situation of isometric contractions.

3.6 **Conclusion**

From this study, it can be seen that sEMG electrode configurations become an important feature when dealing with pennated muscles. This is because the signal travelling along a diagonal plane will be filtered differently by the electrodes in a bipolar configuration and will be attenuated while travelling down. An experimental approach to overcome this problem, using current measurements instead of potentials has been proposed, with results suggesting an increase in the spatial resolution (32, 33). During most functional motor tasks there will be changes in fascicle pennation angle as a result of muscle activation and so this is a dynamically changing feature of the muscle, which will influence what the electrodes record. For this reason, it is important to consider these features when designing EMG electrodes. To provide a foundation from which future guidelines may be set, future work should investigate the effect of dynamic changes in fascicle geometry and include consideration of other anatomical features such as tissue curvature (i.e. skin surface and fascicle) and skeletal elements.

The model presented here is able to evaluate the combined effects of electrode configuration and muscle architecture; it can be used to provide insight into the impact

of changes in muscle pennation angle, on sEMG activity measured [71]. The model in this study focused on a rectangular geometry with straight muscle fibres. The main assumption was to consider the source signal as a representation of the activity of the whole muscle, while the iEMG measurement covered a limited area around the wires electrodes. This was motivated by the fact that the source signal was acquired at low isometric contractions and considering that most of the sEMG signal energy comes from fibres close to the electrodes (so very limited contribution of deeper motor units). To improve the representativeness of the model input, more than one source of signal acquired from different regions of the muscle should be applied. In addition the significantly higher amplitude at IED of 30 mm in the pennation case (Figure 3.11) is likely to be due to the electrode area being close to the termination zone of the signal rather than an increased pick up volume. This “artefact” can be avoided by continuing the signal path and modelling the extinction of the signal. Future work will include the study of fibre end effects on the detected signal, to explore the phenomenon of standing waves that occur as the signal reaches the termination of the fibres. Another possible application of this model involves errors in the estimation of the conduction velocity when the electrodes are not correctly aligned with the fibres direction. Misalignment between the electrode and the fibres leads to a lower estimation of the conduction velocity, since the conduction velocity is estimated through the delay that a certain signal pattern takes when travelling between the pick-up area of an electrode pair [67].

It is recognised that this model only activates a small region of muscle but in practice, real activations may occur across regions of muscle[22], which have different sizes or geometry. Further work could use medical imaging such as ultrasound to quantify active

regions in the muscle which could then be used to provide more accurate estimations of the active muscle region [129].

3.7 Acknowledgments

We thank Mathew Piasecki and Dr. Jamie McPhee for providing the experimental data and Dr. Monica Daley for providing the wavelet function matlab codes.

4. Modelling the Connective Tissue Properties of the Muscle

A detailed description of the constitutive properties of the model used for the case study of age-related changes in muscle fibre spatial distributions, presented in Chapter 5, is provided. The work includes an analytical model, which is used to verify the defined constitutive properties allow the force transmission through shear of the endomysium to the other fibres and to define the minimum length required to for full transmission to occur.

4.1 Function and Properties of Skeletal Muscle Connective Tissue

A description of the function and properties of the connective tissue is given in this section. The connective tissues of skeletal muscles present different structure and composition at different levels (endomysium, perimysium, and epimysium). There is a general pattern that consists of collagen fibres and an amorphous matrix of hydrated proteoglycans which contribute to mechanically link the collagen fibre network [130]. Huijing, [8] reviewed studies with evidence of lateral force transmission between fibres through the connective tissue, suggesting that skeletal muscle can be considered a collagen fibre reinforced composite. In particular, work by Street [102] on the interaction between dissected myofibers and the surrounding fibres, revealed the existence of a lateral force transmission through the ECM when the myofiber strain was large enough to create passive shear stresses capable of deforming the surrounding fibres. In this experiment, the dissected fibre was still able to transmit 75 % of its force through the endomysium to the adjacent fibre when activated [13, 103], indicating that force transmission is possible and relevant.

The collagen fibres in the endomysium change orientation as the muscle length changes [103], increasing the compliance in tension while deforming to accommodate the fibres length change [13]. The endomysium can therefore be seen as a link structure between the fibres which functional role is to distribute the stress transversally to the fibre direction [11]. The perimysium, unlike the endomysium, separates fascicles of different dimensions (primary and secondary fascicles) and is composed of three layers of collagen. The superficial layer is a random network, the intermediate has larger fibre

diameter, while the deep layer has increased space between collagen fibres. This structure underpins the mechanical role of the perimysium, which is to facilitate the connection between synergistic muscular fibres acting toward the same tendon and to act as an interface between fascicles, allowing smooth deformations (fascicle slip within each other) when fascicles have different activation and deformations. At the perimysial level shear strains seems to be greater than at endomysial level, and this could be explained by a rearrangement of the collagen fibres orientation (55° with respect to the fibre direction at resting length, to 80° during activation and 20° when stretched) [12]. In addition the perimysium connects continuously to the tendon, acting as an interface between the muscle and the tendon. This continuity in the properties is possibly due to the same composition of type I collagen and decorin as primary proteoglycan [131]. In the outer layer of the muscle, there is the epimysium which is thicker than the perimysium with larger diameter collagen fibres. It has a role of containment of the muscle bundle and transmission of forces (from perimysium) to tendon or the aponeurotic expansion [132].

4.2 Contribution of Fibres and ECM to Skeletal Muscle Stiffness

Skeletal muscle tissue can be seen as a very complex composite material, which differentiates into sublevel structures. The myofibres are grouped together by the endomysium to form a fibre and the fibres are grouped by the perimysium to form a fascicle. When trying to assess the properties of the connective tissue (extra cellular matrix, ECM) and the muscle fibres experimentally, it is important to use a method that minimises the damage to the tissue structure and composition. Lieber et al. [133]

studied the passive mechanical properties of small muscle fibres bundles of normal and human spastic subjects. The muscle was dissected and soaked in a relaxing solution. A tensile test along the fibre direction was performed. A quasi-static stretch was applied to avoid the influence of any viscoelastic properties and the integrity of the structure was verified. The stiffness of the bundle tissue was calculated in equation 4.1:

$$E_f = \frac{\Delta\sigma_f}{\Delta\varepsilon_f} = \frac{(\sigma_{max} - \sigma_{min})}{\left(\frac{SL_{max} - SL_{min}}{SL_{min}}\right)} \quad , \qquad (4.1)$$

where SL_{max}, SL_{min} are the limits of the linear region of the sarcomere length-stress relationship and σ_{max}, σ_{min} are the limit stresses. The fibres and the ECM were assumed to work in parallel. The results gave fibre bundles tangent modulus (470 KPa) 16 times greater than the single fibre tangent modulus (28 KPa). Applying the rule of mixtures of composite materials (95% volume fraction), the ECM modulus was estimated to be equal to 8.7 GPa. This value differed a lot from previous studies (1-3 GPa) that were affected by the fact that the samples were clamped at the tendon [47, 133, 134].

The passive contribution of the fibre is mainly given by titin. Titin is a giant protein acting as a spring in the sarcomeres that contribute to muscle assembly and resting tension[135]. Prado et al. 2005 [136] explored the titin contribution to the passive tension exerted by the muscle passive tissue of white rabbit skeletal muscles (psoas, EDL, soleus, gastrocnemius, and diaphragm). Results proved that passive stiffness in fibres scales inversely with titin size, but faster muscle fibres can have either high or low titin sizes (slower fibres have large sizes and hence low passive tension). For each

muscle, there was one titin isoform (independent of the muscle from the fibres types present). Some muscles had high contribution (soleus, diaphragm) of the ECM to the total passive stiffness, while others had a lower contribution (i.e. psoas, gastrocnemius) and presented with higher titin stiffness. Either cases, this study proved the substantial contribution of collagens (ECM) in determining the total passive tension. The properties of the fibres are widely discussed and reported in literature ([131]) while the ECM properties are still to be properly assessed because there is a corruption of the material when isolated from the fibres. Corruption refers to both the structure and the biochemical composition, and consequently an indirect approach is generally used to get the stiffness of the ECM and the results of such studies are outlined below [131].

Ward et al. [137] studied human multifidus lumbar muscle and showed a difference in the passive tension of single fibres compared with a bundle of fibres (stiffer). The difference between single and a bundle of fibres stiffness cannot be explained simply by an additive effect. The single fibre stiffness can explain only 12 % of the bundle stiffness, suggesting a big contribution of the ECM. Meyer and Lieber [138] attempted to clarify which contribution is stronger. To avoid corruption of the ECM, the stiffness of the matrix was calculated indirectly applying the rule of mixture of composite materials (no digestion). Despite that, a possible corruption could have occurred at the skinning process of the fibres. The muscle examined was the fifth toe of the extensor digitorum longus muscle in mice. To exclude the possibility of the additive effect when considering a bundle of fibres (which might be at different sarcomere lengths), a group of dissected fibres (no ECM) were tested as well. While the group of fibres reported stiffness similar to the single fibres, the bundle of fibres (that include ECM) showed stiffness 5 folds

greater with a non-linear stress strain relationship. These studies showed that the ECM is generally stiffer than the fibres for extension above the fibre optimal length and has a high non-linear stress-strain relationship. It is not possible to isolate the ECM without corrupting its functional conformation; therefore, indirect methods are used to estimate its mechanical properties. These properties are then fitted to existing constitutive model that best represent their behaviour. Typical models used to characterise the muscle tissues are hyperelastic models such as Mooney Rivlin[139], Ogden[140], Yeoh[141] and customized.

4.1 Ageing of the muscle and the connective tissue

Sarcopenia is the result of cellular processes, whose main consequence is a qualitative deterioration of the muscle tissues [24]. An example is the degeneration of the characteristics of the collagen, which is the cause of an increased stiffness in the muscle connective tissue [142]. This degeneration is believed to be associated with an increase of cross-linking within the collagen fibrils, related with the reduced fibrils turnover [143-145]. Such occurrence was studied in the epimysium by Gao *et al*. [143]. From their study on rats, four regions were outlined in the epimysium stress-strain relationship: low modulus toe (no difference between young and old found), the linear region (98% increased stiffness in old rat population), post yield (ultimate strain lower by 12% in old rat population) and failure region (ultimate stress of old population two times higher). Moreover, the shape of the stress-strain relationship was similar to that observed for the endomysium [13], implying the existence of similar mechanisms and composition between the epi- and endomysium. Results on aged mice and rats also reported a decreased muscle specific force [146, 147] for different muscles. A study on the rat

plantaris muscle revealed a similar specific force in 13 months old rats ($31\ N/cm^2$) compared to 5 months old rats ($27\ N/cm^2$), while a decrease in the specific force was observed when the rats aged to 25 months ($24\ N/cm^2$) [148]. These changes could not be explained by different relative amounts of the non-contractile tissue, i.e. the connective tissue. This might challenge current understanding as during ageing, denervation of the fibres can cause their loss and replacement with fat and connective tissue [30], supposedly altering the force capacity of the muscle. Therefore, modelling can give a clarification on what are the consequences of a different amount of non-contractile tissue. A recent study [149] confirmed also that the muscle aging determinants follow a declining pattern qualitatively consistent across species as confirmed by comparing results from human subjects and aged rats. For this reason, results and properties obtained from experiments on animals such as rats, mice can be meaningful in the understanding of the ageing process in humans, and value from literature can be used to implement mechanical muscle models.

4.1.1 Aim and Objectives

In the literature review given at the beginning of this chapter, it was discussed how ageing can affect the connective tissue properties and what is the tissue functional role. It was found that the increase in connective tissue (collagen fibres) might not be the reason of a decreased later force transmission, but this need to be clarified. Furthermore, the constitutive model formulated will be extended to study an age related alteration of the distribution of the muscle fibres in chapter 5.

Therefore:

- A constitutive model of the muscle tissue is formulated. The properties of the tissues are chosen from literature and fitted to mechanical models
- An analytical model of a single fibre will be used to verify if the properties of the model, are able to guarantee the lateral force transmission. A single fibre analytical model adapted from Sharafi and Blemker [3] is used to verify the consequences of increased connective tissue in transmitting the force laterally through shearing. The minimum fibre length required to have full force transmission is also assessed.
- The constitutive model is used to build an FE model. The mechanical properties of the tissues are taken from literature. A single fibre stretching (to derive the stress-strain relationship) will be simulated first analytically to validate the FE model formulation.

4.2 Modelling the Muscle Tissue

In this section, the constitutive model of the muscle utilized in the mechanical simulations of chapter 5 is formulated. The properties used to describe the tissues mechanical behaviour (strain energy functions), were obtained from literature where mechanical tensile/compressive tests were performed on animals muscle tissue and the results were fit to hyperelastic models (i.e., Monney Rivlin, Ogden, Yeoh).

The hyperelastic constitutive models used to describe the fibre and the endomysium tissues, are defined through strain energy functions W_s which are a function of the

C_{ij} Cauchy-Green tensor's invariants I_i. Once these are defined, the second Piola Kirchoff stress tensor is computed:

$$S_{ij} = 2\frac{\partial W_s}{\partial C_{ij}} \quad . \quad (4.2)$$

This tensor has no direct physical meaning but has the advantage of being symmetric and invariant to rotations. It represents the current stress in the original configuration, meaning also that it tracks the fibre direction. Because of that, the myofibre stress equations were added in the second Piola Kirchhoff stress tensor, to the component of the tensor along the fibre direction.

As a nearly incompressible material, the strain energy was divided into an isochoric and volumetric component:

$$W_s = W_{iso} + W_{vol} \quad . \quad (4.3)$$

The volumetric strain energy will induce a volumetric stress (pressure):

$$p_p = -\frac{\partial W_{vol}}{\partial J} = -k(J-1) \quad . \quad (4.4)$$

As a result the total contribution to the second Piola Kirchhoff stress will be:

$$S_{ij} = -p_p J C^{-1} + 2\frac{\partial W_{iso}}{\partial C_{ij}} \quad . \quad (4.5)$$

For the myofibre specific case, the second Piola Kirchhoff, stress along the axial (fibre) direction was expressed as:

$$S_{axial} = -p_p J C^{-1} + 2\frac{\partial W_{base}}{\partial C_{ij}} + S_{active} \quad . \quad (4.6)$$

The Cauchy stress is computed afterward through the relationship with S_{ij}:

$$\sigma = J^{-1} F S F^T = -p_p I + 2J^{-1} F \frac{\partial W_{iso}}{\partial C} F^T \quad . \quad (4.7)$$

As previously discussed the ECM has a behaviour, which is similar to rubber like materials (i.e. non-linear large deformations). A hyperelastic model would generally be appropriate to describe the ECM mechanical contribution. In the presented model, the connective tissue strain energy W_{base} was described with a Mooney Rivlin strain energy with 5 coefficients calibrated from experimental data (see Table 4-1)[59].

$$W_{base} = C_{10}(\bar{I}_1 - 3) + C_{01}(\bar{I}_2 - 3) + C_{11}(\bar{I}_1 - 3)(\bar{I}_2 - 3) + C_{20}(\bar{I}_1 - 3)^2 + C_{02}(\bar{I}_2 - 3)^2 + \frac{K}{2}(J - 1)^2 \quad , \quad (4.8)$$

where C_{ij}, K are the model parameters (see Table 4-1) and J is the jacobian. W_{iso} is a function of the deviatoric invariants $\bar{I}_1, \bar{I}_2$ of the right Cauchy deformation tensor (C), defined as :

$$\bar{I}_1 = I_{1,C}\left(I_{3,C}\right)^{-1/3} = I_1 J^{-\frac{2}{3}} \quad , \quad (4.9)$$

$$\bar{I}_2 = I_{2,C}\left(I_{3,C}\right)^{-2/3} = I_2 J^{-\frac{4}{3}} \quad . \quad (4.10)$$

The volumetric part is given as:

$$W_{vol} = \frac{1}{2}K(\log J - 1)^2 \quad . \quad (4.11)$$

Table 4-1 Muscle constitutive properties parameters: the strain energy function coefficients, the bulk property and the muscle density taken from Chi et al. 2011

C_{10}	64300 Pa
C_{01}	-38000 Pa
C_{11}	-43 Pa
C_{20}	5400 Pa
C_{02}	5 Pa
K (bulk modulus)	$5x10^7$ Pa
ρ (density)	1000 Kg/m^3

The fibre base material was modelled with a Yeoh strain energy function (equation 4.6) [60, 141]:

$$W_{base} = c_1(I_1 - 3)^1 + c_2(I_1 - 3)^2 + c_3(I_1 - 3)^3 \quad . \quad (4.12)$$

The parameters of the model are reported in Table 4-2.

Table 4-2 Yeoh Model Parameters [60]

c_1	6750 Pa
c_2	0.0278 Pa
c_3	-0.001975 Pa

4.3 FE constitutive Model Validation

To test the FE model accuracy, the analytical solution of the base material constitutive models were compared with an FE model of the tissue simulated on Comsol Multiphysics (version 5.0, Cambridge, UK) for each tissue. A uniaxial tensile stretch simulation (displacement applied with 0-0.5 strain range) was performed. When having a uniaxial stress, for an incompressible material, the stretch $\lambda_1 = \lambda$ along the stress is related to the stretch along the other two directions given by equation 4.7 :

$$\lambda_2 = \lambda_3 = \frac{1}{\sqrt{\lambda}} \quad . \quad (4.13)$$

Therefore, deriving the strain energy with respect to the stretch and combining the equations for two stresses (knowing that along the other directions the stress $\sigma = 0$)

results in the following equation for the stress for a five coefficient Mooney Rivlin function (equation 4.8):

$$\sigma_{eng} = 2C_{10}\left(\lambda - \frac{1}{\lambda^2}\right) + 2C_{11}\left(\frac{1}{\lambda^2} + 2\lambda - 3\right)\left(\lambda - \frac{1}{\lambda^2}\right) + 4C_{20}\left(\lambda^2 + \frac{2}{\lambda^2} - 3\right)\left(\lambda - \frac{1}{\lambda^2}\right) - 2C_{01}\left(\frac{1}{\lambda^3} - 1\right) - 2C_{11}\left(\lambda^2 + \frac{2}{\lambda} - 3\right)\left(\frac{1}{\lambda^3} - 1\right) - 4C_{02}\left(\frac{1}{\lambda^2} + \frac{2}{\lambda} - 3\right)\left(\frac{1}{\lambda^3} - 1\right). \quad (4.14)$$

The stress generated by the fibres base material (Yeoh model) can be expressed analytically as (equation 4.9):

$$\sigma = 2\left(\lambda^2 - \frac{1}{\lambda}\right)\left[c_1 + 2c_2\left(\lambda^2 + \frac{2}{\lambda} - 3\right) + 3c_3\left(\lambda^2 + \frac{2}{\lambda} - 3\right)^2\right] \quad . \quad (4.15)$$

Table 4-3 reports the geometrical parameters of the simulation. These are the same as those used in the single fibre shear force transmission simulation.

Table 4-3 Parameters of the tissue simulation

Geometric Properties	
Length	1400 µm*
Radius	35 µm [150]
Endomysium thickness	0.9092 µm , 95% volume fraction [133]

In the FE model, stationary parametric simulations were performed. A fibre (see Figure 4.1) was fixed at one side and a displacement was applied at the opposite side. The axial strain imposed was the changing parameter.

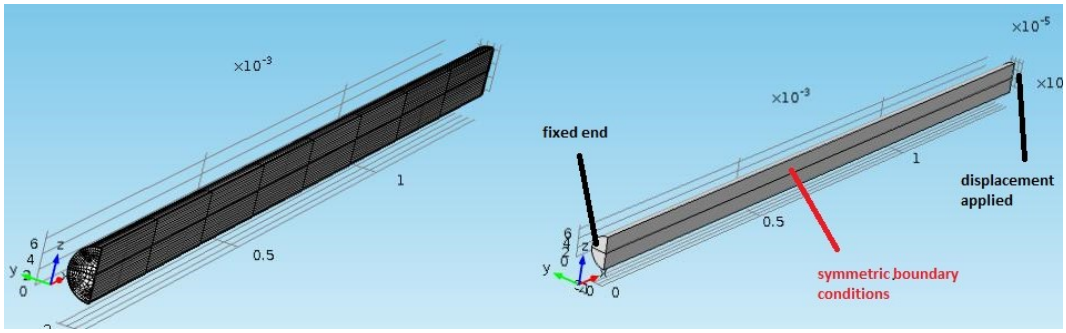

Figure 4.1 FE model of the tissues. A single fibre was simulated to validate the FE model properties against the analytical solution. The fibre properties were those of the endomysium in one simulation and of the fibre base material in the second simulation. The fibre was fixed at one side, and a displacement was applied at the opposite side.

Hexahedral and quadrilateral elements (Lagrange second order shape function) were chosen for the mesh, as they allow a bigger aspect ratio (200 times the thickness of the endomysium) than tetrahedral elements (see

Table 4-4 and Table 4-5 for properties); hence extend more along the fibre permitting a lower number of elements. The mesh set up used in

Table 4-4 is the same used in the FE model of chapter 5.

Table 4-4 FE model mesh parameters

Name	Value
Maximum element size	200*thickness
Minimum element size	thickness
Curvature factor	0.1
Resolution of narrow regions	0.3
Maximum element growth rate	1
Custom element size	Custom

Table 4-5 Mesh elements quality

Property	Value
Minimum element quality	5.574E-4
Average element quality	0.001619
Hexahedral elements	1608
Quadrilateral elements	818

Property	Value
Edge elements	156
Vertex elements	8

Stress-strain data were exported and compared with the analytical solution processed in Matalb R2013a (Cambridge, UK).

4.3.1 Results

Figure 4.2 & 4.3 show the results for the endomysium and fibre based models respectively. They show good agreement (R = 0.99) between the FE simulation and the analytical solution. This validates the mesh and the high aspect ratio used to reduce the number of elements, hence the computational cost. The same aspect ratio will be used to model a bundle of fibres in chapter 5.

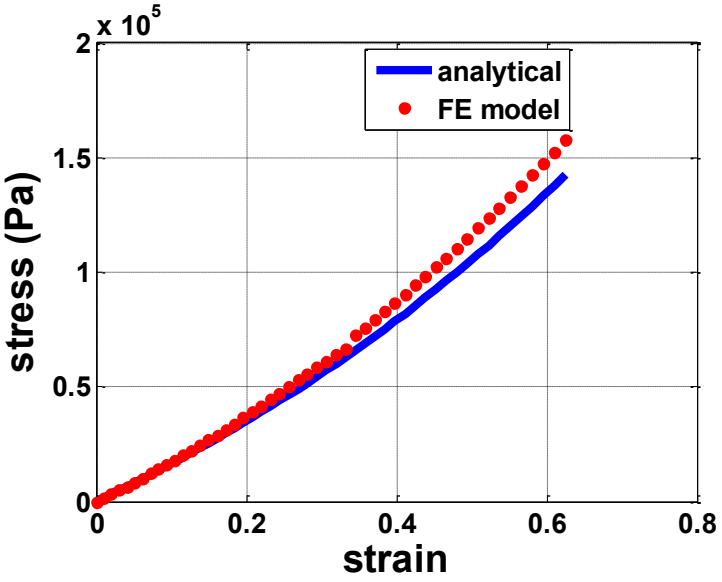

Figure 4.2 Stress-Strain curve. FE simulation VS. the analytical solution for the endomysium tissue (*R* = 0.9999)

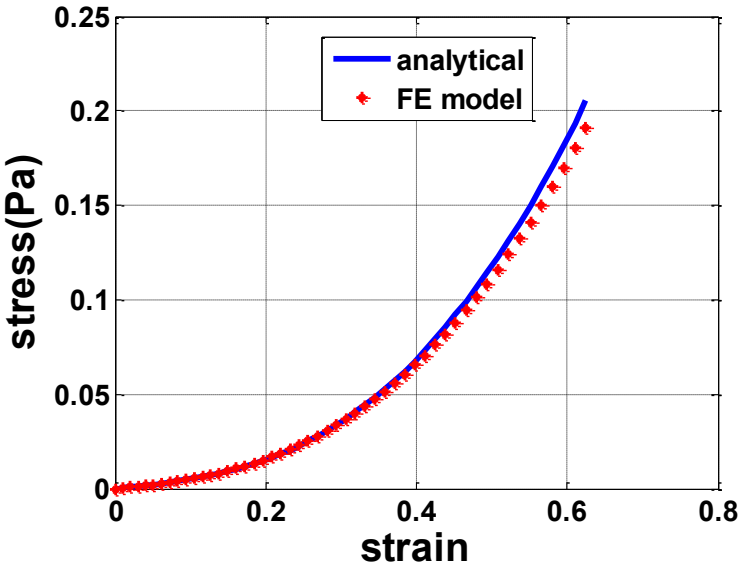

Figure 4.3 Stress-Strain curve. FE simulation VS. the analytical solution for the passive fibres (base material tissue)

4.4 Force transmission

In this section the force transmission to the endomysium is examined analytically in a single fibre. The objective is to find the minimum fibre length needed to transfer the total force through shearing, and verify that with the tissue properties chosen, transmission is still possible even at a reduced volume fraction. The analytical equilibrium equation used by Sharafi and Blemker [3] was applied (see Appendix D for matlab code). The equilibrium is achieved from the force reactions of the endomysium through shearing that counteracts the pulling contracting force of the fibre. The

endomysium force (the values are normalized by the maximal isometric force) is given as [3]:

$$F_{end} = \frac{2\left(\frac{G_{end}}{\sigma_{iso}}\right)\left(\frac{L_0}{r_0}\right)^2 \lambda(1-\lambda)}{-1+\sqrt{1+2k(2+k)\left(\frac{\lambda}{\lambda+1}\right)}} \quad , \tag{4.10}$$

where σ_{iso} is the maximal isometric force, L_0 is the resting length, and k is the ratio between the thickness and the endomysium thickness and the initial fibre radius. G_{end} is the endomysium shear modulus and since the Mooney Rivlin model that represents the endomysium is not linear, the initial shear modulus was considered:

$$G_{end} = 2\ (c_{10} + c_{01}) \quad , \tag{4.11}$$

where c_{10} and c_{01} are the first Mooney Rivlin coefficients (the initial shear modulus depends always on these first coefficients independently from the number of coefficients used for the model). The endomysium force should be equal to the force exerted by the fibre to have equilibrium. The fibre force is composed of the active force and a passive elastic (titin contribution) force. The active force follows a Hill based force-fibre length relationship. The shape of the function $f_l(\lambda)$ was approximated with a polynomial function [60]:

$f_l(\lambda)$=0.534+0.229*cos(w λ)-0.095*cos(2*w λ))+0.024*cos(3w)-
0.021*cos(4w λ)+0.013*cos(5wλ)-0.421*sin(w λ)+0.079*sin(2wλ)-
0.029*sin(3w λ)+0.013*sin(4w λ)+0.002*sin(5w λ) + 0.002*sin(5wλ) (4.12)

where w = 4.957 is a waiting factor.

The passive behaviour of the fibre was modelled as a non-linear elastic material, by fitting a second order polynomial to experimental results on soleus fibre (titin contribution):

$$\sigma = 176340(1-\lambda)^2 - 24703(1-\lambda) + 505.13 \quad . \quad (4.13)$$

Both these forces were normalized by the maximal isometric stress ($\sigma_{iso} = 300\ kPa$) when calculating the equilibrium.

The matlab code provided by Sharafi and Blemker [3] was modified and adapted to this study's constitutive properties. A simulation of a contracting fibre with 95% volume fraction was compared against fibre with 80% volume fraction which corresponds to the difference between young and old populations as reported in experiments on rats [147]. The fibres keep contracting until the equilibrium is reached. The simulation was performed at several fibre length/fibre diameter ratios. The endomysium tissue is

constrained on the outer surface so that it will undergo shear stress as the fibre contracts in both sides.

4.4.1 Results of single fibre analytical model

Figure 4.4 shows that the force transmitted (normalized values) as the ratio between the fibre length and fibre diameter increases tends to be equal to the maximal isometric stress. The plot revealed that for fibre lengths greater than ten times the diameter, the force can be fully transmitted through the endomysium, while for the 80 % volume fraction it must be for a ratio of 20. These ratios are far lower than physiological values that span between 300-4000 [3], and further support the hypothesis of force transmission through the endomysium. Figure 4.5 shows the stretch values as the ratio increase. This tends to be one (no displacement) as the fibre is very long compared to the endomysium thickness.

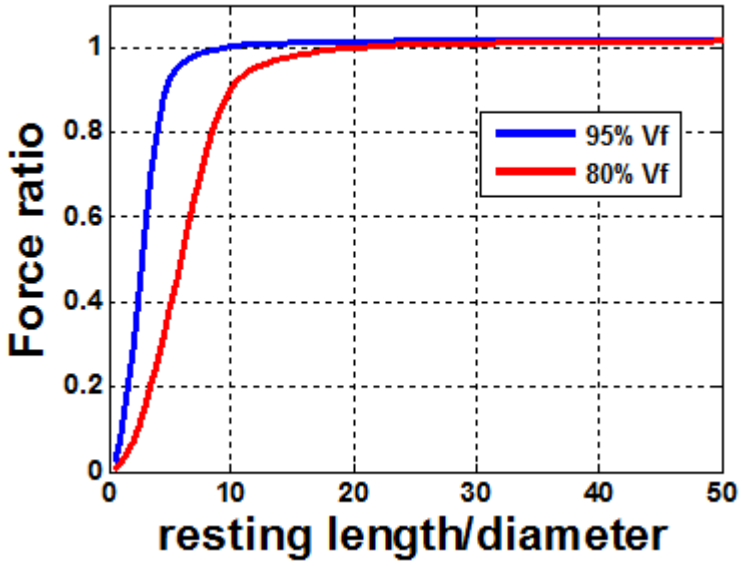

Figure 4.4 Normalized Force transmitted Vs. fibre length. The figure shows that from a ratio fibre length/fibre diameter of ten the fibre is able to transmit the total maximal isometric stress (blue line 95% volume fraction, red line 80%).

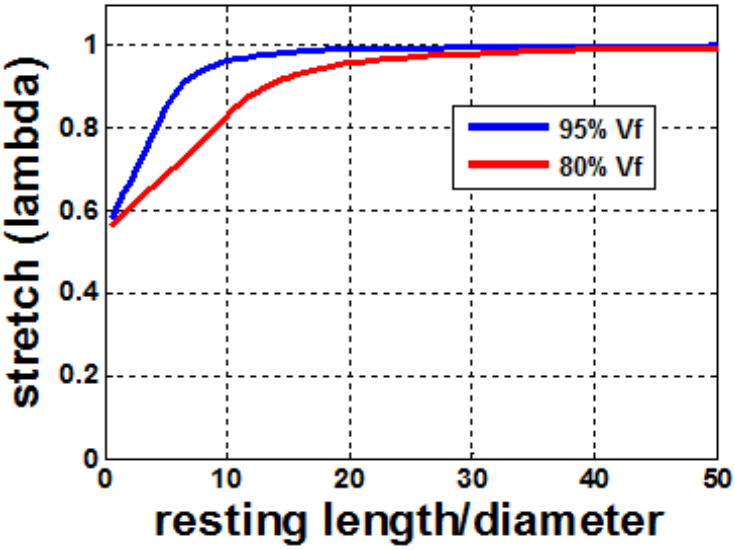

Figure 4.5 Stretch Vs. fibre length. The figure shows that for very long length, the endomysium is relatively very thin and therefore the shear is transmitted without a stretch (blue line 95% volume fraction, red line 80%).

4.4.2 Discussion

The main motivation of studying muscle ageing is to find ways of limiting its progression or reducing functional consequences. A review on skeletal muscle passive extensibility studies [151] delineated the myogenic (and not neurogenic) mechanism of length adaptations (changes) as revealed from studies on immobilized muscles of rats and from studies on human calf muscle. Furthermore, the review mentioned animal studies, which confirmed exercises could prevent connective tissue accumulation on ageing muscles. In the presented model, the properties of the tissue were chosen from literature and are based on experimental data. The single fibre simulation verified that the force transmission through the endomysium is possible as confirmed by the

mathematical model reported by Sharafi and Blemker [3]. A volume fraction of 80 % was chosen to represent the case of reduced volume fraction in aged population, as a consequence of increased interstitial connective tissue (thicker basal lamina, deposit of collagen fibrils) [147]. The force transmission was possible also for this amount of volume fraction, which means that causes of altered force transmission are more likely related to the mechanical properties of the tissue than the volume fraction. This might challenge current understanding of impaired lateral force transmission due to an increased thickness of the connective tissue [152] and indicates the importance of modelling to probe conclusions drawn out from experimental studies.

A possible cause of alterations in muscle mechanical properties is fat infiltration, which has been studied in different FE models [153, 154] and a reduced dystrophin expression (the proteic complex responsible of lateral force transmission). The FE model of a pennated muscle presented by Rahemi *et al*. [154] showed that fat infiltration can be a cause of reduced muscle specific force since it increases the stiffness of the base material, hence altering the quality of the tissue. Virgilio *et al*. [153] model suggested that fat infiltration can reduce the macroscopic shear modulus, but this effect was minimized when the ECM was stiffer than the fibres. In this case, only the reduced volume fraction affected the macromechanical properties. Virgilio *et al*. [153] model was built at a fascicle level and might suggest that volume fraction changes are relevant at a perimysial level rather than at an endomysial level as simulated in the current study. This is because perimysial shear strains are greater than endomysial and therefore shear stresses are lower.

4.5 Conclusion

From the review of literature at the beginning of the chapter, reporting the fibres and the connective tissue tensile properties it is clear that connective tissue is stiffer than the fibres. Despite that, the connective tissue collagen fibres are oriented at certain angle within respect the muscle fibres. This make the tissue compliant along the fibre, and confirms that the force can only be transmitted laterally. This chapter presented a new constitutive model that will be used in the following chapter (Chapter 5) to investigate the tissue behaviour after age-related alterations of the muscle. An analytical model [3] of a fibre was used to verify that the force transmission is possible and for which fibre minimum length. A fibre length 20 times greater (1400 µm) than the endomysium thickness was found to be enough to fully transmit the force through shearing and since it is much lower than physiological ranges, it confirms that the endomysium is capable of force transmission. This will be the fibre length chosen for the FE model in chapter 5.

5 A FEM study of the consequence of motor unit fibre clustering in aged population

Normally muscle fibres belonging to the same motor units are randomly distributed within a certain region [21]. Clustering of fibres within a motor unit is likely to occur in aged muscle, when type II fibres are innervated by slower motor units in a process related to collateral axonal sprouting and re-innervation [155]. Whether that region is localized in a certain area of the muscle or distributed over the whole muscle raised a controversy in the research community [156-158]. However, in this study, the focus is only on the fibres distribution and not the motor unit territory, with the model presented to investigate the effects on the distribution pattern of stress/strain values of the spatial distribution of fibres belonging to the same motor unit.

5.1 Mechanical Models of the muscle tissues

In the previous chapter an overview of the properties of the muscle, tissue and age related decline was given. It was identified that the major decline in the strength of aged muscles is to be found in the quality of the tissue (e.g. integrity of the connective tissue compromised by fat infiltration) rather than quantity (fibres loss). If the muscle is considered as a fibre reinforced composite material [8], where the matrix is the connective tissue; the problem can be split into an intrinsic and an extrinsic degeneration. The intrinsic degeneration refers to the decreased mechanical properties of the fibres and the matrix tissue (i.e. Elastic modulus, Shear Modulus)[137, 143, 159-161]; the extrinsic degeneration refers to the increased proportion of the matrix (fat infiltration, decreased fibres diameter)[146] relative to the fibres, the decreased length of the fibres and the motor unit's reinnervation[25, 155]. Muscle models can be useful tools to better understand the weight of each feature in determining the muscle strength and therefore have the potential to delineate optimal approaches/interventions required to limit or recover muscle decline.

Recent research [2-4, 105, 107, 162, 163] has focused on developing further models that can simulate sophisticated behaviours when considering the muscle tissue constitutive properties. Blemker et al.,[57] reported a constitutive model that included a component directly linked with the muscle's transverse fibres and along fibres shear modulus. Sharafi and Blemker [2]used this model to study the effect of fibres and fascicle geometry in the micromechanical constitution. Histological samples were digitized to get the fibres and fascicles cross-sectional pattern. Results indicated that the microstructure of the muscle (fascicle shape) is likely to be explained by the need to

accommodate larger deformation along specific planes due to the macroscopic geometry, which is in line with the experimental findings of the role of the perimysium [12]. This also explained the higher anisotropy of fascicles compared to fibre geometry and results in significant transverse anisotropy in shear. The model showed also that the direction with higher shear modulus corresponded to the direction where fascicles are more elongated.

Further implementations of the Blemker et al., [57] model were applied at a microscopic level to study the fibre's lateral force transmission through the endomysium, which confirmed the feasibility of full lateral force transmission at physiological length ranges. Further work [3] studied the force transmission of intra-fascicularly terminating muscle fibres at a microscopic level. An analytically simplified model (used in chapter 4) of a fibre surrounded by its connective tissue was implemented with some assumptions (shear strain constant across the thickness of endomysium, fibre rigid in shear, circular cross section). This simplified model predicted that both longer fibre resting length and higher endomysium shear modulus increased force transmission. Results also suggested that force transmission is more effective as fibre length and volume fraction increase, which is in line with the thought of age related muscle weakness, since both length and volume fraction of the fibres decrease.

Zhang and Gao's [162] 2D finite element model of a single myofibre, investigated the effect of the tapering end of the fibre and the stiffness of the connective tissue on the lateral force transmission. This model included both the tensile and the shear force transmission in order to be able to evaluate which one is the dominant component. Results indicated that an increased stiffness of the connective tissue improves the force

transmission and shear force transmission is dominant and significant only at the end of the myofibre in contrast with the role of intrafascicularly terminating fibres described by Sharafi and Blemker's model [3] . Another study of the myofascial force transmission through modelling, was carried out by Yucesoy *et al*. [105]. In this study, a 3D finite element model of the muscle considered the fibres and the connective tissue as two separated domains (different meshes) linked with an elastic element through which the force is transmitted. The case where all the links were highly stiff (control) was compared against possible pathological cases where some links were complaint. The model gave results consistent with other works [164]. Internal excessive strain values were found in the models with compliant links. This resulted in a lower force transmission specifically when the muscle extension was above the optimal length. Different stiffness within the muscle can also be caused by a regionalized activation pattern of the muscle as was reported by Rahemi *et al*. [60] in a FEM of the lateral gastrocnemius. For the same overall muscle activity, a different regionalization of the muscle activity resulted in changes in muscle force magnitude, direction and hence architectural final configuration. In this case, as well, the connective tissue is of relevant importance to transfer the force to inactive regions. All these models were made to enable investigations of relative contributions of different muscle components for force production, which is not possible to do in experimental studies. From the outcomes, it can be confirmed that lateral force transmission is mechanically feasible and that features such as connective tissue stiffness, fibre length together with variation in activation patterns, have an influence on the overall force transmitted. This is of relative importance when considering age related alterations of the fibre geometry. Aged muscle presents with fat infiltration and fibrosis [146] that might alter the volume

fraction, altering the quality of the connective tissue surrounding the fibres. The altered volume fraction can also be caused by a decrease of type II fibre diameter. This fact was studied in the previous chapter and a minimum fibre length that can guarantee full lateral force transmission with the constitutive model presented was found. Furthermore, the denervation of type II fibres and consequent collateral re-innervation by slower motor units might cause a regional packing of fibres belonging to the same motor unit. Experimental studies reviewed by Monti *et al*. [21] indicate that fibre distribution within motor unit showed a random distribution in most of the results. The size of the territory occupied by a motor unit depends on the muscle and motor unit type [21], which is subject specific. Therefore, a possible altered force transmission could be caused by a change in the distribution of the activated fibres (belonging to the same motor unit). To our knowledge this specific phenomenon has not been investigated yet either experimentally or through modelling. The current work will therefore use a micromechanical muscle model to investigate the redistribution of the fibres belonging to the same motor unit as a consequence of age related denervation of type II fibres. The phenomenon that is being investigated is the clustering of fibres (belonging to the same motor unit) resulting from the reinnervation of fibres in aged muscles. The hypothesis is that a clustered fibre distribution creates greater, concentrated stress or strain within a fascicle.

5.2 Method

5.2.1 FE model

Comsol Multiphysics (version 5.0, Cambridge, UK) finite element solver, which suits multiphysics simulations, was used. This is a general-purpose solver, which allows access to the constitutive equations and the state variables in order to customize the problem set. In these simulations, a bundle of 19 muscle fibres surrounded by the endomysium sheet contracts as they are activated. A mesh of hexahedral (fibre) and quadrilateral (endomysium) elements with a Lagrange quadratic shape function was used. The constitutive properties of the fibres and the connective tissue are those detailed in chapter 4. The bundle of 19 fibres (representative of a fascicle) was used to simulate different spatial distributions of activated fibres (see Figure 5.1 and Figure 5.2).

The active fibres represent type I fibres which are distributed randomly across the area or due to age related re-innervation, are clumped to cover a region of the fascicle cross section. Therefore, two cases of clumped active fibres and two cases of distributed active fibres were examined (see Figure 5.1). In addition, the fibre recruitment was set to be 21 % and 37 % (4 fibres and 7 fibres activated).

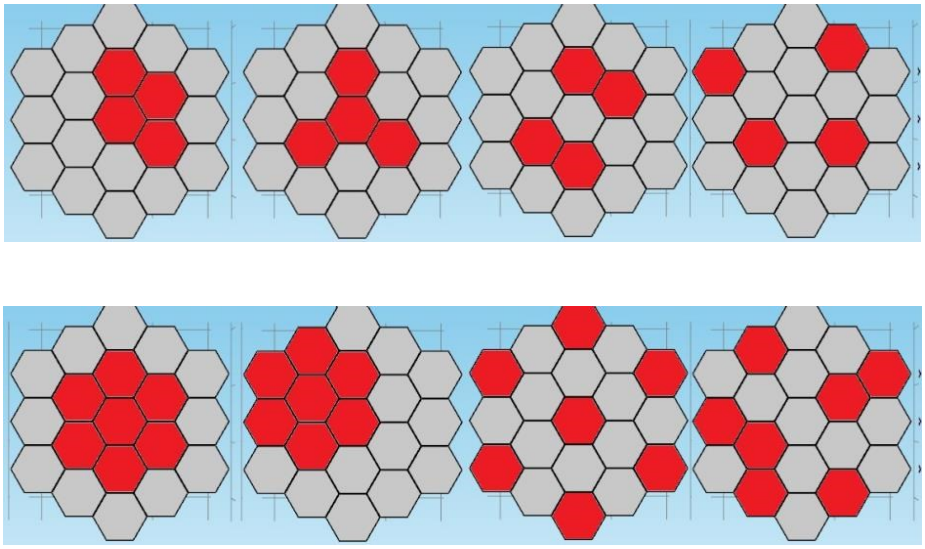

Figure 5.1 Eight cases of activation pattern (red color). Top: 21 % activation was simulated with four conditions: two clumped activated fibres conditions and two randomly distributed activation pattern. Bottom: the same fibre distribution categories but for an activation of 37 %.

Figure 5.2 shows the mesh of the model and the specifics are reported in Table 5-1. These are the same as the model used for the validation of the FE properties in chapter 4 (the grow rate is one point higher).

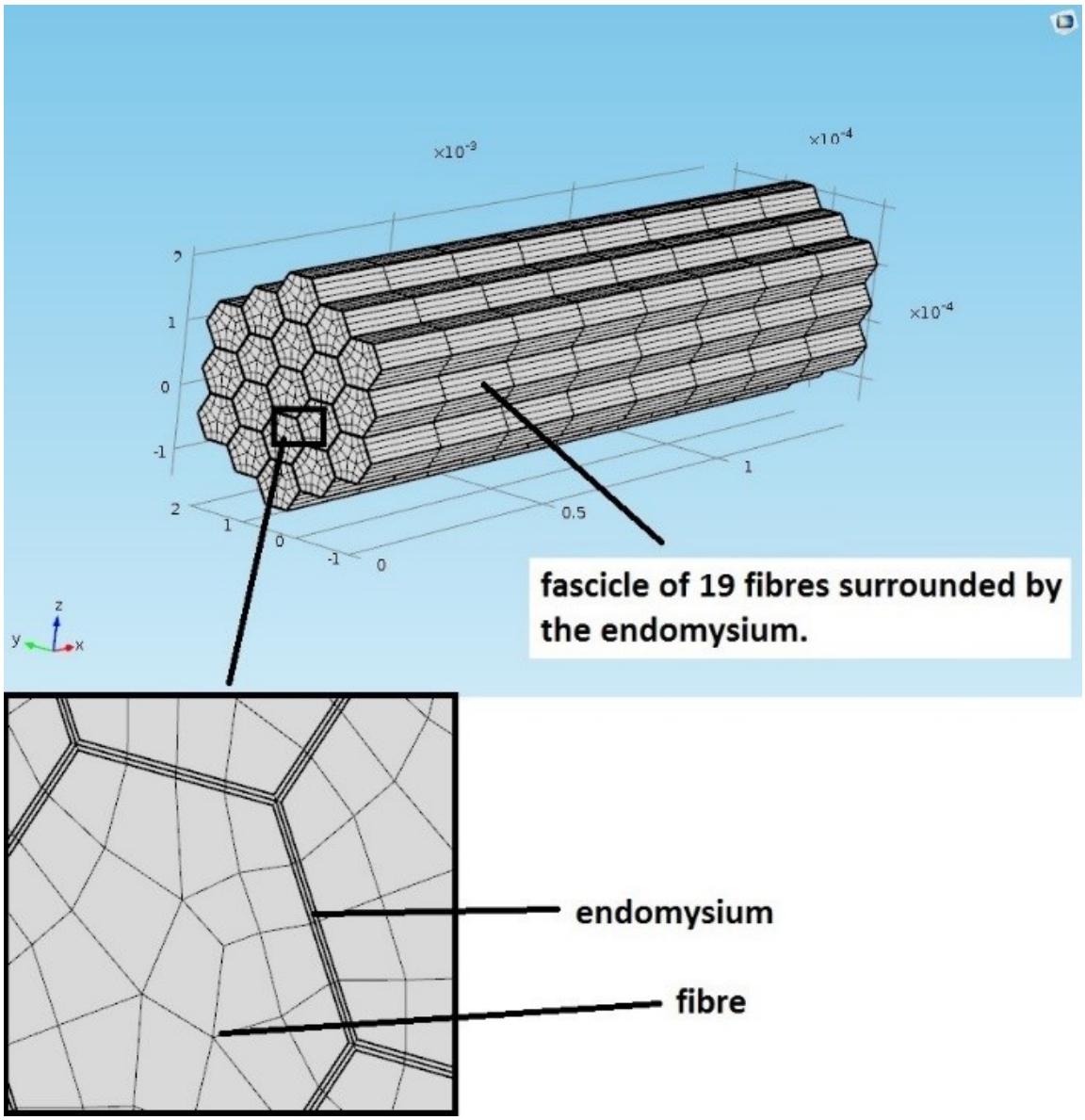

Figure 5.2 Mesh of the bundle of fibres

Table 5-1 Mesh specifics of the bundle of fibres

Maximum element size	200 × thickness (aspect ratio 50)
Minimum element size	0.9092 µm(endomysium thickness[131])
Maximum element grow rate	2
Curvature factor	0.3
Resolution of narrow region	0.1

5.2.2 Convergence study

A mesh study was performed to verify the accuracy of the solution. To reduce the computational cost only a bundle of seven fibres was simulated using a symmetrical boundary condition (see Figure 5.3). The symmetry condition was applied only on the mesh study and not on the bundle of 19 fibres used in the case study.

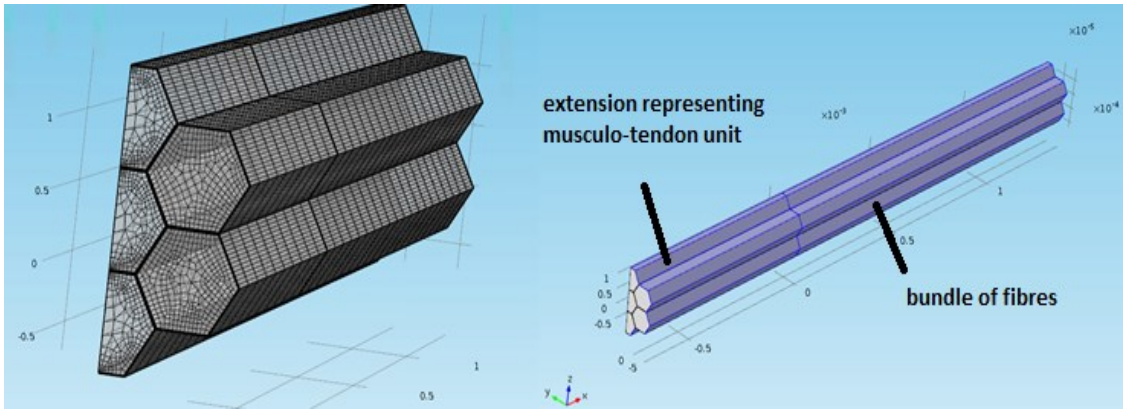

Figure 5.3 Mesh (left) and domain (right) of the model for the mesh study. A bundle of seven fibres was simulated applying a symmetry condition to reduce the computational cost. The model has two material properties: one representing the musculo-tendon unit and one representing the section of bundle of fibres.

The bundle included the extended tissue representing the muscle tendon unit, and the fibre bundle. No axial displacement was set at the extremities of the whole bundle, while a fixed constraint was applied on the boundaries surrounding the bundle. The fibre in the center was activated and four probes were located in the middle of the bundle (see Figure 5.4).

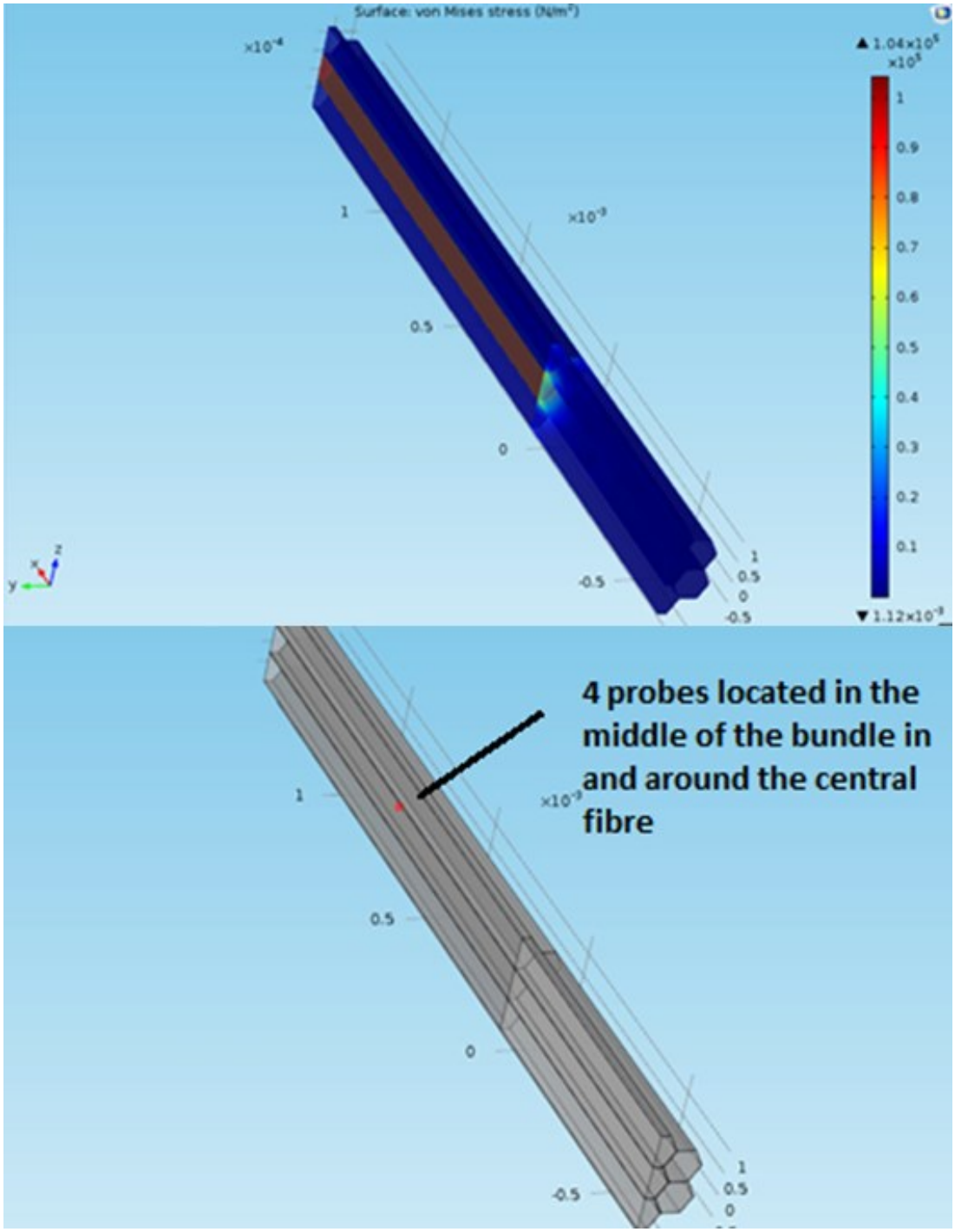

Figure 5.4 Simulated bundle of fibres. (Right) the fibre in the centre of the bundle was activated (red domain). (Left) four probes in the middle of the bundle recorded the Cauchy axial stress values at different mesh refinement.

The bundle of fibres in the simulation represents a small section in the middle of the fascicle (to exclude the tapering of the fibres end). Therefore, an extending domain was added to include the stiffness contribution of the continuing tissues (muscle tendon unit). In addition, the fascicle was enveloped by a domain representing the surrounding muscle tissue (see Figure 5.5).

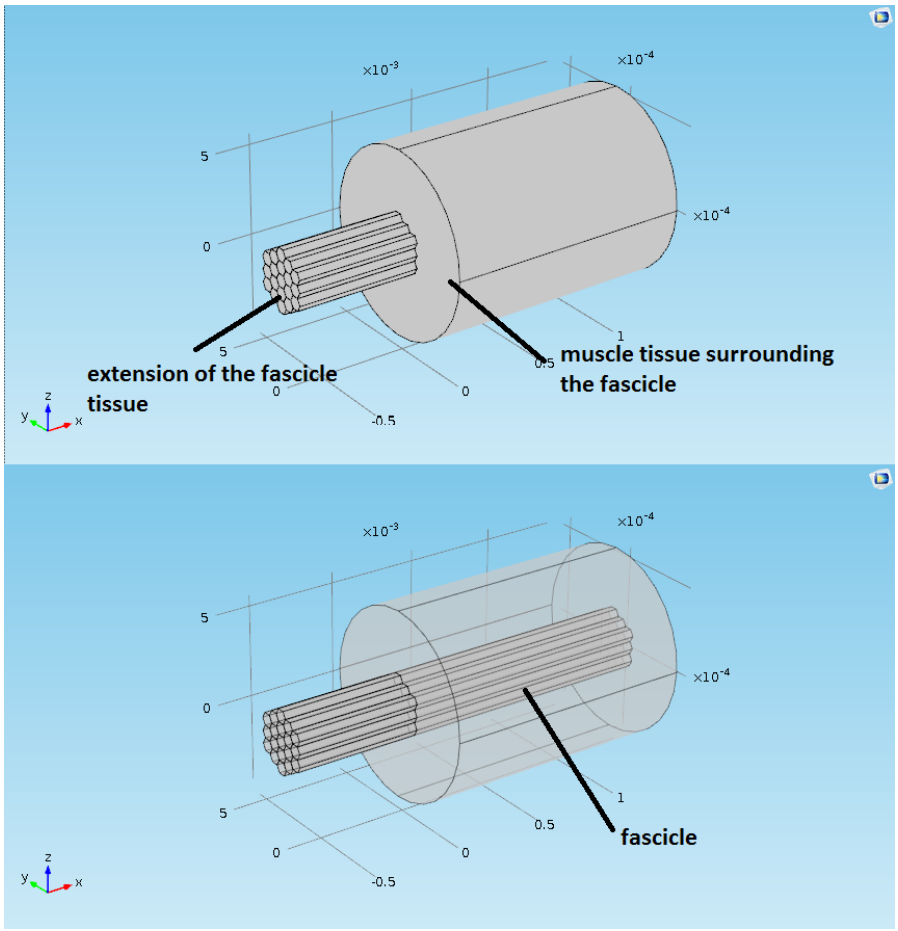

Figure 5.5 Fascicle surrounded by the muscle tissue. An extension of the fibre was added to represent the musculo-tendon complex.

The constitutive properties and the FE formulation are described in chapter 4.2. The muscle tissue passive behaviour (titin contribution) was modelled (see equation 5.1) as a non-linear elastic material, by fitting a second order polynomial (equation 5.1) to experimental results on soleus fibres (titin contribution) [136].

$$\sigma = 176340\varepsilon^2 - 24703\varepsilon + 505.13 \quad . \quad (5.1)$$

In this case the stress-strain relationship defines the axial behaviour of the fibre which was added as a Second Piola Kirchhoff stress in the base material stress formulation.

The surrounding tissue represents the overall muscle and connective tissue and an Ogden hyperelastic model (see equation 5.2) was used to model it [165]:

$$W(\lambda_1, \lambda_2, \lambda_3) = \sum_{p=1}^{N} \frac{\mu_p}{\alpha_p} (\lambda_1^{\alpha_p} + \lambda_2^{\alpha_p} + \lambda_3^{\alpha_p} - 3) \quad . \quad (5.2)$$

This strain energy is a function of the principal stretches. The parameters were fitted using in vivo experimental compressive tests data ($\mu_p = 15.6\ kPa$, α_p= 21.4) of the tibialis anterior of rats [165]. This model was chosen because as the fibres contract, it compresses the surrounding tissue. The extension of the fascicle tissue represents the muscle-tendon unit, modelled as a linear elastic material. Stiffness values were based on data results of the Achilles tendon of young and middle aged rats (1.390 ± 0.138 and 1.984 ± 0.146 N/mm respectively) reported by Plate [159]. The rats were 8 months (young) and 24 months (middle) old; which correspond to 18 and 52 human years

assuming that 13.7 rat days is equivalent to 1 human year. Two Young's Moduli were derived from these stiffness values from the linear elastic theory:

$$E = Young's\ Modulus = \frac{KL}{A} \quad , \qquad (5.3)$$

where K is the stiffness, L is the length of the tissue considered (half of the fibre length) and A is the total area.

5.2.3 Boundary conditions

The model is simulating an isometric contraction; therefore, the fascicle is constrained to no axial displacement at the extremities. The outer layer of the surrounding muscle tissue domain is fixed to represent the inertia of the whole muscle (See Figure 5.6).

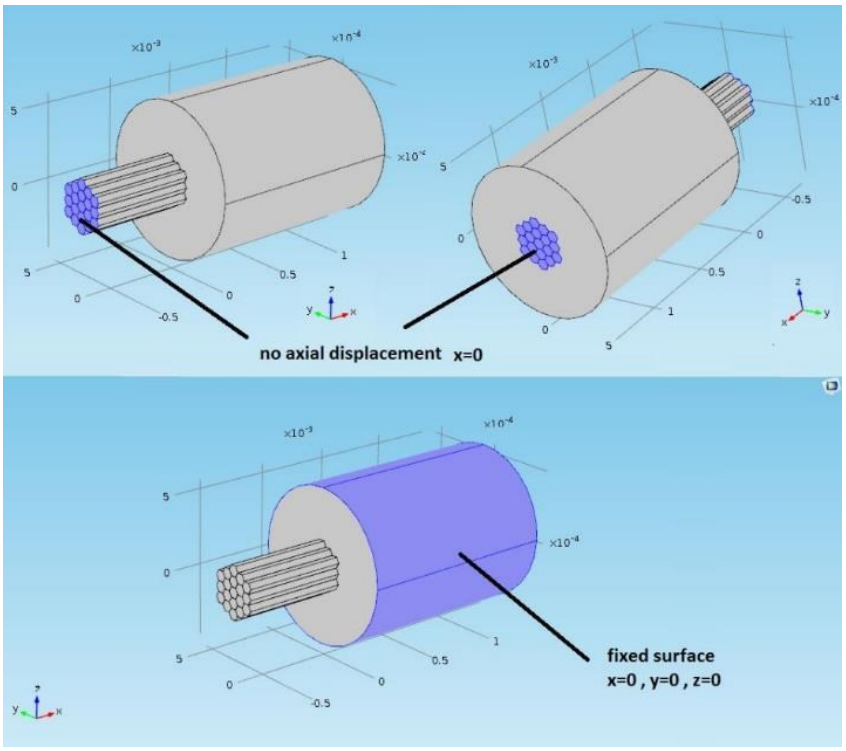

Figure 5.6 Illustration of the boundary conditions. The fibre and the extension are constrained at the extremities (no axial displacement), but can expand in the z and y directions. The surrounding tissue is completely fixed at the outer layer.

5.3 Results

5.3.1 Convergence Study

The probes recorded the axial stress and four levels of mesh refinement (from 2716 to 9312 elements) were simulated. The results reported in Figure 5.7 show that the model has converged and that a mesh with this design could be used to model the muscle

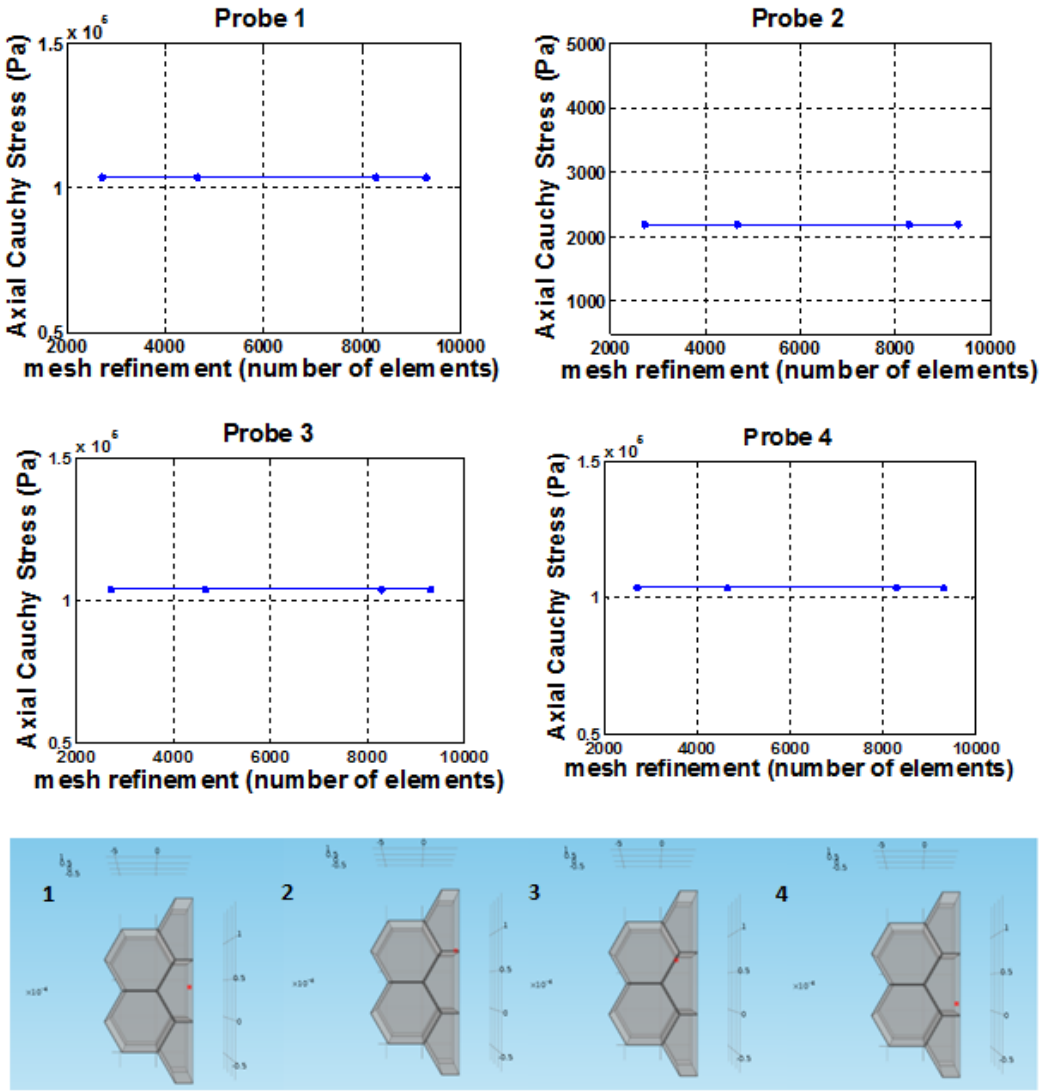

Figure 5.7 Mesh refinement study for a seven fibres bundle. The axial stress is reported for each of the four probes at different mesh refinement. All the results converged.

5.3.2 Bundle of fibre

The results for the bundle of 19 fibres showed no differences in the total force transmitted to the passive fibres with different activation patterns (see Figure 5.8).

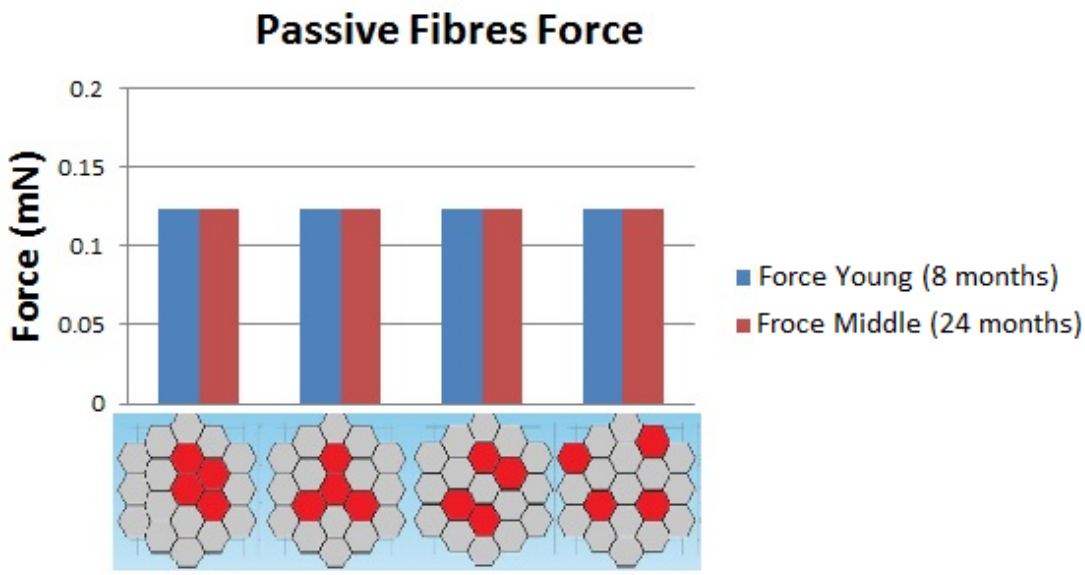

Figure 5.8 Passive fibres force (20% activation). There is no difference in the force transmitted to the passive fibres (grey fibres) between activation cases and between age population.

In the case of 37 % of activation the results are still equivalent, although the total force recorded is lower as there are fewer passive fibres (see Figure 5.9).

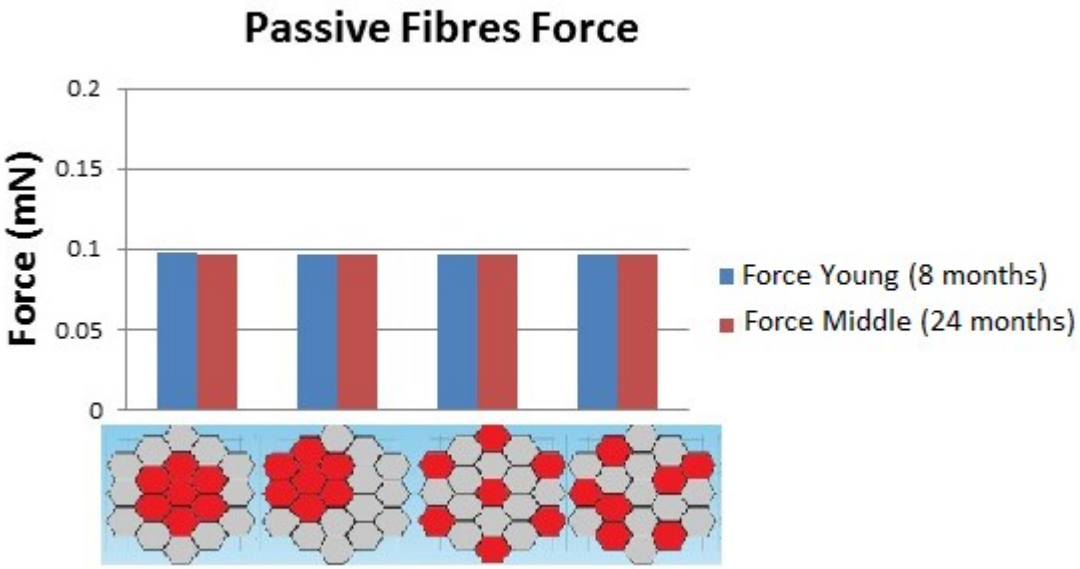

Figure 5.9 Passive fibres force (40% activation). There is no significant difference of the force transmitted to the passive fibres (grey fibres) between activation cases and between age populations.

Considering one activation pattern (distribution 1 of 20 %, see Figure 5.1 Eight cases of activation pattern (red color).) case, two more simulations were performed with a compliant extended tissue (E = 5 kPa) and a stiffer (E = 30 MPa) extended tissue. This to verify whether changes occur with more radical properties. These simulations did not show a significant difference, in line with the previous results (see Figure 5.10).

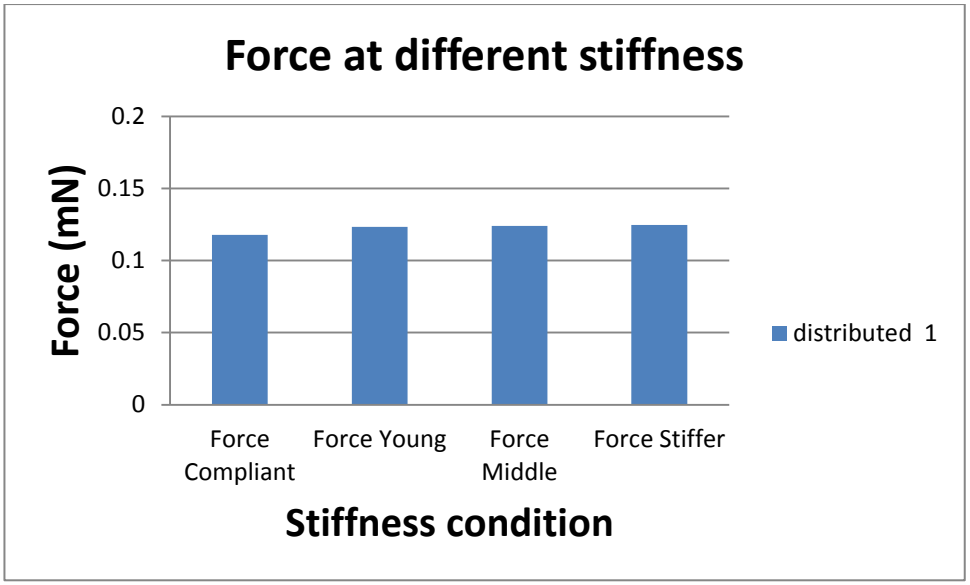

Figure 5.10 Passive fibre forces with a range of tissue stiffnesses simulated. There is no difference in the passive force transmitted to the fibres between stiffness cases of the extended tissue. A compliant stiffness (5 KPa), a young (8 months rat) and middle age (24 months rat) stiffness taken from literature and a stiffer case (30 MPa) were considered.

A cross section in the middle of the fibre was considered to explore the distribution of the strain and the stresses (see Figure 5.11 and Figure 5.12). No significant differences were found between the young and the middle age cases. In Figure 5.11, the axial stress is represented, normalized by the maximal isometric stress (101800 Pa). Hence the active fibres have a value of one while the surrounding fibres reach a value of almost 2 % (~ 2000 Pa) due to the force transmission. The strain seems to be greater (see Figure 5.12) toward the middle of the fascicle away from the interface with the surrounding tissue which is stiffer and has a bigger dimension. Similar results were found for a 40 %

activation (see Figure 5.13 and Figure 5.14), with higher value of strain due to the fact that more fibres are activated.

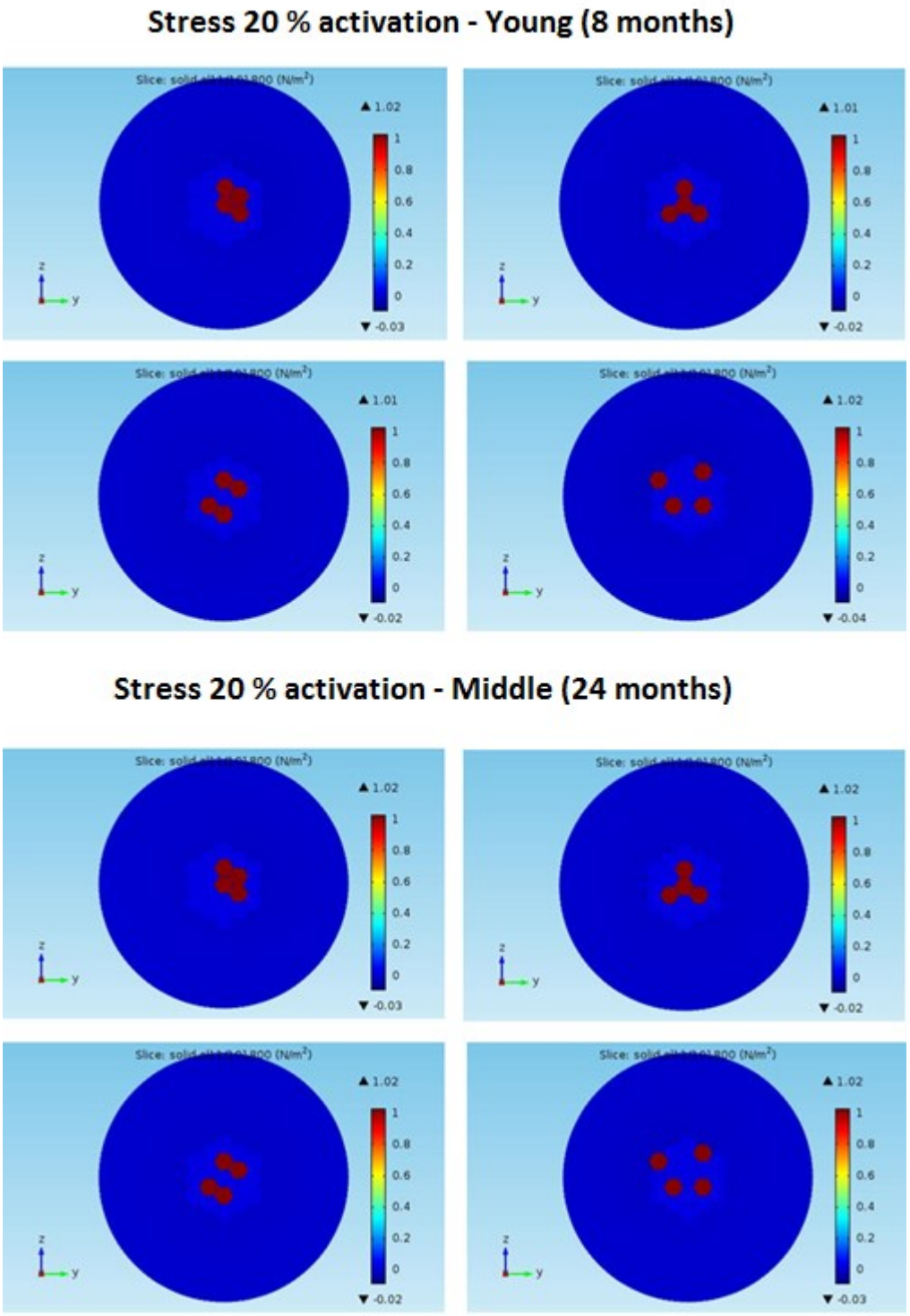

Figure 5.11 Cross Section (Stress). A cross section in the middle of the bundle of fibres reveals the activation pattern (in the colour bar, red= maximum stress).

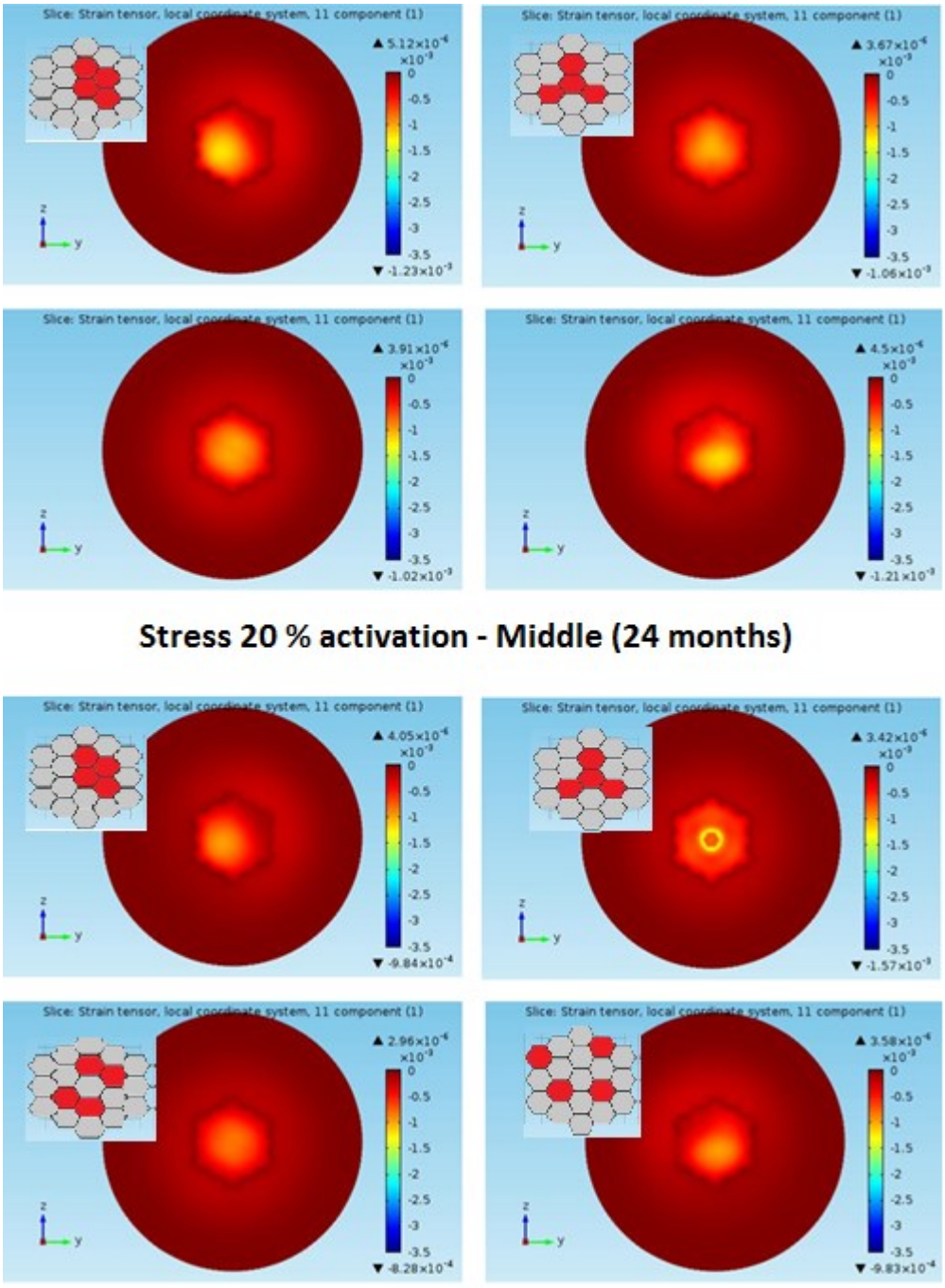

Figure 5.12 Cross Section (strain). The strain tends to be higher toward the centre of the bundle, specifically for the second clumped activation (top right). These differences are very small due to the isometric nature of the simulated contraction.

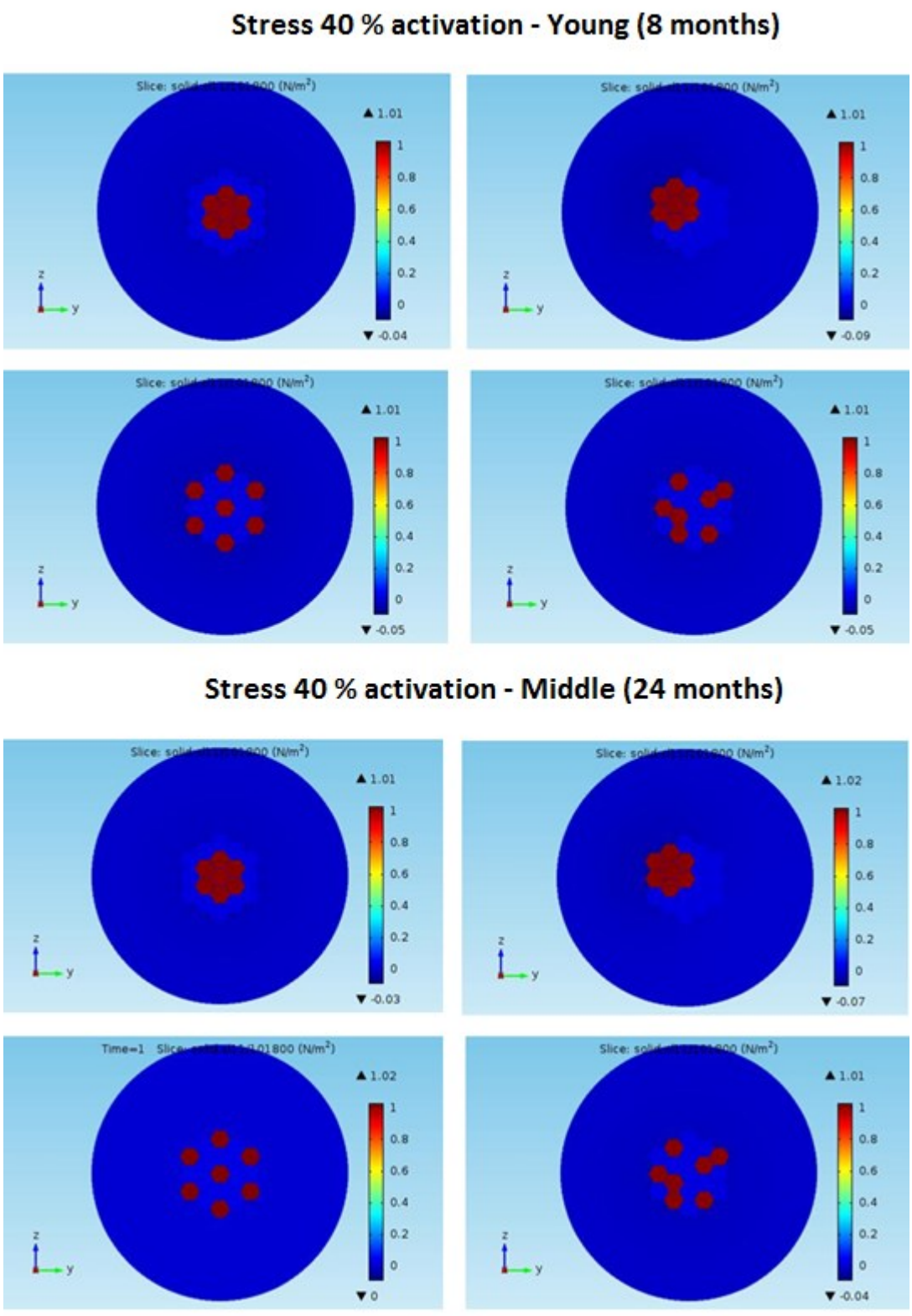

Figure 5.13 Cross Section (Stress). Activation stress pattern when 40 % activation, the stress values are normalized by the maximal isometric stress.

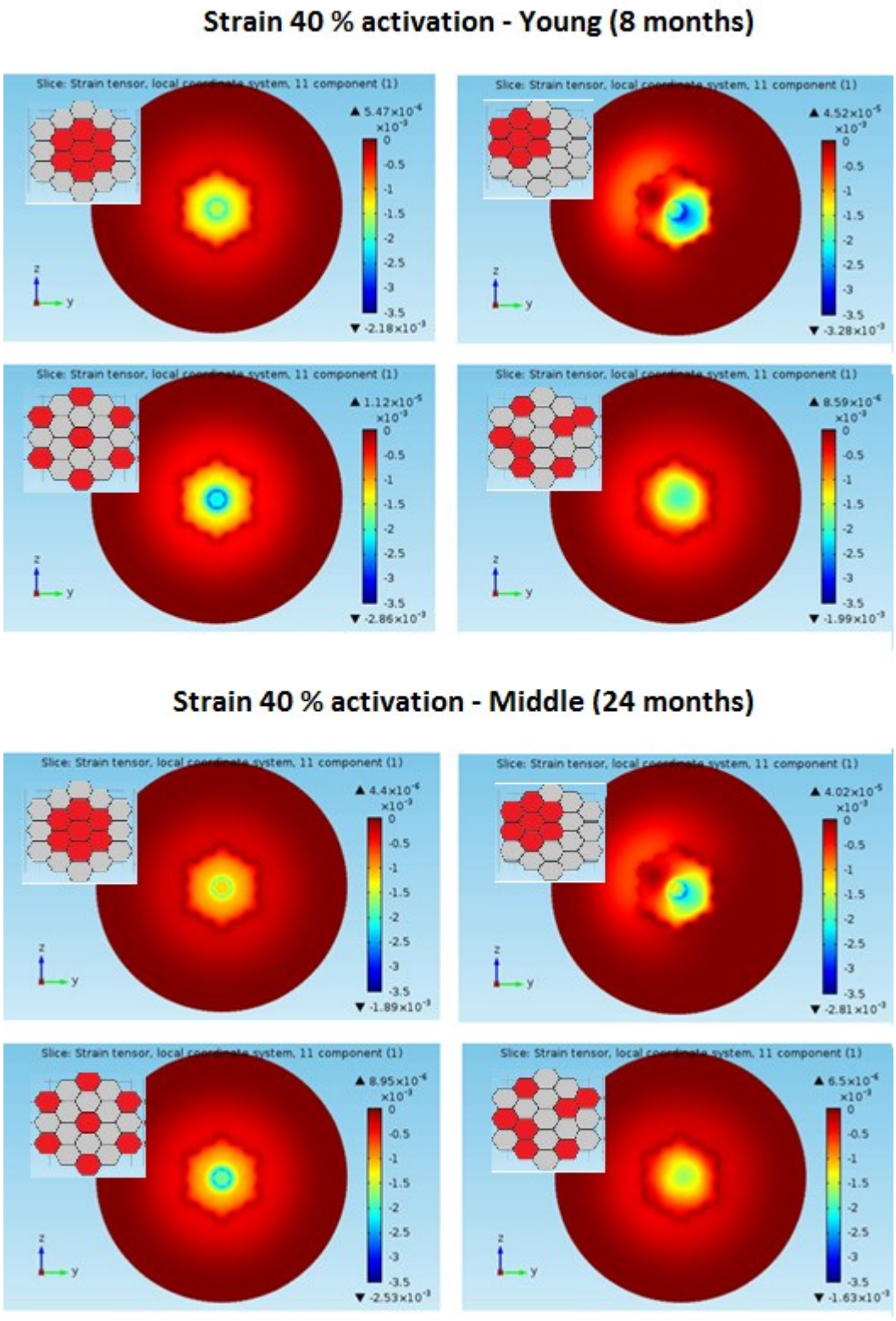

Figure 5.14 Cross Section (Strain). The strain tends to be higher in the middle of the bundle, away from the stiffer surrounding tissue the same as the 20% activation pattern.

5.4 Discussion

The fibre packing is the clustering of fibres belonging to the same motor unit. This is not a normal physiological condition as fibres belonging to the same motor unit are randomly distributed across the muscle or across a region of the muscle[157]. This fibre packing/clustering occurs in aged muscle [25, 35] and is the consequence of what is called axonal sprouting where slower motor units recruit denervated fibres from faster motor units[166]. The consequence of this remodelling (change in the fibre number per motor unit and number of motor units) is a decrease of the total muscle force [25, 155]. There are not many sources in the literature, which specifically discuss the consequence of the altered distribution of the muscle activation due to aging. A new method to quantify the age-related packing or clustering was implemented only recently by Greising *et al*. [167]. The focus is more on the phenomenon of slower motor units recruiting fibres of faster (type II) motor units [25] and not on the morphological consequences of it, which is the fibre packing.

There are not muscle models that address this either and that is the reason that motivated this investigation. The results showed no significant differences in transmitting the force when the activation pattern is changed, but the strain pattern showed in Figure 5.12 and Figure 5.14 revealed that in the fascicle the strain is higher in regions far from the interface with the surrounding tissue. And when the active fibres are activated and packed close to the interface, higher strains are observed on the opposite side (see Figure 5.12 first clumped activation and Figure 5.14 second clumped activation). The potential effect of this is an unbalanced distribution of the stress, which could cause damage of the fascicle during dynamic and/or high loading conditions. In

the performed simulation, the strains were small since only an isometric contraction was considered and the stress transmitted to the passive fibres was only 2 % of the maximal isometric stress. Therefore, an implication of the outcome of this work is that the motor units remodelling associated with aging, does not decrease the force capacity only, but could lead also to unbalanced strains and a damage of the tissue at high strain levels and dynamic conditions.

When changing the stiffness of the extended tissue, no significant changes occurred to the force transmitted (see Figure 5.10), indicating that strains are unaltered within the muscle tissue. A possible alteration can occur at the muscular-tendon junction as suggested by Sharafi *et al.* [4]. The model showed that peak strains occur when the endomysium is more compliant, and that this peak strains are located near the muscular-tendon junction.

This model was built using constitutive properties taken from literature. The bundle of fibres model represents only a portion of the total fascicle length, and that motivated the addition of a domain as an extension to the tendon. Considering only a portion is a limitation in term of representing the whole fibre, but gives the advantage of a less computational cost plus the exclusion of the tapering of the fibre, which was not meant to be part of the study. Each material property was taken from a different source and ideally, a study, which is carried out along with experimental micromechanical tests would be ideal. Future studies will take into consideration the portion of fibres at the muscular-tendon junction. In this case, the tapering of the fibres should be taken into consideration. This model can also represent a bundle of fascicle (bigger scale) and the consequence of different volume fraction studied in chapter 4, must be revisited since

bigger dimensions are involved. Indeed fascicle seems to play a different role from the endomysium [11], allowing higher strain to accommodate the shape changes of the muscle.

5.5 Conclusion

The clustering of fibres of the same motor units is one of the consequences of motor unit loss and reinnervation. In this study, isometric contractions of a bundle of fibres were simulated at different activations patterns. Two patterns described the normal physiological condition (random distribution), and the other two described the condition of fibres clustering. Results did not reveal significant quantitative changes, but the strain pattern might suggest an uneven redistribution of the force within the fascicle that can cause damage for higher level of strains.

6 . Thesis Discussion

6.1 Overview

In this thesis two factors that contribute to features of skeletal muscle mechanics were considered: i) the activation signal that triggers muscle contraction and ii) the connective tissue, which contributes different roles at different dimensional scale levels. The activation signal can be analysed through sEMG, but research need to be done to be able to properly interpret these measurements. The role of the connective tissue is another research area, which is becoming important due to the discovery of its functional role in force transmission. In the literature review (chapter 2), It has been shown how FE models can answer some of the research questions in these areas. New FE models that used a different approach were proposed and discussed in chapter 3 and chapter 4,5. In this chapter, the contribution to the knowledge and the conclusion will be discussed. Furthermore, future perspective will be presented.

6.2 sEMG Electrode Design Study

Skeletal muscle activation can be monitored through sEMG or iEMG. These measurements are affected by noise or other signal sources and by the complex muscle structure and the dielectric property that alters the input signal detected. For instance, the pennation will lead the signal to travel away from and toward the detecting electrodes, a consequence of which is an alteration of the signal, which should not be accredited to a different motor unit's activity or tissue properties. Therefore, methods that optimize and increase the selectivity and accuracy of these measurements are needed. The findings presented here can be useful to work focused on updating current guidelines [92] on electrodes configuration for sEMG recording. This has been a topic

brought to the attention in the ISEK (International Society of Electrophysiology and Kinesiology) Conference in 2014, which dedicated a specific session: “Is it time to update recommended sEMG?”. The reason the guidelines were drawn out was not only to promote good practice, but also to guarantee common recognized standards that help evaluation of the validity of research outcomes. Further guidelines can be added to take into account the muscle sizes (fibre length, muscle CSA, skin and fat tissues thickness, etc.), the three dimensional pennation and the interpretation of the EMG during dynamic contractions. Muscle FE models can provide a very useful tool to explore different scenarios that can lead to new guiding principles for different muscles. Several models have previously been implemented to describe the muscle tissue volume conductor properties. From analytical models [66-68] to more advanced FE models [5, 6, 76]. Mesin *et al.* [71] FE model considered the curvature of the fibres while contracting. The implications of dynamic contractions are changes of the conductivity properties of the tissue, the relative distance between the electrode and the source and the relative position of the tendons (the end-effect of action potential becomes more relevant). The consequences of these are changes in the amplitude and frequency content. For instance, the model showed that the average rectified value can be reduced of one third when the fibre shorten to 50% and this effect is less pronounced for superficial fibre since their relative position respect to the electrodes does not change significantly. The shortening muscle also affects the detection systems differently. Monopolar measurements are less affected than bipolar because of a higher contribution of the non-propagating component (standing wave at the interface between muscle and tendon). A limitation of this model was the lack of the skin and fat layer, which are essential to represent properly the filtering properties of the muscle as

discussed in chapter 2. Lowery *et al.*[6] cylindrical model showed that the presence of the fat and skin layer increase the potential amplitude while the rate of decay with angular displacement of the detecting electrodes from the source signal decreases. Lowery *et al.*[6] investigated also the consequence of the presence of the bone. It was shown that the potential on top of the bone increases when the source is close above the bone (decreases on the opposite side) and when bone is close to the surface. The presence of the bone did not bring significant variations when located in the middle of the muscle and far from the source signal. Later on Lowery *et al* [5] proposed a detailed anatomical based FE model and compared it with a cylindrical layered symmetric model. The anatomical model included the fat and skin layers, the bone and vessels. Furthermore, the model presented an asymmetry geometry. All these factors contributed significantly to change the shape of the single action potential detected, but for general feature of the EMG such as the rate of decay and firing rates, the cylindrical model was revealed enough representative.

The main limitation of these FE models is the fact that they are phenomenological and no direct comparison with experimental data is possible since the source signal is also simulated. A mutli-scale chemo-electrical mechanical FE structural model was recently implemented by Mordhorst *et al.* [168]. This model incorporated an electrical model to an improved version of the physiologically based mechanical model proposed by Rohrle *et al.*[106]. The bidomain continuum model (defined in all the space), typically used to describe the heart electrophysiology, was used to link the intracellular and extracellular potential. This model opened perspective in study physiological aspects of the muscle, such as the muscle fatigue reflected into the electrical activity. Despite this, it is very

complex and it would not be suitable for the phenomenological aspects described so far. The main reason being the fact that it is not possible to estimate the number of fibres unless the muscle is dissected and analysed in vitro. In addition, the motor units' distribution is unknown and cannot be accurately estimated. The proposed model tried to overcome this issue by using experimental data as source signal. This implies some assumptions as well that will be discussed.

6.2.1 Contribution to existing knowledge

Previous FE models were able to clarify the effect of some muscle characteristics on the detected surface EMG. These models used a phenomenological approach that simulate the current/potential source of a single action potentials or group of single action potentials distributed in the muscle. The main limitation of this models, is that fact that they cannot replicate the experimental source condition, since it is not possible to know some features such as the number of fibres and motor units distribution.

In the work presented within this thesis (Chapter 3), a new approach is used. An experimental iEMG is used as source signal and represents the total sum of the action potentials from different MUs. The models study the effect of different electrode configurations on the time-frequency properties of the sEMG signal, whilst also considering the implications of a pennate architecture. To my knowledge, these factors have not previously been deeply investigated using the more representative FE

modelling approach, although the surface potential solution of an analytical model of a bipennate architecture was given by Mesin and Farina [125].

The novelty of the work presented in this thesis is to consider the source signal as the overall MUAPs acting at a certain depth in the muscle, hence use experimentally recorded myoelectric signals. This allows a direct way of evaluating the results with experimental sEMG (given a realistic anatomical model). In addition, the time-frequency analysis applied gives insight into the filtering properties of the tissues and can be used to estimate a correction or weighting factor in muscle models where slower and faster motor unit activities are considered independently [20]. Specifically, the study reported in chapter 3 revealed a strong low pass filtering of the signal when pennation is high. The higher frequency signal components were more affected, which indicates that interpretation of motor unit recruitment may be influenced by pennation angle.

Limitations in the acquisition of the source signal used in the presented work did not allow a direct validation of these data, as the fine-wire electrodes and amplifier used had a bipolar-configuration which detected only a limited amount of fibre activity in the pick-up volume range, so no comparison is presented with the surface signal. Furthermore, the experiment involved low level isometric contractions to reduce the number of motor units involved so that the iEMG could be more representative. The capacitive effect of the tissue were not included in this work. Lowery et al. [5] model showed that capacitive effects induce a temporal low pass filtering (phase shift) of the measured potential, and a decreased amplitude of the end-fibre effect component. In the presented model, there is one source signal representing the sum of the MUAPs. Therefore the whole signal will be delayed and the consequences are not as relevant as

with multiple sources being filtered in different way and time. Despite this, a further investigation is needed to clarify the capacitive effects. This model presented also a planar geometry, which allowed the control of the pennation and the travelling source. Despite this, it is necessary to include the curvature and eventually the bone to be able to compare the results with experimental data. This approach can be of direct use for developing electrodes systems with the best configuration and design for a given muscle or activity to be studied. An early example of application was presented in chapter 3 along with the formulation.

6.2.2 Future perspective

The electrical model presented within this thesis should be considered to be an early work, aimed at laying the foundations for future development of more anatomically realistic FE models where the source signal is based on experimental data. Therefore future development of the presented work should include:

- The fibres curvature and the bone in the model:

The curvature of the fibres can change the action potential shape and hence the spectral content of the signal [71, 169, 170]. In addition, the curvature and inhomogeneity of the whole muscle tissue is also an influencing factor [6]. The model proposed by Lowery *et al.* [6] had also showed how the bone can increase the amplitude of the sEMG if it is close to the skin, while the effect is negligible if it is located deeper. Mesin *et al*. [71] introduced a conductivity tensor to take into account the curvature of the fibres, demonstrating that this feature changed the detected potential spectral content when

the muscle is shortening. Therefore, an improvement to the model presented within this thesis would be to extend it to include the curvature of the tissue and the bone, which in turn would require the source signal to run also on a curved surface.

- Incorporation of monopolar signal acquisition to improve the representativeness of the source signal:

As monopolar acquisitions have wider pick up volume [68] they can give a source signal that is more representative of the motor units action potentials of the whole muscle. A further study comparing monopolar iEMG at different depths can further confirm the validity of using one source signal in the model for lower values of isometric activation.

- Validation and applications of the model:

To validate the model reported here, the geometry should first include features that are proven to consistently influence the potential detected on the surface (e.g. curvature, bone and source signal, as described above). Once the model is improved, it can be adjusted to fit the anatomical dimension of the muscle(s) of interest. A comparison then will be possible between the experimental surface potential and the simulated surface potentials. Another validation involves the comparison of the model results with sEMG of pennated muscles where the pennation geometry is known. Based on Darby *et al.* [171] work (see Figure 6.1), it is possible to track the fascicle curvature of muscle fascicles through B-mode ultrasound image sequences. The gastrocnemius has short fibres compared to other propulsive muscles of the lower limb; hence, it is suitable for ultrasound imaging where the scanning transducers are small and can detect only a limited portion of the muscle tissue at a time. A novel technique allows a simultaneous detection of ultrasound images and sEMG [129]. This can help to set the model

geometrical parameters and compare the sEMG recorded with the sEMG simulated, or confirm the filtering behaviour.

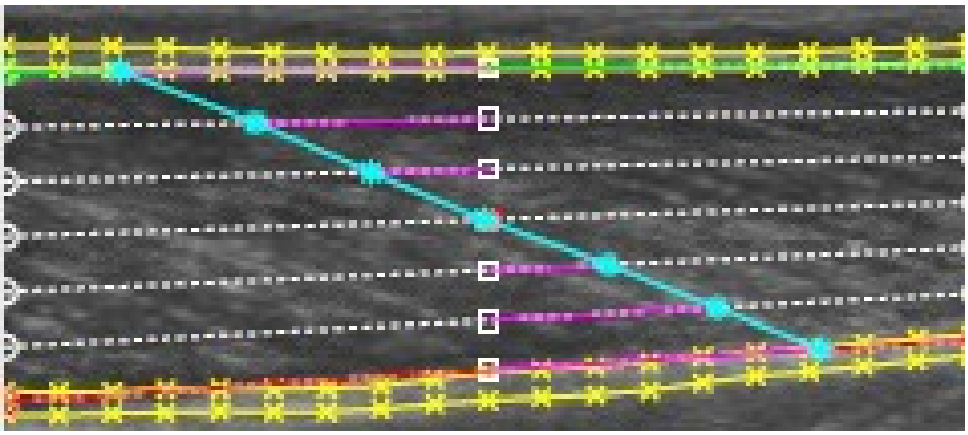

Figure 6.1 Fascicle tracking technique from ultrasound imaging (adapted from [171]) of the gastrocnemius. It is possible to see how the algorithm detect the deep and superficial aponeurosis (yellow markers) and estimate/track the fascicle orientation (blue line) as the fascicle is contracting.

6.3 Micromechanical Model of Skeletal Muscle

The connective tissue in skeletal muscle is composed of layers of collagen fibres in an amorphous matrix. The type of collagen fibres and their organisation changes according to the dimensional scale. This is because the connective tissue assumes different roles in different scales [131]. The endomysium surrounds the myofibers and its role is to transmit the force laterally, the perimysium has more collagen layers and its role is to

accommodate shape changes and transmit the force to the tendon aponeurosis. The epimysium contains the muscle and also contributes to the force transmission [130]. Purslow [13] showed how the perimysium allows fascicle translation whereas the endomysium transmits the force laterally and drags the passive fibres as the active ones are contracted.

Age related alterations of the muscle tissue, such as those related to sarcopenia, presents serious personal, societal and economic challenges related to the increasingly ageing demographic. These challenges are largely related to reduced capabilities to live independently and increased risk of injuries related to falls, which occur due to muscle weakness that compromises the normal muscle function, co-ordination and hence completion of motor tasks. The higher injury risks are exacerbated by co-factors such as bone frailty (osteoporosis) [172]. Clinical conditions such as sarcopenia reflect alterations in skeletal muscle properties. The stiffness and content of the connective tissue can increase [143, 160] and motor unit remodelling can lead to clustering of active fibres [167]. Investigation of the specific functional consequences of these changes to the material properties of the muscles is required to lead to a better understanding of how to improve the quality of life of people affected by sarcopenia. Modelling is a method to explore these consequences and overcome the limits of experimental study, specifically when carrying out invasive experiments on human subjects.

The FE method upgrades and extends the capabilities of lumped parameters muscle models. The advantages of FE models mainly relate to the possibility to extend the physical problem to complex “non-ideal” geometries, whereas analytical problems often require an idealization of the architecture such as infinite layers or symmetric and

simpler geometries. Currently, mathematical models are being developed to enable investigation of how this force is transmitted and which mechanical or geometrical (such as fibres length) properties can permit such transmission [3, 143]. Blemker *et al.* [57] FE model, introduced a new formulation that can be used for macro and micro studies, and where the longitudinal/transverse to fibres shear properties were incorporated in the constitutive model. These characteristics made the model suitable for studying the interaction between the fibres and the endomysium. Sharafi and Blemker [3] mathematical model verified how lateral force transmission through endomysium is possible at physiological ranges even with a low shear modulus due to the very thin endomysium layer (while the fibre is much longer). Another Sharafi et al. [4] model suggested that higher likelihood of injuries during muscle active lengthening, could be because of higher strain at the myotendinuos junction and that the endomysium play an important role in reducing these strains. In this thesis, the focus is to build a micromechanical model that can be used to study age related alterations of the muscle tissue. The mechanical study in chapter 5 investigated the micromechanical properties of the muscle tissue when affected by tissue stiffness and spatial organisation of activated fibres, which reflect changes reported to occur with age related degeneration.

6.3.1 Contribution to the knowledge

The FE model implemented in this thesis (bundle of fibres, Chapter 5) offer tools that can be used to investigate the functional implications of altered properties of the muscle tissue at a microscopic level. The functional effects of clustering of fibres belonging to the same motor units, to my knowledge had not been investigated in detail before, but

is known to be a consequence of age-related motor unit remodelling [167]. Results in the presented study showed that at the microscopic level there is a very small variability of the stress in the passive fibres due to the nature of the simulation applied (small bundle, isometric contractions), however high stress concentrations might occur if larger, deformations were considered. From the results presented, it can be inferred that higher strains occur toward the middle of the fascicle. These higher strains can lead to an injury of the fascicle in a similar way described by Sharafi *et al.* [4] when considering higher strain at the myotendinous junction. This model present the limitation of considering low level of activation contractions and higher stress/strain can occur during muscle dynamic. The possible variability of the fibre geometry was not considered, but it was showed that the myofibers are more uniform and tend to have a rounded shape [2], therefore an homogeneous structure is a good approximation of the fibre bundle.

6.3.2 Future Perspectives

This study is part of a bigger project that aims to combine computer simulations with experimental studies, because this approach can provide a better understanding of the functional role of each determinants of the muscle force (activation, connective tissue, geometry, etc..). For this reason, future work will include validation of the model with experimental studies and the creation of new homogenous constitutive properties based on experimental tests. One component of future work it is hoping to achieve is to test mice myofibers *in vitro* to evaluate the force exerted, the fibre type and the shear interaction with the connective tissue. This work is required, as the literature review

revealed that one of the main gaps in the literature is the availability of experimental values of muscle properties, which are required to develop FE models such as the ones presented. Collecting such experimental data is technically challenging, and it may not be possible to gain data from individual fibres within a small bundle as currently no technique exists to activate only one or a few fibres within a bundle as the whole bundle is stimulated altogether. In addition, due to the chemical process involved in fibre typing, the type of fibres can be estimated only after the mechanical test which means that a selection of the fibre type to test cannot be made prior to the mechanical test. In addition to these ideas the presented work also lays the foundations for further studies of the functional significance of changes in skeletal muscle properties which may occur as a result of ageing, injury, pathology or therapeutic interventions.

Suggestions for such studies include:

- Studying the effects of changes in material properties associated with ageing:

From mechanical tests, it is possible to acquire the fibre behaviour (stress-strain relationship. These data can be used to be fitted to hyperelastic mechanical models. Equipment to perform mechanical tests on single or bundle of fibres, are available in the . Dissected muscle sample from old mice and rats, can be available and therefore constitutive models of young and aged muscle can be obtained.

- Extension of the proposed model to a macroscopic level

Changes in muscle functional capabilities may be significantly affected by factors such fat infiltration and fibrosis [154], which occur in relation to ageing, myopathies (e.g.

Musclular dystrophy), neuropathies (e.g. Motor Neurone Disease) and other diseases (e.g. diabetes). It is therefore proposed that the model presented here could be extended to a macroscopic level to verify whether decreased volume fraction due to fat infiltration has a bigger impact at a fascicle/muscle level than it has at endomysium level. Within such work, at a fascicle level the formulation can be the same, while when considering the whole muscle, the model should be able to track also the fibres direction during the contraction. A typical formulation that can satisfy that criteria is a strain energy function which depends on the invariants defined by Weiss *et al* (as in Rahemi et al., [60] Rohrle et al.[168]) and eventually the invariants defined by Criscione *et al*. [101] to include the shear properties as was successfully implemented by Blemker *et al*. [57]. In this way, the work presented can be used to provide a multi-resolution assessment of the skeletal muscle properties which can aid understanding of basic principles related to form and function and contribute to better clinical understanding of disabilities related to diseases of the musculoskeletal system.

6.4 FE model limitations

Both the electrical and micromechanical models could be further improved and by more rigorous validation with experimental studies. The general limitations are the numerical instability meaning that the FE simulation does not always converge; the complexity of anatomically based geometry (very challenging in the mechanical simulations) and the acquisition of experimental data. In this thesis, assumptions were made to overcome these problems, such as using a planar surface for the electrical model or considering a small portion of the fibres bundle. But future implementation will consider these

features. For the simulation, an intel core i7 machine with 3.40 GHz CPU clock speed and 16 MB of RAM was used. This machine allowed simulation times that range between 50 minutes (electrical model) to 120 minutes (mechanical models). A direct linear system solver was chosen. An iterative solver would have decreased the simulation time by reducing the memory and computational cost. The issue with the iterative solvers is that it does not guarantee always a convergence.

7 Thesis Conclusion

7.1 Conclusion

This thesis has focused on developing and evaluating the capabilities of FE muscle models, with respect to understanding skeletal muscle form and function. It lays the foundation for future work by developing two new FE models that can be used for an electrode design/experimental protocol and investigation of factors, which influence muscle force production. Two types of studies were presented. The first study is a design study that can be used either for designing new EMG electrodes with the best configuration according to the muscle properties (mainly architecture) and may be valuable in the development of new guidelines for the use of bipolar EMG electrodes, revising the current internationally recognized SENIAM guidelines [92]. The second study is a micromechanical model of the muscle, which can explore some of the functional consequences of age related alterations of the muscle properties. The main findings from this work are that experimental EMG studies may not have yet optimised the experimental, hardware design to enable collection of the most insightful myoelectric data. For example, for pennation angle greater than 20°, more than 50% of the source signal was attenuated, which can be compensated by increasing the IED to 25 mm. In terms of the micromechanical properties of skeletal muscle, connective tissue is clearly important for force transmission. While no significant differences in strain were identified in the conditions simulated, changes in the strain patterns might suggest an uneven redistribution of the force within the fascicle that could cause damage at higher levels of force production or dynamic contractions. Both the models could be further improved and by more rigorous validation with experimental studies. The general limitations are the numerical instability meaning that the FE simulation does not always converge; the complexity of anatomically based geometry (very challenging

in the mechanical simulations) and the acquisition of experimental data. In this thesis assumptions were made to overcome these problems, such as using a planar surface for the electrical model or considering a small portion of the fibres bundle. Taken together however, the work represents a new approach to link experimental results with computer simulations that explore the functional significance of the muscle force determinants. The final aim is to be able to understand the impact of these determinants on aged muscle deterioration. Future work should aim to extend the models presented here to enable multi-resolution evaluation of skeletal muscle properties and fuller understanding of the consequences of electrode design on recorded experimental data.

References

[1] N. D. Reeves, M. V. Narici, and C. N. Maganaris, “Myotendinous plasticity to ageing and resistance exercise in humans,” *Exp Physiol,* vol. 91, no. 3, pp. 483-98, May, 2006.

[2] B. Sharafi, and S. S. Blemker, “A micromechanical model of skeletal muscle to explore the effects of fiber and fascicle geometry,” *J Biomech,* vol. 43, no. 16, pp. 3207-13, Dec, 2010.

[3] B. Sharafi, and S. S. Blemker, “A mathematical model of force transmission from intrafascicularly terminating muscle fibers,” *J Biomech,* vol. 44, no. 11, pp. 2031-9, Jul, 2011.

[4] B. Sharafi, E. G. Ames, J. W. Holmes, and S. S. Blemker, “Strains at the myotendinous junction predicted by a micromechanical model,” *J Biomech,* vol. 44, no. 16, pp. 2795-801, Nov, 2011.

[5] M. M. Lowery, N. S. Stoykov, J. P. Dewald, and T. A. Kuiken, “Volume conduction in an anatomically based surface EMG model,” *IEEE Trans Biomed Eng,* vol. 51, no. 12, pp. 2138-47, Dec, 2004.

[6] M. M. Lowery, N. S. Stoykov, A. Taflove, and T. A. Kuiken, “A multiple-layer finite-element model of the surface EMG signal,” *Biomedical Engineering, IEEE Transactions on,* vol. 49, no. 5, pp. 446-454, 2002.

[7] C. A. Oatis, *Kinesiology : the mechanics and pathomechanics of human movement*, 2nd ed., Baltimore: Lippincott Williams & Wilkins, 2009.

[8] P. A. Huijing, “Muscle as a collagen fiber reinforced composite: a review of force transmission in muscle and whole limb,” *J Biomech,* vol. 32, no. 4, pp. 329-45, Apr, 1999.

[9] A. K. Peter, H. Cheng, R. S. Ross, K. U. Knowlton, and J. Chen, “The costamere bridges sarcomeres to the sarcolemma in striated muscle,” *Progress in Pediatric Cardiology,* vol. 31, no. 2, pp. 83-88, 5//, 2011.

[10] T. J. Patel, and R. L. Lieber, “Force transmission in skeletal muscle: from actomyosin to external tendons,” *Exerc Sport Sci Rev,* vol. 25, pp. 321-63, 1997.

[11] P. P. Purslow, “The structure and functional significance of variations in the connective tissue within muscle,” *Comp Biochem Physiol A Mol Integr Physiol,* vol. 133, no. 4, pp. 947-66, Dec, 2002.

[12] P. P. Purslow, “The ¤intramuscular connective tissue matrix and cell/matrix interactions in relation meat toughness,” in Proceedings of the 45th International Congress on Meat Science and Technology,, Yokohama., 1999.

[13] P. P. Purslow, and J. A. Trotter, “The morphology and mechanical properties of endomysium in series-fibred muscles: variations with muscle length,” *J Muscle Res Cell Motil,* vol. 15, no. 3, pp. 299-308, Jun, 1994.

[14] C. Sherrington, “Ferrier Lecture: Some Functional Problems Attaching to Convergence,” vol. 105, no. 737, pp. 332-362, 1929.

[15] B. M. Nigg, and W. Herzog, *Biomechanics of the musculo-skeletal system*, 3. ed., New Jersey: John Wiley & Sons, 2007.

[16] R. E. Burke, D. N. Levine, P. Tsairis, and F. E. Zajac, “Physiological types and histochemical profiles in motor units of the cat gastrocnemius,” *J Physiol,* vol. 234, no. 3, pp. 723-48, Nov, 1973.

[17] E. Henneman, and C. B. Olson, “Relation Between Structure and Function in the Design of Skeletal Muscles,” *J Neurophysiol,* vol. 28, pp. 581-98, May, 1965.

[18] H. P. Clamann, “Motor unit recruitment and the gradation of muscle force,” *Phys Ther,* vol. 73, no. 12, pp. 830-43, Dec, 1993.

[19] E. F. Hodson-Tole, and J. M. Wakeling, “Motor unit recruitment for dynamic tasks: current understanding and future directions,” *J Comp Physiol B,* vol. 179, no. 1, pp. 57-66, Jan, 2009.
[20] J. M. Wakeling, S. S. Lee, A. S. Arnold, M. de Boef Miara, and A. A. Biewener, “A muscle's force depends on the recruitment patterns of its fibers,” *Ann Biomed Eng,* vol. 40, no. 8, pp. 1708-20, Aug, 2012.
[21] R. J. Monti, R. R. Roy, and V. R. Edgerton, “Role of motor unit structure in defining function,” *Muscle Nerve,* vol. 24, no. 7, pp. 848-66, Jul, 2001.
[22] T. M. Vieira, I. D. Loram, S. Muceli, R. Merletti, and D. Farina, “Postural activation of the human medial gastrocnemius muscle: are the muscle units spatially localised?,” *J Physiol,* vol. 589, no. Pt 2, pp. 431-43, Jan, 2011.
[23] E. Commission. "The 2015 Ageing Report: Economic and budgetary projections

for the 28 EU Member States (2013-2060)," 10/02/2016; http://ec.europa.eu/economy_finance/publications/european_economy/2015/ee3_en.htm.
[24] T. Lang, T. Streeper, P. Cawthon, K. Baldwin, D. R. Taaffe, and T. B. Harris, “Sarcopenia: etiology, clinical consequences, intervention, and assessment,” *Osteoporos Int,* vol. 21, no. 4, pp. 543-59, Apr, 2010.
[25] J. A. Faulkner, L. M. Larkin, D. R. Claflin, and S. V. Brooks, “Age-related changes in the structure and function of skeletal muscles,” *Clin Exp Pharmacol Physiol,* vol. 34, no. 11, pp. 1091-6, Nov, 2007.
[26] S. Barbat-Artigas, Y. Rolland, M. Zamboni, and M. Aubertin-Leheudre, “How to assess functional status: a new muscle quality index,” *J Nutr Health Aging,* vol. 16, no. 1, pp. 67-77, Jan, 2012.
[27] R. Roubenoff, and V. A. Hughes, “Sarcopenia: current concepts,” *J Gerontol A Biol Sci Med Sci,* vol. 55, no. 12, pp. M716-24, Dec, 2000.
[28] J. Lexell, “Human aging, muscle mass, and fiber type composition,” *J Gerontol A Biol Sci Med Sci,* vol. 50 Spec No, pp. 11-6, Nov, 1995.
[29] M. V. Narici, C. Maganaris, and N. Reeves, “Myotendinous alterations and effects of resistive loading in old age,” *Scand J Med Sci Sports,* vol. 15, no. 6, pp. 392-401, Dec, 2005.
[30] J. Lexell, C. C. Taylor, and M. Sjostrom, “What is the cause of the ageing atrophy? Total number, size and proportion of different fiber types studied in whole vastus lateralis muscle from 15- to 83-year-old men,” *J Neurol Sci,* vol. 84, no. 2-3, pp. 275-94, Apr, 1988.
[31] M. V. Narici, N. Maffulli, and C. N. Maganaris, “Ageing of human muscles and tendons,” *Disabil Rehabil,* vol. 30, no. 20-22, pp. 1548-54, 2008.
[32] M. V. Narici, C. N. Maganaris, N. D. Reeves, and P. Capodaglio, “Effect of aging on human muscle architecture,” *J Appl Physiol,* vol. 95, no. 6, pp. 2229-34, Dec, 2003.
[33] M. V. Narici, and N. Maffulli, “Sarcopenia: characteristics, mechanisms and functional significance,” *Br Med Bull,* vol. 95, pp. 139-59, 2010.
[34] N. D. Reeves, “Adaptation of the tendon to mechanical usage,” *J Musculoskelet Neuronal Interact,* vol. 6, no. 2, pp. 174-80, 2006 Apr-Jun, 2006.
[35] J. Lexell, C. C. Taylor, and M. Sjöström, “What is the cause of the ageing atrophy? Total number, size and proportion of different fiber types studied in whole vastus lateralis muscle from 15- to 83-year-old men,” *J Neurol Sci,* vol. 84, no. 2-3, pp. 275-94, Apr, 1988.
[36] V. M. Zatsiorsky, and B. I. Prilutsky, *Biomechanics of skeletal muscles*, Champaign, IL: Human Kinetics, 2012.
[37] D. H. Paterson, and D. E. Warburton, “Physical activity and functional limitations in older adults: a systematic review related to Canada's Physical Activity Guidelines,” *Int J Behav Nutr Phys Act,* vol. 7, pp. 38, 2010.

[38] G. S. Lynch, “Tackling Australia's future health problems: developing strategies to combat sarcopenia--age-related muscle wasting and weakness,” *Intern Med J,* vol. 34, no. 5, pp. 294-6, May, 2004.

[39] D. M. Needham, *Machina carnis : the biochemistry of muscular contraction and its historical development*, 1971.

[40] N. Steno, *Nicolai Stenonis De musculis et glandulis observationum specimen. Cum epistolis duabus anatomicis. [Epistola I. De anatome rajæ. II. De vitelli in intestina pulli transitu.]*, 1664.

[41] A. F. Huxley, “Muscle structure and theories of contraction,” *Prog Biophys Biophys Chem,* vol. 7, pp. 255-318, 1957.

[42] C. H. Fiske, and Y. Subbarow, “THE NATURE OF THE "INORGANIC PHOSPHATE" IN VOLUNTARY MUSCLE,” *Science,* vol. 65, no. 1686, pp. 401-3, Apr, 1927.

[43] P. Eggleton, and G. P. Eggleton, “The Inorganic Phosphate and a Labile Form of Organic Phosphate in the Gastrocnemius of the Frog,” *Biochem J,* vol. 21, no. 1, pp. 190-5, 1927.

[44] A. V. Hill, “The Heat of Shortening and the Dynamic Constants of Muscle,” vol. 126, no. 843, pp. 136-195, 1938.

[45] E. Eisenberg, T. L. Hill, and Y. Chen, “Cross-bridge model of muscle contraction. Quantitative analysis,” *Biophys J,* vol. 29, no. 2, pp. 195-227, Feb, 1980.

[46] E. M. Arnold, S. R. Hamner, A. Seth, M. Millard, and S. L. Delp, “How muscle fiber lengths and velocities affect muscle force generation as humans walk and run at different speeds,” *J Exp Biol,* vol. 216, no. Pt 11, pp. 2150-60, Jun, 2013.

[47] F. E. Zajac, “Muscle and tendon: properties, models, scaling, and application to biomechanics and motor control,” *Crit Rev Biomed Eng,* vol. 17, no. 4, pp. 359-411, 1989.

[48] T. S. Buchanan, D. G. Lloyd, K. Manal, and T. F. Besier, “Neuromusculoskeletal modeling: estimation of muscle forces and joint moments and movements from measurements of neural command,” *J Appl Biomech,* vol. 20, no. 4, pp. 367-95, Nov, 2004.

[49] A. J. van den Bogert, K. G. Gerritsen, and G. K. Cole, “Human muscle modelling from a user's perspective,” *J Electromyogr Kinesiol,* vol. 8, no. 2, pp. 119-24, Apr, 1998.

[50] C. W. Spoor, J. L. van Leeuwen, W. J. van der Meulen, and A. Huson, “Active force-length relationship of human lower-leg muscles estimated from morphological data: a comparison of geometric muscle models,” *Eur J Morphol,* vol. 29, no. 3, pp. 137-60, 1991.

[51] T. L. Wickiewicz, R. R. Roy, P. L. Powell, and V. R. Edgerton, “Muscle architecture of the human lower limb,” *Clin Orthop Relat Res*, no. 179, pp. 275-83, Oct, 1983.

[52] S. R. Ward, C. M. Eng, L. H. Smallwood, and R. L. Lieber, “Are current measurements of lower extremity muscle architecture accurate?,” *Clin Orthop Relat Res,* vol. 467, no. 4, pp. 1074-82, Apr, 2009.

[53] B. J. Fregly, “Design of Optimal Treatments for Neuromusculoskeletal Disorders using Patient-Specific Multibody Dynamic Models,” *Int J Comput Vis Biomech,* vol. 2, no. 2, pp. 145-155, Jul, 2009.

[54] A. Erdemir, S. McLean, W. Herzog, and A. J. van den Bogert, “Model-based estimation of muscle forces exerted during movements,” *Clin Biomech (Bristol, Avon),* vol. 22, no. 2, pp. 131-54, Feb, 2007.

[55] M. Sartori, M. Reggiani, D. Farina, and D. G. Lloyd, “EMG-Driven Forward-Dynamic Estimation of Muscle Force and Joint Moment about Multiple Degrees of Freedom in the Human Lower Extremity,” *PLoS One,* vol. 7, no. 12, pp. e52618, 2012.

[56] D. Staudenmann, K. Roeleveld, D. F. Stegeman, and J. H. van Dieën, “Methodological aspects of SEMG recordings for force estimation--a tutorial and review,” *J Electromyogr Kinesiol,* vol. 20, no. 3, pp. 375-87, Jun, 2010.

[57] S. S. Blemker, P. M. Pinsky, and S. L. Delp, “A 3D model of muscle reveals the causes of nonuniform strains in the biceps brachii,” *J Biomech,* vol. 38, no. 4, pp. 657-65, Apr, 2005.

[58] S. S. Blemker, and S. L. Delp, “Rectus femoris and vastus intermedius fiber excursions predicted by three-dimensional muscle models,” *J Biomech,* vol. 39, no. 8, pp. 1383-91, 2006.

[59] S. W. Chi, J. Hodgson, J. S. Chen, V. Reggie Edgerton, D. D. Shin, R. A. Roiz, and S. Sinha, “Finite element modeling reveals complex strain mechanics in the aponeuroses of contracting skeletal muscle,” *J Biomech,* vol. 43, no. 7, pp. 1243-50, May, 2010.

[60] H. Rahemi, N. Nigam, and J. M. Wakeling, “Regionalizing muscle activity causes changes to the magnitude and direction of the force from whole muscles-a modeling study,” *Front Physiol,* vol. 5, pp. 298, 2014.

[61] J. V. Basmajian, C. J. De Luca, and C. J. Deluca, *Muscles alive : their functions revealed by electromyography*, 5th / John V. Basmajian, Carlo J. De Luca. ed., Baltimore ; London: Williams & Wilkins, 1985.

[62] P. A. Lynn, N. D. Bettles, A. D. Hughes, and S. W. Johnson, “Influences of electrode geometry on bipolar recordings of the surface electromyogram,” *Med Biol Eng Comput,* vol. 16, no. 6, pp. 651-60, Nov, 1978.

[63] A. J. Fuglevand, D. A. Winter, A. E. Patla, and D. Stashuk, “Detection of motor unit action potentials with surface electrodes: influence of electrode size and spacing,” *Biol Cybern,* vol. 67, no. 2, pp. 143-53, 1992.

[64] S. Andreassen, and A. Rosenfalck, “Relationship of intracellular and extracellular action potentials of skeletal muscle fibers,” *Crit Rev Bioeng,* vol. 6, no. 4, pp. 267-306, Nov, 1981.

[65] J. M. Wakeling, “Patterns of motor recruitment can be determined using surface EMG,” *J Electromyogr Kinesiol,* vol. 19, no. 2, pp. 199-207, Apr, 2009.

[66] R. Merletti, L. Lo Conte, E. Avignone, and P. Guglielminotti, “Modeling of surface myoelectric signals--Part I: Model implementation,” *IEEE Trans Biomed Eng,* vol. 46, no. 7, pp. 810-20, Jul, 1999.

[67] R. Merletti, S. H. Roy, E. Kupa, S. Roatta, and A. Granata, “Modeling of surface myoelectric signals--Part II: Model-based signal interpretation,” *IEEE Trans Biomed Eng,* vol. 46, no. 7, pp. 821-9, Jul, 1999.

[68] S. Andreassen, and A. Rosenfalck, “Recording from a single motor unit during strong effort,” *IEEE Trans Biomed Eng,* vol. 25, no. 6, pp. 501-8, Nov, 1978.

[69] K. A. Wheeler, H. Shimada, D. K. Kumar, and S. P. Arjunan, “A sEMG model with experimentally based simulation parameters,” *Conf Proc IEEE Eng Med Biol Soc,* vol. 2010, pp. 4258-61, 2010.

[70] N. S. Stoykov, M. M. Lowery, A. Taflove, and T. A. Kuiken, “Frequency- and time-domain FEM models of EMG: capacitive effects and aspects of dispersion,” *IEEE Trans Biomed Eng,* vol. 49, no. 8, pp. 763-72, Aug, 2002.

[71] L. Mesin, M. Joubert, T. Hanekom, R. Merletti, and D. Farina, “A finite element model for describing the effect of muscle shortening on surface EMG,” *IEEE Trans Biomed Eng,* vol. 53, no. 4, pp. 593-600, Apr, 2006.

[72] M. M. Lowery, N. S. Stoykov, and T. A. Kuiken, “Independence of myoelectric control signals examined using a surface EMG model,” *Biomedical Engineering, IEEE Transactions on,* vol. 50, no. 6, pp. 789-793, 2003.

[73] H. P. Ludin, “Microelectrode study of normal human skeletal muscle,” *Eur Neurol,* vol. 2, no. 6, pp. 340-7, 1969.

[74] D. Farina, and R. Merletti, “A novel approach for precise simulation of the EMG signal detected by surface electrodes,” *IEEE Trans Biomed Eng,* vol. 48, no. 6, pp. 637-46, Jun, 2001.

[75] T. H. J. M. Gootzen, D. F. Stegeman, and A. Heringa, “On numerical problems in analytical calculations of extracellular fields in bounded cylindrical volume conductors,” *Journal of Applied Physics,* vol. 66, no. 9, pp. 4504-4508, 1989.

[76] J. H. Blok, D. F. Stegeman, and A. van Oosterom, “Three-layer volume conductor model and software package for applications in surface electromyography,” *Ann Biomed Eng,* vol. 30, no. 4, pp. 566-77, Apr, 2002.

[77] K. Roeleveld, J. H. Blok, D. F. Stegeman, and A. van Oosterom, “Volume conduction models for surface EMG; confrontation with measurements,” *J Electromyogr Kinesiol,* vol. 7, no. 4, pp. 221-232, Dec, 1997.

[78] P. Rosenfalck, “Intra- and extracellular potential fields of active nerve and muscle fibres. A physico-mathematical analysis of different models,” *Acta Physiol Scand Suppl,* vol. 321, pp. 1-168, 1969.

[79] S. Gabriel, R. W. Lau, and C. Gabriel, “The dielectric properties of biological tissues: II. Measurements in the frequency range 10 Hz to 20 GHz,” *Phys Med Biol,* vol. 41, no. 11, pp. 2251-69, Nov, 1996.

[80] C. Gabriel, S. Gabriel, and E. Corthout, “The dielectric properties of biological tissues: I. Literature survey,” *Phys Med Biol,* vol. 41, no. 11, pp. 2231-49, Nov, 1996.

[81] S. Gabriel, R. W. Lau, and C. Gabriel, “The dielectric properties of biological tissues: III. Parametric models for the dielectric spectrum of tissues,” *Phys Med Biol,* vol. 41, no. 11, pp. 2271-93, Nov, 1996.

[82] R. Merletti, and L. R. Lo Conte, “Surface EMG signal processing during isometric contractions,” *J Electromyogr Kinesiol,* vol. 7, no. 4, pp. 241-250, Dec, 1997.

[83] L. Mesin, “Volume conductor models in surface electromyography: computational techniques,” *Comput Biol Med,* vol. 43, no. 7, pp. 942-52, Aug, 2013.

[84] M. Gazzoni, D. Farina, and R. Merletti, “A new method for the extraction and classification of single motor unit action potentials from surface EMG signals,” *J Neurosci Methods,* vol. 136, no. 2, pp. 165-77, Jul, 2004.

[85] D. Farina, R. Merletti, and R. M. Enoka, “The extraction of neural strategies from the surface EMG,” *Journal of Applied Physiology,* vol. 96, no. 4, pp. 1486-1495, 2004.

[86] C. J. De Luca, S. H. Nawab, and J. C. Kline, “Clarification of methods used to validate surface EMG decomposition algorithms as described by Farina et al. (2014),” *J Appl Physiol (1985),* vol. 118, no. 8, pp. 1084, Apr, 2015.

[87] D. Farina, R. Merletti, and R. M. Enoka, “Reply to De Luca, Nawab, and Kline: The proposed method to validate surface EMG signal decomposition remains problematic,” *J Appl Physiol (1985),* vol. 118, no. 8, pp. 1085, Apr, 2015.

[88] M. J. Zwarts, and D. F. Stegeman, “Multichannel surface EMG: basic aspects and clinical utility,” *Muscle Nerve,* vol. 28, no. 1, pp. 1-17, Jul, 2003.

[89] R. Merletti, D. Farina, and M. Gazzoni, “The linear electrode array: a useful tool with many applications,” *J Electromyogr Kinesiol,* vol. 13, no. 1, pp. 37-47, Feb, 2003.

[90] G. Drost, D. F. Stegeman, B. G. van Engelen, and M. J. Zwarts, “Clinical applications of high-density surface EMG: a systematic review,” *J Electromyogr Kinesiol,* vol. 16, no. 6, pp. 586-602, Dec, 2006.

[91] R. Merletti, A. Holobar, and D. Farina, “Analysis of motor units with high-density surface electromyography,” *J Electromyogr Kinesiol,* vol. 18, no. 6, pp. 879-90, Dec, 2008.

[92] H. J. Hermens, B. Freriks, C. Disselhorst-Klug, and G. Rau, “Development of recommendations for SEMG sensors and sensor placement procedures,” *J Electromyogr Kinesiol,* vol. 10, no. 5, pp. 361-74, Oct, 2000.

[93] E. Otten, “Concepts and models of functional architecture in skeletal muscle,” *Exerc Sport Sci Rev,* vol. 16, pp. 89-137, 1988.

[94] J. L. Van Leeuwen, and C. W. Spoor, “Modelling mechanically stable muscle architectures,” *Philos Trans R Soc Lond B Biol Sci,* vol. 336, no. 1277, pp. 275-92, May, 1992.

[95] J. L. v. Leeuwen, and W. M. Kier, “Functional design of tentacles in squid: linking sarcomere ultrastructure to gross morphological dynamics,” *Philosophical Transactions of the Royal Society B: Biological Sciences,* vol. 352, no. 1353, pp. 551-571, 1997.

[96] M. A. Crisfield, *Non-linear finite element analysis of solids and structures*, West Sussex: Wiley, 1997.

[97] W. Herzog, *Skeletal muscle mechanics from mechanisms to function*, Chichester: Wiley, 2000.

[98] T. Johansson, P. Meier, and R. Blickhan, “A Finite-Element Model for the Mechanical Analysis of Skeletal Muscles,” vol. 206, no. 1, pp. 131-149, 2000.

[99] T. Sussman, and K.-J. Bathe, “A finite element formulation for nonlinear incompressible elastic and inelastic analysis,” vol. 26, no. 1–2, pp. 357-409, 1987.

[100] G. P. Pappas, D. S. Asakawa, S. L. Delp, F. E. Zajac, and J. E. Drace, “Nonuniform shortening in the biceps brachii during elbow flexion,” *J Appl Physiol (1985),* vol. 92, no. 6, pp. 2381-9, Jun, 2002.

[101] J. C. Criscione, A. S. Douglas, and W. C. Hunter, “Physically based strain invariant set for materials exhibiting transversely isotropic behavior,” *Journal of the Mechanics and Physics of Solids,* vol. 49, no. 4, pp. 871-897, 4//, 2001.

[102] S. F. Street, “Lateral transmission of tension in frog myofibers: a myofibrillar network and transverse cytoskeletal connections are possible transmitters,” *J Cell Physiol,* vol. 114, no. 3, pp. 346-64, Mar, 1983.

[103] J. A. Trotter, and P. P. Purslow, “Functional morphology of the endomysium in series fibered muscles,” *J Morphol,* vol. 212, no. 2, pp. 109-22, May, 1992.

[104] A. I. Namburete, M. Rana, and J. M. Wakeling, “Computational methods for quantifying in vivo muscle fascicle curvature from ultrasound images,” *J Biomech,* vol. 44, no. 14, pp. 2538-43, Sep, 2011.

[105] C. A. Yucesoy, B. H. Koopman, P. A. Huijing, and H. J. Grootenboer, “Three-dimensional finite element modeling of skeletal muscle using a two-domain approach: linked fiber-matrix mesh model,” *J Biomech,* vol. 35, no. 9, pp. 1253-62, Sep, 2002.

[106] O. Röhrle, J. B. Davidson, and A. J. Pullan, “A physiologically based, multi-scale model of skeletal muscle structure and function,” *Front Physiol,* vol. 3, pp. 358, 2012.

[107] Y. Berranen, M. Hayashibe, B. Gilles, and D. Guiraud, “3D volumetric muscle modeling for real-time deformation analysis with FEM,” *Conf Proc IEEE Eng Med Biol Soc,* vol. 2012, pp. 4863-6, 2012.

[108] A. Teklemariam, E. F. Hodson-Tole, N. D. Reeves, N. P. Costen, and G. Cooper, “A Finite Element Model Approach to Determine the Influence of Electrode Design and Muscle Architecture on Myoelectric Signal Properties,” *PLoS One,* vol. 11, no. 2, pp. e0148275, 2016.

[109] R. L. Lieber, and J. Fridén, “Functional and clinical significance of skeletal muscle architecture,” *Muscle Nerve,* vol. 23, no. 11, pp. 1647-66, Nov, 2000.

[110] R. L. Lieber, and S. R. Ward, “Skeletal muscle design to meet functional demands,” *Philos Trans R Soc Lond B Biol Sci,* vol. 366, no. 1570, pp. 1466-76, May, 2011.

[111] J. V. Trontelj, J. Jabre, and M. Mihelin, "Needle and Wire Detection Techniques," *Electromyography*, pp. 27-46: John Wiley & Sons, Inc., 2005.

[112] R. Merletti, and D. Farina, “Analysis of intramuscular electromyogram signals,” *Philos Trans A Math Phys Eng Sci,* vol. 367, no. 1887, pp. 357-68, Jan, 2009.

[113] A. Teklemariam, G. Cooper, E. F. Hodson-Tole, N. D. Reeves, and N. P. Costen, "A Finite Element Model simulation of surface EMG signals based on muscle tissue dielectric properties and electrodes configuration." pp. 193-197.

[114] R. Plonsey, and D. B. Heppner, “Considerations of quasi-stationarity in electrophysiological systems,” *Bull Math Biophys,* vol. 29, no. 4, pp. 657-64, Dec, 1967.
[115] Ltd, and Comsol, "Comsol Multiphysics 5.0 AC/DC User Manual, Fundamental of Electromagnetism," pp. 32-41.
[116] F. L. Gielen, W. Wallinga-de Jonge, and K. L. Boon, “Electrical conductivity of skeletal muscle tissue: experimental results from different muscles in vivo,” *Med Biol Eng Comput,* vol. 22, no. 6, pp. 569-77, Nov, 1984.
[117] D. Andreuccetti, R. Fossi, and C. Petrucci. "An Internet resource for the calculation of the dielectric properties of body tissues in the frequency range 10 Hz - 100 GHz.," 2014, 2014/2015; http://niremf.ifac.cnr.it/tissprop/.
[118] V. von Tscharner, “Intensity analysis in time-frequency space of surface myoelectric signals by wavelets of specified resolution,” *J Electromyogr Kinesiol,* vol. 10, no. 6, pp. 433-45, Dec, 2000.
[119] J. M. Wakeling, M. Kaya, G. K. Temple, I. A. Johnston, and W. Herzog, “Determining patterns of motor recruitment during locomotion,” *J Exp Biol,* vol. 205, no. Pt 3, pp. 359-69, Feb, 2002.
[120] E. F. Hodson-Tole, and J. M. Wakeling, “Variations in motor unit recruitment patterns occur within and between muscles in the running rat (Rattus norvegicus),” *J Exp Biol,* vol. 210, no. Pt 13, pp. 2333-45, Jul, 2007.
[121] J. M. Wakeling, S. A. Pascual, B. M. Nigg, and V. von Tscharner, “Surface EMG shows distinct populations of muscle activity when measured during sustained sub-maximal exercise,” *Eur J Appl Physiol,* vol. 86, no. 1, pp. 40-7, Nov, 2001.
[122] C. J. De Luca, M. Kuznetsov, L. D. Gilmore, and S. H. Roy, “Inter-electrode spacing of surface EMG sensors: reduction of crosstalk contamination during voluntary contractions,” *J Biomech,* vol. 45, no. 3, pp. 555-61, Feb 2, 2012.
[123] E. J. De la Barrera, and T. E. Milner, “The effects of skinfold thickness on the selectivity of surface EMG,” *Electroencephalogr Clin Neurophysiol,* vol. 93, no. 2, pp. 91-9, Apr, 1994.
[124] V. von Tscharner, C. Maurer, F. Ruf, and B. M. Nigg, “Comparison of electromyographic signals from monopolar current and potential amplifiers derived from a penniform muscle, the gastrocnemius medialis,” *J Electromyogr Kinesiol,* vol. 23, no. 5, pp. 1044-51, Oct, 2013.
[125] L. Mesin, and D. Farina, “Simulation of surface EMG signals generated by muscle tissues with inhomogeneity due to fiber pinnation,” *IEEE Trans Biomed Eng,* vol. 51, no. 9, pp. 1521-9, Sep, 2004.
[126] M. A. Cavalcanti Garcia, and T. M. M. Vieira, “La electromiografía de superficie: ¿qué es, qué se busca con ella y cómo usarla?,” *Revista Andaluza de Medicina del Deporte,* vol. 08, no. 02, pp. 17-28, 2015.
[127] E. F. Hodson-Tole, I. D. Loram, and T. M. Vieira, “Myoelectric activity along human gastrocnemius medialis: different spatial distributions of postural and electrically elicited surface potentials,” *J Electromyogr Kinesiol,* vol. 23, no. 1, pp. 43-50, Feb, 2013.
[128] L. Mesin, R. Merletti, and T. M. Vieira, “Insights gained into the interpretation of surface electromyograms from the gastrocnemius muscles: A simulation study,” *J Biomech,* vol. 44, no. 6, pp. 1096-103, Apr, 2011.
[129] A. Botter, T. M. Vieira, I. D. Loram, R. Merletti, and E. F. Hodson-Tole, “A novel system of electrodes transparent to ultrasound for simultaneous detection of myoelectric activity and B-mode ultrasound images of skeletal muscles,” *J Appl Physiol (1985),* vol. 115, no. 8, pp. 1203-14, Oct, 2013.
[130] P. P. Purslow, “Muscle fascia and force transmission,” *J Bodyw Mov Ther,* vol. 14, no. 4, pp. 411-7, Oct, 2010.

[131] A. R. Gillies, and R. L. Lieber, "Structure and function of the skeletal muscle extracellular matrix," *Muscle Nerve,* vol. 44, no. 3, pp. 318-31, Sep, 2011.
[132] A. Turrina, M. A. Martínez-González, and C. Stecco, "The muscular force transmission system: role of the intramuscular connective tissue," *J Bodyw Mov Ther,* vol. 17, no. 1, pp. 95-102, Jan, 2013.
[133] R. L. Lieber, E. Runesson, F. Einarsson, and J. Fridén, "Inferior mechanical properties of spastic muscle bundles due to hypertrophic but compromised extracellular matrix material," *Muscle Nerve,* vol. 28, no. 4, pp. 464-71, Oct, 2003.
[134] R. F. Ker, R. M. Alexander, and M. B. Bennett, "Why are mammalian tendons so thick?," vol. 216, no. 2, pp. 309-324, 1988.
[135] S. Labeit, and B. Kolmerer, "Titins: giant proteins in charge of muscle ultrastructure and elasticity," *Science,* vol. 270, no. 5234, pp. 293-6, Oct, 1995.
[136] L. G. Prado, I. Makarenko, C. Andresen, M. Krüger, C. A. Opitz, and W. A. Linke, "Isoform diversity of giant proteins in relation to passive and active contractile properties of rabbit skeletal muscles," *J Gen Physiol,* vol. 126, no. 5, pp. 461-80, Nov, 2005.
[137] S. R. Ward, A. Tomiya, G. J. Regev, B. E. Thacker, R. C. Benzl, C. W. Kim, and R. L. Lieber, "Passive mechanical properties of the lumbar multifidus muscle support its role as a stabilizer," *J Biomech,* vol. 42, no. 10, pp. 1384-9, Jul, 2009.
[138] G. A. Meyer, and R. L. Lieber, "Elucidation of extracellular matrix mechanics from muscle fibers and fiber bundles," *J Biomech,* vol. 44, no. 4, pp. 771-3, Feb, 2011.
[139] M. Mooney, "A Theory of Large Elastic Deformation," *Journal of Applied Physics,* vol. 11, no. 9, pp. 582-592, 1940.
[140] R. W. Ogden, "Large Deformation Isotropic Elasticity - On the Correlation of Theory and Experiment for Incompressible Rubberlike Solids," *Proceedings of the Royal Society of London A: Mathematical, Physical and Engineering Sciences,* vol. 326, no. 1567, pp. 565-584, 1972.
[141] O. H. Yeoh, "Some Forms of the Strain Energy Function for Rubber," *Rubber Chemistry and Technology,* vol. 66, no. 5, pp. 754-771, 2015/05/05, 1993.
[142] A. Galeski, J. Kastelic, E. Baer, and R. R. Kohn, "Mechanical and structural changes in rat tail tendon induced by alloxan diabetes and aging," *J Biomech,* vol. 10, no. 11/12, pp. 775-82, 1977.
[143] Y. Gao, T. Y. Kostrominova, J. A. Faulkner, and A. S. Wineman, "Age-related changes in the mechanical properties of the epimysium in skeletal muscles of rats," *J Biomech,* vol. 41, no. 2, pp. 465-9, 2008.
[144] C. J. Rodrigues, A. J. Rodrigues Júnior, and G. M. Bohm, "Effects of aging on muscle fibers and collagen content of the diaphragm: a comparison with the rectus abdominis muscle," *Gerontology,* vol. 42, no. 4, pp. 218-28, 1996.
[145] M. Kjaer, "Role of extracellular matrix in adaptation of tendon and skeletal muscle to mechanical loading," *Physiol Rev,* vol. 84, no. 2, pp. 649-98, Apr, 2004.
[146] L. R. Smith, and E. R. Barton, "Collagen content does not alter the passive mechanical properties of fibrotic skeletal muscle in mdx mice," *Am J Physiol Cell Physiol,* vol. 306, no. 10, pp. C889-98, May, 2014.
[147] K. S. Ramaswamy, M. L. Palmer, J. H. van der Meulen, A. Renoux, T. Y. Kostrominova, D. E. Michele, and J. A. Faulkner, "Lateral transmission of force is impaired in skeletal muscles of dystrophic mice and very old rats," *J Physiol,* vol. 589, no. Pt 5, pp. 1195-208, Mar, 2011.
[148] H. Degens, L. Hoofd, and R. A. Binkhorst, "Specific force of the rat plantaris muscle changes with age, but not with overload," vol. 78, no. 3, pp. 215-219, 1995.
[149] S. B. Ballak, H. Degens, A. de Haan, and R. T. Jaspers, "Aging related changes in determinants of muscle force generating capacity: a comparison of muscle aging in men and male rodents," *Ageing Res Rev,* vol. 14, pp. 43-55, Mar, 2014.

[150] H. Schmalbruch, "Skeletal Muscle Fibres," *Skeletal Muscle*, Handbook of Microscopic Anatomy, pp. 35-158: Springer Berlin Heidelberg, 1985.
[151] R. L. Gajdosik, "Passive extensibility of skeletal muscle: review of the literature with clinical implications," *Clin Biomech (Bristol, Avon),* vol. 16, no. 2, pp. 87-101, Feb, 2001.
[152] C. Zhang, and Y. Gao, "Effects of aging on the lateral transmission of force in rat skeletal muscle," *J Biomech,* vol. 47, no. 5, pp. 944-8, Mar, 2014.
[153] K. M. Virgilio, K. S. Martin, S. M. Peirce, and S. S. Blemker, "Multiscale models of skeletal muscle reveal the complex effects of muscular dystrophy on tissue mechanics and damage susceptibility," *Interface focus,* vol. 5, no. 2, pp. 20140080, 2015/04//, 2015.
[154] H. Rahemi, N. Nigam, and J. M. Wakeling, "The effect of intramuscular fat on skeletal muscle mechanics: implications for the elderly and obese," *J R Soc Interface,* vol. 12, no. 109, pp. 20150365, Aug, 2015.
[155] V. A. Kadhiresan, C. A. Hassett, and J. A. Faulkner, "Properties of single motor units in medial gastrocnemius muscles of adult and old rats," *J Physiol,* vol. 493 (Pt 2), pp. 543-52, Jun, 1996.
[156] M. E. Héroux, H. J. Brown, J. T. Inglis, G. P. Siegmund, and J. S. Blouin, "Motor units in the human medial gastrocnemius muscle are not spatially localized or functionally grouped," *J Physiol,* vol. 593, no. 16, pp. 3711-26, Aug, 2015.
[157] T. M. Vieira, J. M. Wakeling, and E. F. Hodson-Tole, "Is there sufficient evidence to claim muscle units are not localised and functionally grouped within the human gastrocnemius?," *J Physiol,* vol. 594, no. 7, pp. 1953-4, Apr, 2016.
[158] J. S. Blouin, H. J. Brown, M. E. Héroux, J. T. Inglis, and G. P. Siegmund, "Reply from J. S. Blouin, H. J. Brown, M. E. Héroux, J. T. Inglis and G. P. Siegmund," *J Physiol,* vol. 594, no. 7, pp. 1955, Apr, 2016.
[159] J. F. Plate, W. F. Wiggins, P. Haubruck, A. T. Scott, T. L. Smith, K. R. Saul, and S. Mannava, "Normal aging alters in vivo passive biomechanical response of the rat gastrocnemius-Achilles muscle-tendon unit," *J Biomech,* vol. 46, no. 3, pp. 450-5, Feb, 2013.
[160] L. K. Wood, E. Kayupov, J. P. Gumucio, C. L. Mendias, D. R. Claflin, and S. V. Brooks, "Intrinsic stiffness of extracellular matrix increases with age in skeletal muscles of mice," *J Appl Physiol (1985),* vol. 117, no. 4, pp. 363-9, Aug, 2014.
[161] C. Z. Wang, T. J. Li, and Y. P. Zheng, "Shear modulus estimation on vastus intermedius of elderly and young females over the entire range of isometric contraction," *PLoS One,* vol. 9, no. 7, pp. e101769, 2014.
[162] C. Zhang, and Y. Gao, "Finite element analysis of mechanics of lateral transmission of force in single muscle fiber," *J Biomech,* vol. 45, no. 11, pp. 2001-6, Jul, 2012.
[163] C. Y. Tang, G. Zhang, and C. P. Tsui, "A 3D skeletal muscle model coupled with active contraction of muscle fibres and hyperelastic behaviour," *J Biomech,* vol. 42, no. 7, pp. 865-72, May, 2009.
[164] B. J. J. J. Van der Linden, Faculty of Mechanical Engineering, University of Twente, Enschede, 1998.
[165] E. M. Bosboom, M. K. Hesselink, C. W. Oomens, C. V. Bouten, M. R. Drost, and F. P. Baaijens, "Passive transverse mechanical properties of skeletal muscle under in vivo compression," *J Biomech,* vol. 34, no. 10, pp. 1365-8, Oct, 2001.
[166] M. C. Brown, R. L. Holland, and W. G. Hopkins, "Motor nerve sprouting," *Annu Rev Neurosci,* vol. 4, pp. 17-42, 1981.
[167] S. M. Greising, J. S. Medina-Martínez, A. K. Vasdev, G. C. Sieck, and C. B. Mantilla, "Analysis of muscle fiber clustering in the diaphragm muscle of sarcopenic mice," *Muscle Nerve,* vol. 52, no. 1, pp. 76-82, Jul, 2015.
[168] M. Mordhorst, T. Heidlauf, and O. Röhrle, "Predicting electromyographic signals under realistic conditions using a multiscale chemo-electro-mechanical finite element model," *Interface Focus,* vol. 5, no. 2, pp. 20140076, Apr, 2015.

[169] S. Xiao, K. C. McGill, and V. R. Hentz, “Action potentials of curved nerves in finite limbs,” *IEEE Trans Biomed Eng,* vol. 42, no. 6, pp. 599-607, Jun, 1995.
[170] G. V. Dimitrov, and N. A. Dimitrova, “Modelling of the extracellular potentials generated by curved fibres in a volume conductor,” *Electromyogr Clin Neurophysiol,* vol. 20, no. 1, pp. 27-40, 1980 Jan-Feb, 1980.
[171] J. Darby, B. Li, N. Costen, I. Loram, and E. Hodson-Tole, “Estimating skeletal muscle fascicle curvature from B-mode ultrasound image sequences,” *IEEE Trans Biomed Eng,* vol. 60, no. 7, pp. 1935-45, Jul, 2013.
[172] I. o. M. U. D. o. H. P. a. D. Prevention, and C. J. Berg RL, editors., *Promoting Health and Preventing Disability.*, [1992].
[173] M. Epstein, and W. Herzog, *Theoretical models of skeletal muscle*, Chichester: Wiley, 1998.
[174] W. Herzog, K. Powers, K. Johnston, and M. Duvall, “A new paradigm for muscle contraction,” *Front Physiol,* vol. 6, pp. 174, 2015.
[175] A. M. Gordon, A. F. Huxley, and F. J. Julian, “The variation in isometric tension with sarcomere length in vertebrate muscle fibres,” *J Physiol,* vol. 184, no. 1, pp. 170-92, May, 1966.
[176] G. T. Mase, R. M. Smelser, and G. E. Mase, *Continuum mechanics for engineers*, 3rd ed., Boca Raton: CRC Press, 2010.

Appendix A

Cross Bridge Theory

Sarcomeres and cross-bridge binding [173]

The smallest unit of skeletal muscle is the sarcomere, which is the contractile element of a muscle (see Figure A.1). The sarcomere is a compartment bordered by a protein indicated as a Z-line and where thin filaments are alternated with thick filaments along the fibre direction. The thick filament is a group (~180) of myosin proteins with tails pointing at the centre of the sarcomere and an outward head pointing in the opposite direction. The thin filament is a helical double woven actin filament, stiffened by the protein tropomyosin, with troponin proteins complexes attached along the actin filament.

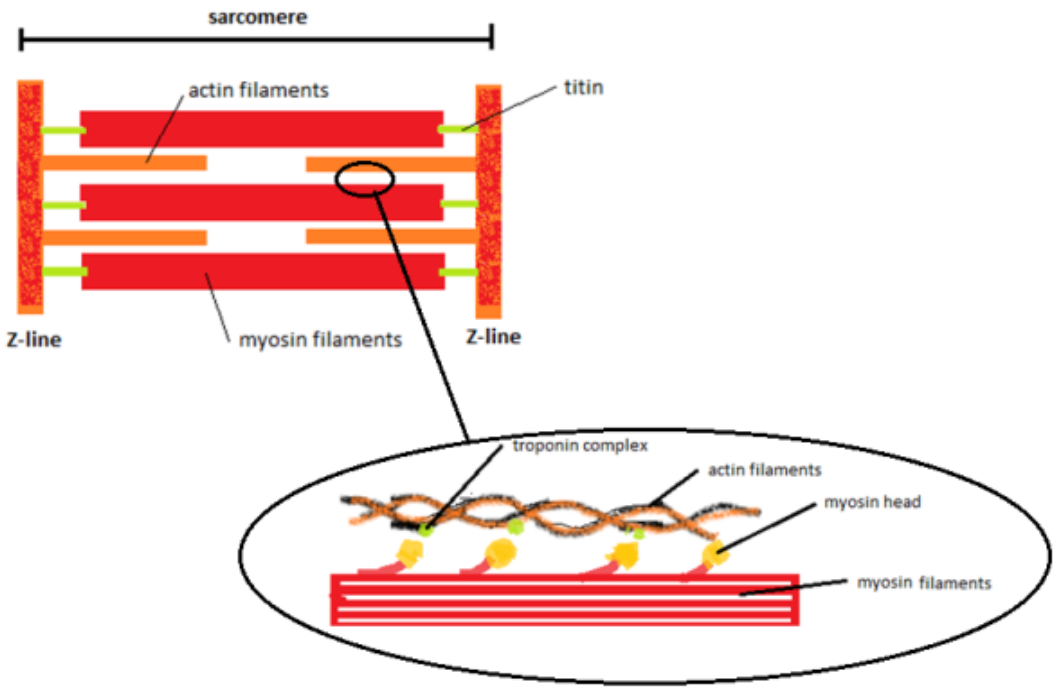

Figure A.0.1 A sarcomere unit scheme. The actin (thin) filaments are located between the myosin (thick) filaments and bonded to them through the troponin complexes. The sarcomere unit is bordered by a proteic structure called Z-line. Note that the myosin are connected to the Z-line through the titin proteins which act like springs and balance the tension in the sarcomere so that it is equal on both sides.

When an action potential spreads along the fibres, Ca^{2+} ions are released from the sarcoplasmic reticulum into the sarcomere. The calcium attaches to troponin C and the Troponin complex changes structure in order to make available an active binding site on the actin filament and thus allowing the myosin head attachment to form the so called Cross-Bridge (see **Figure A.0.1**). The hydrolization of ATP bound to the myosin head, liberates the energy necessary to move the head and so the actin filament toward the centre of the sarcomere. During a contraction, the interaction between actin and myosin is cyclic, requiring a continuous ATP supply with the amount of Ca^{2+} released in part

determining the number of cross-bridges formed. In addition the myosin is attached to the Z-line through a protein called titin, which is believed to act as a spring and maintain the equilibrium between the two halves of the sarcomere contractions [174].

Huxley's Cross Bridge Model

A structural model that describes the cross-bridge force production is the Huxley's Cross Bridge Model [41]. In this model, the myosin and the actin are considered as rigid filaments that can slide over each other. The constitutive equation is the Huxley-Zahalak equation:

$$\frac{\partial n}{\partial t} + \frac{\partial n}{\partial x}\, v = \left(\frac{1}{l_a} - n\right) f(x) - n g(x) \qquad \text{(A.1)}$$

This equation describes the rate of proportion of attached $\mathrm{n(x,t)}$ sites along the direction x, based on the distribution functions $\mathrm{f(x)}$ the probability of attachment and $\mathrm{g(x)}$ the probability of broken connection. $\mathrm{l_a}$ is the distance between two consecutive actin attachment sites. Knowing the force exerted from a single site, makes it possible to obtain a Force-Velocity relationship at a macroscopic level of a muscle section:

$$F(t) = \frac{mAs}{2} \int_{-\infty}^{+\infty} kxn(x,t)\, dx \qquad \text{(A.2)}$$

Where m is the number of sites per volume, s the average sarcomere length, A the cross sectional area, k is the elastic constant and $\mathrm{n}(\mathrm{x},\mathrm{t})$ will act as a weighting function. Integrating this equation provides an estimate of the total force:

$$F = \frac{mAsk\alpha}{2(\alpha+\beta)l_a}\left[\frac{1}{2}h^2 + (1 - e^{\left(\frac{(\alpha+\beta)}{2v}\right)h^2})\left(\frac{v}{\alpha+\beta} - \left(\frac{v}{g_o}\right)^2\right)\right] \quad \text{(A.3)}$$

Where, h is the initial x point, and α, β , are two parameters belonging to the solution of the first order differential equation of Huxley-Zahalak equation. The constitutive parameters are directly obtainable from the underlying chemical reactions occurring during attachment. . The cross-bridge model can explain the discontinuous stress-stretch behaviour on a micro scale (see), of the single sarcomere as proved by [175] in its their experiments on isolated fibres of frog muscle, where the force depends on the proportion of overlapping cross-bridges . This function becomes a continuous smoothed bell shaped function at a macroscopic level, defining the force-fibre length relationship (see section 1.3).

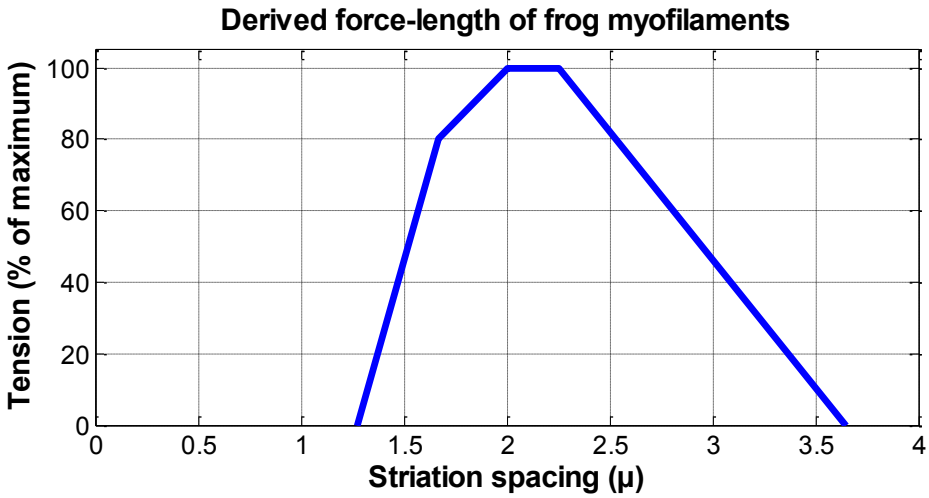

Figure A.0.2 force-sarcomere overlapping curve. The tension generated between the myofilaments is related with to the proportion of overlapping cross-bridges (striation spacing on the x-axis) as it was proved in Gordon et al., 1966 experiment on a frog muscle. This experiment validated the cross-bridge model at a microscopic level.

Appendix B

Continuum Mechanics

In continuum mechanics, a material body B can be considered as a set of material points (particles) which can be put with a one-to-one correspondence within the points of a regular region R of physical space [176]. The changes of the body physical and kinematic properties can be expressed in terms of a reference (initial, X) configuration according to the Lagrangian description. Thus, changes to the spatial coordinate can be written as:

$$x = \chi(X, t) \tag{B.1}$$

Deformation

Where x is the current configuration and X is the reference configuration. χ is a mapping function that relates the current configuration to the reference one. Assuming non-dependence on time and a smooth mapping function, the distance between two points in the current configuration (see Figure B. 0.1) is given by:

$$dx_i = \frac{\partial \chi_i}{\partial X_A} dX_A \quad , \tag{B.2}$$

$\frac{\partial \chi_i}{\partial X_A}$ is the deformation gradient referred as F_{iA} (invertible due to smoothness condition of χ).

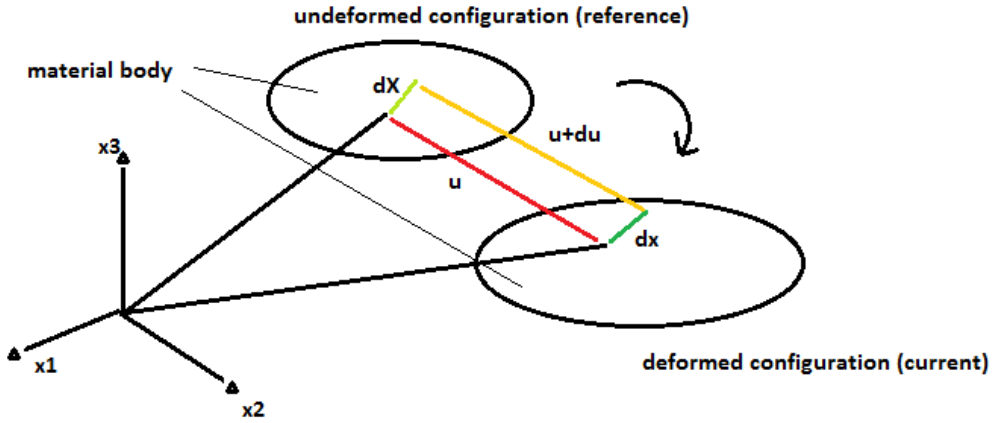

Figure B. 0.1 Deformation of a material body

In the figure the displacement vector (u) and the distance between particles dX (reference configuration), dx(current configuration) are showed.

Moreover, the deformation can be expressed in different ways. When it is considered as the change of the squared magnitude of the distance between the particles (see Figure B. 0.1), the Cauchy Green's right deformation tensor C is obtained:

$$C = F^T \cdot F \quad . \qquad \text{(B.3)}$$

The Green's deformation tensor is a symmetric second order tensor. Thus it follows the same mathematical consideration as the Cauchy stress tensor, and an analogous definition of strain invariants, spherical strain tensor and principal strains. From the

Green's deformation tensor it is possible to define the Green-Lagrangian finite strain tensor E that is related with C as follows:

$2E = C-I$ (C, Cauchy Green's deformation tensor, I, identity matrix). (B.4)

This tensor can be expressed in terms of displacement gradient.

Stress

The current state of stress of a homogenous isotropic material, within respect a certain cutting plane is defined by the Cauchy second order (rank 2) symmetric stress tensor. The physical meaning of this tensor can be understood by idealizing the infinitesimal point as a cube, with three force vectors applied to each face. The vectors normal to each face are the normal stresses, while the vectors tangents are the shear stresses. In total there are 9 component, which can be reduced to 6 component since the tensor is symmetric (see Figure B.2).

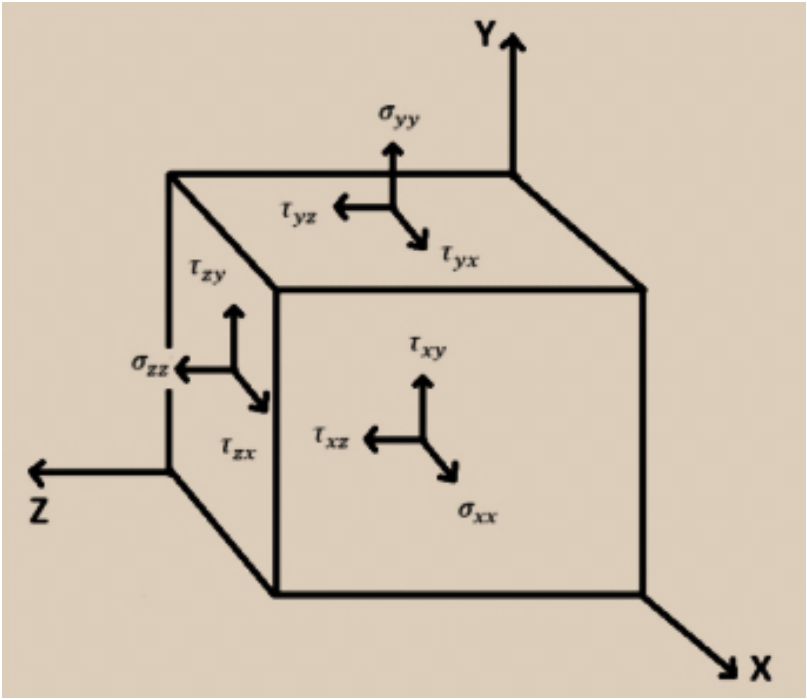

Figure B.2 The stress components of the Cauchy stress tensor. The stress components of the Cauchy stress tensor in an ideal cube that represent an infinitesimal point. The σ components are the normal stress while the τ components represent the shear stresses. The Cauchy stress tensor is symmetric, which means that only six components are required to be known. Besides, it expresses the current state of stress of a point in a body.

The Cauchy stress tensor expresses the stress relative to the present configuration. Furthermore, Cauchy stress is variant to pure rotation while the deformation strain is not. For these reasons, it is useful to express the stress in another form, since in muscle models it is required to express stresses in the reference configuration. The second Piola-Kirchoff stress tensor expresses the stress relative to the reference configuration; in particular, the second Piola-Kirchoff stress tensor relates forces in the reference configuration to areas in the current configuration:

$$S = J \cdot F^{-1} \cdot \sigma \cdot F^{-T} \quad , \qquad \text{(B.5)}$$

S=second Piola Kirchoff stress tensor, F= deformation gradient,

J= determinant of F, Jacobian determinant, σ= Cauchy stress tensor.

This tensor is symmetric and invariant to pure rotations and can be used to express the initial muscle fibres stress. In the linear simulation, the stress is added as a second Piola-Kirchoff stress since it must be in the reference configuration.

Appendix C

Hyperelasticity

During deformation the work done by external forces is stored in the material in the form of strain energy W, expressed as a scalar function of the deformation. When formulating the problem, it is good to have quantities that are not influenced by rigid body rotations. For this reason, the strain energy is derivate from the stretch invariants that are invariant to both the coordinate system and the strain measure. Due to an easier computation the Cauchy Green right (C) or left (B) tensors are used to calculate the stretch invariants[96]:

$$\mathrm{I}_1 = \lambda_1^2 + \lambda_2^2 + \lambda_3^2 = \mathrm{tr}(\mathrm{C}) \quad , \quad \text{(C.1)}$$

$$\mathrm{I}_2 = \lambda_2^2\lambda_3^2 + \lambda_3^2\lambda_1^2 + \lambda_1^2\lambda_2^2 = \frac{1}{2}\left(\mathrm{I}_1{}^2 - \mathrm{tr}(\mathrm{C}^2)\right) \quad , \quad \text{(C.2)}$$

$$\mathrm{I}_3 = \lambda_1^2\lambda_2^2\lambda_3^2 + \lambda_3^2\lambda_1^2 + \lambda_1^2\lambda_2^2 = \det(\mathrm{C}) = \mathrm{J}^2 \quad , \quad \text{(C.3)}$$

where:

$\mathrm{J} = \det(\mathrm{F}) = \mathrm{I}_3{}^{\frac{1}{2}}$ is called the Jacobian.

A strain energy for an isotropic material using the stretch ratios should satisfy the following criteria:

- The energy function is zero for the ground state $\lambda_1 = \lambda_2 = \lambda_3 = 1$;
- The energy function is symmetric in $\lambda_1 - \lambda_3$;
- The energy function is always ≥ 0.

A function that satisfies these criteria has the following form:

$$\varphi = \sum_{p,q,r=0}^{\infty} C_{pqr} \ (I_1 - 3)^p (I_2 - 3)^q (I_3 - 1)^r \quad . \quad \text{(C.4)}$$

From this function is derivate a special form used for incompressible rubber like materials, implemented by Mooney-Rivlin:

$$\varphi = C_{10}(I_1 - 3) + C_{01}(I_2 - 3) \quad . \quad \text{(C.5)}$$

Pure compressible materials formulation leads to numerical problems, for which an additional term is used to treat the material as a nearly incompressible (where the bulk modulus K tend to be infinite) material:

$$\varphi_b = \frac{K}{2}(J - 1)^2 \quad . \quad \text{(C.6)}$$

Furthermore, the function can be split into the deviatoric and volumetric component defining modified stretch ratio as follow:

$$\bar{\lambda} = J^{-\frac{1}{3}}\lambda \quad , \qquad \text{(C.7)}$$

which preserve the volume:

$$\bar{J} = \bar{\lambda}_1\bar{\lambda}_2\bar{\lambda}_3 = 1 \quad . \qquad \text{(C.8)}$$

Following the modified invariants are:

$$I_{1,M} = I_{1,C}\left(I_{3,C}\right)^{-1/3} = \bar{I}_1 J^{-\frac{2}{3}} \qquad \text{(C.9)}$$

$$I_{2,M} = I_{2,C}\left(I_{3,C}\right)^{-2/3} = \bar{I}_2 J^{-\frac{4}{3}}$$

(2.27)

$$I_{3,M} = \left(I_{3,C}\right)^{1/2} \quad \text{(volume dependent quantity)} \quad , \qquad \text{(C.10)}$$

And the resultant modified Mooney-Rivlin function will result to be:

$$\varphi = \varphi_d + \varphi_b = C_{10}(\bar{I}_1 - 3) + C_{01}(\bar{I}_2 - 3) + \frac{K}{2}(J-1)^2 \quad . \qquad \text{(C.11)}$$

This function is used to describe rubber materials, and its behaviour fits also the typical behaviour of the muscle connective tissue, i.e. large deformation and non-linear stress strain.

Appendix D

Matlab Code

Mechanical model of the shear force transmission

The following code is a modified version of the code provided by Sharafi and Blemker [3].

```
Author: Bahar Sharafi
% This program is part of the supplementary material for the article
% B. Sharafi, S. Blemker, "A mathematical model of force transmission
from
% intrafascicularly terminating fibers", J Biomech, in review
% Please cite this article if you use the program in your work.
%
%
% This script calculates and plots the ratio of force to peak isometric
% force as a function of fiber resting length to fiber diameter, assuming
% the fiber is initially at resting length
clear all;
close all;
clc;

global alpha beta beta_old sigma_star
alpha = 1;                                  % activation level
```

```
sigma_star = 300e5;                          % peak isometric stress (Pa)

w=4.957;



fiber_volume_fraction = 0.95;
beta =2*(1-sqrt(fiber_volume_fraction))/sqrt(fiber_volume_fraction);

fiber_volume_fraction_old = 0.8;
beta_old                                                              =2*(1-
sqrt(fiber_volume_fraction_old))/sqrt(fiber_volume_fraction_old);

% endomysium shear moduli, normalized by sigma_star
L_hats = [[1:100],[102:2:300],[310:10:4000]];




%% Solving the equilibrium equation  for lambda (lambdas)

lambdas = zeros(1,length(L_hats));



    for i = 1:length(L_hats)
        global L_hat term1 term3
        L_hat = L_hats(i);
      % Solving the equilibrium equation for lambda:
        lambdas(i) = fzero(@eqnfunc_shear,1.0);
        clear L_hat
    end
```

```
    % Calculating fiber force :
    for k = 1:length(lambdas)

        force_ratio(k)    =    (0.534    +    0.229*cos(w*lambdas(k))-
0.095*cos(2*w*lambdas(k))+                  0.024*cos(3*w*lambdas(k))-
0.021*cos(4*w*lambdas(k))+0.013*cos(5*w*lambdas(k))-
0.421*sin(w*lambdas(k))+0.079*sin(2*w*lambdas(k))-
0.029*sin(3*w*lambdas(k))+0.013*sin(4*w*lambdas(k))+0.002*sin(5*w*lamb
das(k)) + 0.002*sin(5*w*lambdas(k))) ;

    end


    lambdas_old = zeros(1,length(L_hats));

    for i = 1:length(L_hats)
        global L_hat term1old term3old
        L_hat = L_hats(i);
      % Solving the equilibrium equation for lambda:
        lambdas_old(i) = fzero(@eqnfunc_shear_old,1.0);
        clear L_hat
    end


    % Calculating fiber force :
    for k = 1:length(lambdas_old)
```

```
        force_ratio_old(k)   =   (0.534   +   0.229*cos(w*lambdas_old(k))-
0.095*cos(2*w*lambdas_old(k))+           0.024*cos(3*w*lambdas_old(k))-
0.021*cos(4*w*lambdas_old(k))+0.013*cos(5*w*lambdas_old(k))-
0.421*sin(w*lambdas_old(k))+0.079*sin(2*w*lambdas_old(k))-
0.029*sin(3*w*lambdas_old(k))+0.013*sin(4*w*lambdas_old(k))+0.002*sin(
5*w*lambdas_old(k)) + 0.002*sin(5*w*lambdas_old(k))) ;

    end


    % Plotting force ratio as a function of fiber resting length/diamter
    figure(1)
    plot
(L_hats/2,force_ratio,L_hats/2,force_ratio_old,'r','LineWidth',3)
%     title('Force Vs. Fibre length','FontSize',24,'FontWeight','bold');
    xlabel('resting
length/diameter','FontSize',24,'FontWeight','bold');
    ylabel('Force ratio','FontSize',24,'FontWeight','bold')
    set(gca,'FontSize',15,'FontWeight','bold')
    axis([0 50 0 1.1])
    hold on
    grid on


    % Plotting lambda as a function of fiber resting length/diamter
    figure(2)
    plot(L_hats/2,lambdas,L_hats/2,lambdas_old,'r','LineWidth',3)
%                                   title('Stretch       Vs.       Fibre
length','FontSize',24,'FontWeight','bold');
```

```
    xlabel('resting
length/diameter','FontSize',24,'FontWeight','bold');
    ylabel('stretch (lambda)','FontSize',24,'FontWeight','bold')
    set(gca,'FontSize',15,'FontWeight','bold')
    axis([0 50 0 1.1])
    hold on
    grid on
hold off
```

Two equilibrium equation functions were defined. One for a young adult population with fibre volume fraction 95% and the other for an old population with fibre volume fraction of 80%.

Function for 95 % volume fraction

```
% eqnfunc_shear(lambda) = 0 is the equation of equilibrium (2.1.1.2)
function y = eqnfunc_shear(lambda)

global L_hat  sigma_star  beta

% Mooney Rivlin coefficient of the connective tissue
c10 = 64300;
c01 = -38000;
c20 = 9400;
c11 = -43;
c02 = 5;
```

```
Gend = 2*(c10+c01);
w=4.957;
r0 = 35e-6;
radius = 35e-6/sqrt(lambda);
thickness = 0.9092e-6;

kappa = thickness/r0;
Af = pi*(r0^2);



% Terms of eqn (2.1.1.2)
term1      =      2*(Gend/sigma_star)*(L_hat^2)*(1-lambda)*(lambda)./(-
1+sqrt(1+2*beta*(2+beta)*lambda./(lambda+1)));

term2 = -(1/sigma_star)*((2.499e5)*(lambda-1)^2 + (5.056e4)*(lambda-1)
+ 2198);

term3    =    -(0.534    +    0.229*cos(w*lambda)-0.095*cos(2*w*lambda)+
0.024*cos(3*w*lambda)-0.021*cos(4*w*lambda)+0.013*cos(5*w*lambda)-
0.421*sin(w*lambda)+0.079*sin(2*w*lambda)-
0.029*sin(3*w*lambda)+0.013*sin(4*w*lambda)+0.002*sin(5*w*lambda)     +
0.002*sin(5*w*lambda));

y = term1+term2+term3;
```

Function for 80 % volume fraction

```
% eqnfunc_shear(lambda) = 0 is the equation of equilibrium (2.1.1.2)
function y = eqnfunc_shear(lambda)

global L_hat  sigma_star   beta_old

% Mooney Rivlin coefficient of the connective tissue
c10 = 64300;
c01 = -38000;
c20 = 9400;
c11 = -43;
c02 = 5;

Gend = 2*(c10+c01);
w=4.957;
r0 = 35e-6;
radius = 35e-6/sqrt(lambda);
thickness = 50.1312e-6;

kappa = thickness/r0;
Af = pi*(r0^2);



% Terms of eqn (2.1.1.2)
```

```
term1      =      2*(Gend/sigma_star)*(L_hat^2)*(1-lambda)*(lambda)./(-
1+sqrt(1+2*beta_old*(2+beta_old)*lambda./(lambda+1)));

term2 = -(1/sigma_star)*((2.499e5)*(lambda-1)^2 + (5.056e4)*(lambda-1)
+ 2198);

term3    =    -(0.534    +    0.229*cos(w*lambda)-0.095*cos(2*w*lambda)+
0.024*cos(3*w*lambda)-0.021*cos(4*w*lambda)+0.013*cos(5*w*lambda)-
0.421*sin(w*lambda)+0.079*sin(2*w*lambda)-
0.029*sin(3*w*lambda)+0.013*sin(4*w*lambda)+0.002*sin(5*w*lambda)     +
0.002*sin(5*w*lambda));

y = term1+term2+term3;
```